Investigation of Sub-wet bulb Temperature Evaporative Cooling System for Cooling in Buildings

By

Abdulrahman Alharbi

Thesis submitted to the University of Nottingham

for the degree of Doctor of Philosophy

October 2014

Contents

Abstract

The work presented in this thesis investigates design, computer modelling and testing a sub-wet bulb temperature evaporative cooling system for space air conditioning in buildings. The context of this evaporative cooling technology design is specifically targeted at locations with a hot and dry climate such as that prevailing in most regions of Middle East countries. The focus of this technology is to address the ever-escalating energy consumption in buildings for space cooling using mechanical vapour compression air conditioning systems. In this work, two evaporative cooling configurations both based on sub-wet bulb temperature principle have been studied. Furthermore, in these designs, it was sought to adopt porous ceramic materials as wet media for the evaporative cooler and as building element and use of heat pipes as heat transfer devices. In the first test rig, the prototype system uses porous ceramic materials as part of a functioning building wall element. Experimental and modelling results were obtained for ambient inlet air dry bulb temperature of 30 and 35^{o}C, relative humidity ranging from 35% to 55% and intake air velocity less than 2 (m/s). It was found that the design achieved sub-wet bulb air temperature conditions and a maximum cooling capacity approaching 242 W/m^2 of exposed ceramic material wet surface area. The wet bulb effectiveness of the system was higher than unity. The second design exploits the high thermal conductivity of heat pipes to be integrated as an effective heat transfer device with wet porous ceramic flat panels for evaporative cooling. The thermal performance of the prototype was presented and the computer model was validated using laboratory tests at temperatures of 30 and 35^{o}C and relative humidity ranging from 35% to 55%. It was found that at airflow rates of 0.0031kg/s, inlet dry-bulb temperature of 35^{o}C and relative humidity of 35%, the supply air could

be cooled to below the inlet air wet bulb temperature and achieve a maximum cooling capacity of about 206 W/m^2 of wet ceramic surface area.

It was shown that the computer model and experimental tests are largely in good agreement.

Finally, a brief case study on direct evaporative cooling thermal performance and environmental impact was conducted as part of a field trip study conducted on an existing large scale installation in Mina Valley, Saudi Arabia. It was found that the evaporative cooling systems used for space cooling in pilgrims' accommodations and in train stations could reduce energy consumption by as much as 75% and cut carbon dioxide emission by 78% compared to traditional vapour compression systems. This demonstrates strongly that in a region with a hot and dry climate such as Mina Valley, evaporative cooling systems can be an environmentally friendly and energy-efficient cooling system compared to conventional vapour compression systems.

Publications

- Rabah Boukhanouf, Abdulrahman Alharbi, Hatem G Ibrahim and Jie Zhu. Design and testing of a sub wet bulb temperature ceramic evaporative cooler for buildings. Applied Thermal engineering **In Press**.

- Alharbi, A. Boukhanouf R. Habeebullah and Ibrahim, H., 2014. Thermal Performance and Environmental Assessment of Evaporative Cooling Systems: Case of Mina Valley, Saudi Arabia. International Journal of Civil, Architectural science and Engineering Vol;8 No: 5 pp 499-503.

- R. Boukhanouf, A. Alharbi, O. Amer, and H. G. Ibrahim. Experimental and Numerical Study of a Heat Pipe based Indirect Porous Ceramic Evaporative Cooler In 5th International Conference on Environmental Engineering and Applications (ICEEA), 3-5 July Nottingham University, 2014.

- Boukhanouf, R., Ibrahim, H., Alharbi, A and Kanzari, 2014. Investigation of an evaporative cooler for buildings in hot and dry climates Journal of Clean Energy Technologies. 2(3), 221-225.

- Boukhanouf, R., Alharbi, A., Ibrahim, H and Kanzari, M., 2013. Investigation of a sub-wet bulb temperature evaporative cooler for buildings In: Sustainable Building and Construction Conference, Coventry University, 2013. pp 70-79.

Acknowledgement

First and foremost, I thank ALLAH Almighty who gave me the strength through all my ups and downs during this project and whose invaluable grace I cannot quantify.

Next, I am very grateful to my supervisor Dr. Rabah Boukhanouf for his unlimited supports, encouragement and patience during the entire period of my study.

A great many thanks goes out to my wife and my children, who have encouraged me from the beginning to pursue my dreams and who have supported me every step along the way.

I would like to thank the Saudi government, which supported me by providing me with a full scholarship and the people working in the higher education ministry in Saudi Arabia and in the Cultural Bureau in London who helped me during the time I studied in the UK.

I would like also to thank Dr. Turki Habeebullah for his support during my scientific trip to The Institute of The Two Holy Mosques for Hajj and Omrah Research, Umm Al-Qura University, Saudi Arabia.

Finally, I would like to thank all the staff in the workshop and laboratory to name David Taylor, Jonathan Moss and David Oliver.

Nomenclature

Symbol	description	Unit
A	Heat and mass transfer area	(m^2)
A_f	The finned section heat transfer area	(m^2)
A_{dh}	Hydraulic diameter of rectangular ducts	(m^2)
C_c	Cost of electricity consumption	(SAR/kWh)
C_p	Specific heat of humid air	(J kg^{-1} K^{-1})
C_{pfw}	Specific heat of water	(J kg^{-1} K^{-1})
E_c	The power consumption	(kWh)
g_a	Air moisture content in wet channel	(kg water/ kg dry air)
g_d	Air moisture content in dry channel	(kg water/ kg dry air)
g_{fw}	Saturated air moisture content	(kg water/ kg dry air)
h	Specific enthalpy	(J/kg)
h_{fg}	Latent heat of vaporization of water	(kJ/kg)
K_s	Overall heat transfer coefficient	($Wm^{-2}K^{-1}$)
l_1	Length of the wick	(m)
Le	Lewis number	
m	Depends on the fin properties	
m_a	Air mass flow rate dry channel	(kg/s)
m_d	Air mass flow rate wet channel	(kg/s)
m_s	Supply mass flow rate ($m_d - m_a$)	(kg/s)
Nu	Nusselt number	
P	Power input	(W)
q	Specific cooling capacity	(W/m^2)

Q_c	Cooling load	(kWh)
r_1	Inner of the wick	(m)
r_2	Outer of the wick	(m)
R_a	Rayleigh number	
R_{ao}	Thermal resistance of the wet channel	(W/m^2)
R_{cp}	Thermal resistance of the saturated ceramic panel wall	(K/W)
R_{di}	Thermal resistance of the dry channel	(K/W)
R_{me}	Thermal resistance of the heat pipe wick of the evaporator and condenser	(K/W)
R_w	Thermal resistance of the water in the ceramic container	(K/W)
t	Thickness	(m)
t_a	Air temperature in the wet channel	(^oC)
T_d	Air temperature in the dry channel	(^oC)
T_{fw}	Water film temperature	(^oC)
T_{wb}	Wet bulb temperature	(^oC)
$\dot{V}$	Air flow rate	(m^3/s)
ρ	Air density	(kg/m^3)
α	Convective heat transfer coefficient	($W/(m^2\ K)$)
σ	Mass transfer coefficient	($kg_{water}/s\ m^2)/kg_{dry}$)
δ_f	Fins thickness	(m)
λ_1	Thermal conductivity of the liquid phase of the working fluid	(W/mK)

λ_c	Thermal conductivity of the dry ceramic container	(W/mK)
λ_f	Fins thermal conductivity	(W/mK)
λ_s	Thermal conductivity of heat pipe wick material	(W/mK)
λ_w	Water thermal conductivity	(W/mK)
λ_{wick}	Thermal conductivity of the wick	(W/mK)
ϕ_c	Ceramic container porosity	(%)
ϕ_{wick}	Wick porosity	(%)
η_f	Efficiency of the finned section heat exchanger	
ε_{db}	Wet bulb effectiveness	
ε_{dp}	Dew point effectiveness	

Subscript	description
a	Wet channel
d	Dry channel
i	Inlet
o	Outlet
w	Water
fw	Film of water
wb	Wet bulb temperature

dp	Dry bulb temperature

List of Figures

List of Tables

Chapter 1

Introduction

1.1 Background

Today, the demand for energy is growing rapidly, and the world is hungry for energy. Energy is used for everything we do in its different forms, including heat, electricity, nuclear energy, light, etc. These are overwhelmingly transformed from other forms of fossil fuels. According to Energy Resources [1] "fossil fuels provide around 66% of the world's electrical power, and 95% of the world's total energy demands (including heating, transport, electricity generation and other uses". Burning fossil fuel in turn produces carbon dioxide (CO_2) which contributes to the "greenhouse effect" warming of the earth [2].

The building sector consumes a large amount of the total primary energy compared to other sectors. Energy consumption in buildings stands at between 30–40% of the total primary energy use globally [3, 4]. For example, in the developed countries such as USA, 41% of primary energy was consumed by residential and commercial buildings compared to 30% and 29% by industrial and transportation sectors respectively[5], while in the developing countries such as Kingdom of Saudi Arabia where air conditioning is required for the majority of the year, 70% of primary energy is consumed by the building sector to provide comfortable indoor climatic conditions for occupants.

The growth in air conditioning systems in the world is mainly driven by an increase in living standards, affordability, population growth and cheap electrical energy in some regions such as the Middle East. This has put severe strains on electricity grids in many countries to build new power generation plants and extend grid infrastructure to meet peak electricity loads, which in turn negatively impact the environment by emitting more greenhouse gases.

Therefore, adoption of more energy efficient systems and passive cooling techniques would significantly reduce energy consumption and CO_2 emissions. One of these is evaporative cooling systems, which are based on using the process of evaporating water to cool air. Where its application is suitable, evaporative cooling systems have the advantage of low energy consumption, being environmentally benign and having low capital and maintenance costs. Existing evaporative cooling systems can be divided into two main categories: direct and indirect evaporative cooling systems. During the process of direct evaporative cooling, the moving air passes over an open water surface or a wetted medium. The heat and mass transfer between the warm dry air and water saturated medium results in a temperature decrease of air and an increase in its water content while its overall enthalpy remains constant. On the other hand, in indirect evaporative cooling, the supply is cooling through a heat exchanger that separates it from the water stream. Hence, the water content of the cooled air remains unchanged.

The effectiveness of direct evaporative coolers is primarily influenced by the air wet bulb temperature, and in a well-designed system the air could be cooled to within 2 to 3^oC. However, the strong influence of the ambient air wet bulb temperature on its thermal performance represents a severe thermodynamic limitation [6]. This limitation also applies to indirect evaporative cooling systems' counterparts, although the

increase in humidity is overcome. Therefore, this has led several researchers to develop and modify the thermal process of direct and indirect evaporative cooling systems to achieving sub-wet bulb temperature, referred to as Dew point or Sub-wet bulb temperature evaporative cooling. The thermodynamic cycle of a sub-wet bulb temperature evaporative cooling system was first introduced by Maisotesnkois in 2003 and is known as the M-cycle [6]. Currently, the M-cycle is available in the form of a commercial product mainly sold in the USA under the name of "Coolorado".

Currently, there are several researchers who have investigated design, building and testing of direct and indirect evaporative cooling systems in the context of reducing energy consumption for space air conditioning in buildings. The overall aim of this thesis is to expand on the works of Ibrahim et al. [7], Schiano-Phan [8] and Riffat and Zhu [9] to develop a sub-wet bulb temperature evaporative cooling system using porous ceramic materials for integration into building elements.

1.2 Research Aims and Objectives

The main aims of this research are to investigate the design, building and testing of a sub-wet bulb temperature evaporative cooling system using porous ceramic materials as wet media material. The main focus is to provide space cooling for building occupants in the regions with hot and dry climate such as the Middle East. The specific objectives of the research are following;

1.2.1 Comparison of traditional and modern cooling technology

Traditional passive cooling techniques for buildings such as windcatchers, earth cooling and evaporative cooling used in hot and dry climates were reviewed and compared to modern cooling technologies, which are predominantly based on vapour compression. This includes the principle of operation, thermal performance and application. Evaporative cooling technologies, particularly the direct systems, were reviewed in some details to highlight current research, development, application and thermal performance prediction.

1.2.2 Review of existing state-of-the-art research work on sub-wet bulb temperature of indirect evaporative cooling system and porous materials

The review focuses on system designs of thermal performances and the current application of sub-wet bulb temperature. In addition, the porous materials used as wet media for evaporative cooling are addressed.

1.2.3 Developing a computer model using common energy and mass conservation equations for each design configuration

Common energy and mass conservation equations were used to develop a computer model to analyse the performance of the sub-wet bulb temperature evaporative coolers using Matlab software. The model includes evaluating the effect of inlet temperature, humidity and air flow.

1.2.4 Testing small-scale laboratory prototypes

Two small-scale prototypes were design and tested under various operation conditions to establish operating performance and to validate the computer

model by comparing the results to those obtained from the computer model, such as cooling effectiveness and energy efficiency.

1.2.5 Analysing thermal performance and assessing the environmental impact of direct evaporative cooling application in Makkah as a case study

By adopting a case study that resulted from field trips to Mina Valley in Saudi Arabia, a brief economic and environmental comparison between existing direct evaporative cooling installations and vapour compression systems was conducted.

1.3 Research description

Two regenerative configurations of an indirect evaporative cooling system were designed, modelled, built and tested to achieve sub-wet bulb temperature. The main idea of the study of the two coolers is to redirect a portion of the dry channel air for water evaporation in the wet channel to break the limitation that supplied air cannot be cooled below its wet bulb and achieve product air at sub-wet bulb temperature.

The air streams in the dry and wet channel flow in counter flow arrangement, and the supply air exchanges sensible heat with the water in the porous ceramic materials that in turn are cooled through water evaporation on the wet channel side. This results in a drop in temperature of the air in the dry channel without changing its moisture content while the air in the wet channel is rejected at the saturation state.

In the first scale rig, porous ceramic materials in the form of hollow flat shells were used as wet media in a sub-wet bulb temperature evaporative cooler. The porous ceramic panels were placed between the dry and wet air ducts to form small and narrow ducts with air flowing at low velocity. The dry channel side of the porous

ceramic panel is sealed with a thin non-permeable membrane while the wet channel side allows water to sip through its micro-pores onto its surface forming a thin water film. This allows direct contact with the airflow and hence causes water evaporation.

In the second cooler, a prototype porous ceramic material was combined with 12 bundles of finned heat pipes. The porous ceramic was installed in wet channel to be used as wet media and finned heat pipes were placed in dry channel to be a heat transfer device between the cold water in ceramic containers in wet duct and inlet dry air in the dry duct.

A huge application of evaporative cooling technology in Mina Valley, Saudi Arabia, was visited during July and August 2013 to investigated the thermal performance and environmental impact of this application. A detailed description of evaporative cooling systems used for space cooling in Mina Valley, Saudi Arabia, was presented. The thermal performance and environmental impact of the evaporative cooling systems used for space cooling in pilgrims' accommodations at the Aljamaraat Bridge and in the train stations were evaluated.

1.4 Contributions to knowledge

The research work carried out in this thesis contributed to advancing general knowledge of energy conservation by reviewing the practical advantages and limitations of traditional and modern engineering methods of providing thermal comfort in buildings. The work also contributed to the specific field of research of evaporative cooling systems in general and the sub-wet bulb temperature sub-category in particular in the following way:

- Design of a small-scale sub-wet bulb temperature evaporative cooling system for integration into building element using porous ceramic materials.
- Developing a computer model for a sub-wet bulb temperature evaporative cooling system using energy and mass conservation laws.
- Conducting experimental validation of the theoretical model and providing strong evidence on the viability of the evaporative cooling system for hot and dry climate.
- Demonstrating the feasibility of incorporating porous ceramic materials as wet media for sub-wet bulb temperature evaporative cooling directly into a building element or using heat transfer devices such as a heat pipe.
- Carrying out a brief economic analysis of a case study on existing large-scale evaporative cooling systems.

1.5 Thesis structure

The thesis is organised into 8 chapters.

Chapter 1 covers mainly the context of the research topic, the intended aims and objectives, and the contribution achieved.

Chapter 2 presents a short review on the traditional cooling techniques used particularly in the hot and dry climate of Middle East countries as well as the principle of operation of the main modern refrigerant based technologies.

Chapter 3 is about a focused literature review of indirect evaporative cooling technologies and wet media materials. This covers the principle work of sub-wet bulb temperature and its advantages compared with mechanical vapour compression, materials such as porous ceramic and heat pipes and the performance were also described.

Chapter 4 describes the theoretical analysis and computer model of the sub-wet bulb temperature evaporative cooler using porous ceramic materials. A physical description of the cooling system, a mathematical model that was developed by solving common energy and mass conservation laws, and the computer algorithm used to develop the codes are introduced. In addition, the mathematical model results are discussed in details.

Chapter 5 reports on experimental results of a laboratory prototype porous ceramic sub-wet bulb temperature evaporative cooler. The results were discussed and compared to those obtained through computer modelling. The experiments include studying the effects of various parameters on the performance of the cooling system such as the intake air dry-bulb temperature, intake air humidity, velocity, etc. Further, discrepancies between experimental and modelling results are examined.

Chapter 6 investigates a second configuration of a sub-wet bulb temperature evaporative cooling system in which the design integrates a cylindrical heat pipe and porous ceramic panels. It covers a discussion on both the experimental and computer modelling results.

Chapter 7 presents a case study of a large-scale application of evaporative cooling technology in Mina Valley, Saudi Arabia. Detailed descriptions of evaporative cooling systems used for space cooling in different locations including the pilgrims' accommodations at Aljamaraat Bridge and train stations were given. A simplified economic an environmental analysis is also conducted.

Chapter 8 discusses the research work and main findings on the theoretical and experimental analysis and recommends the direction of further work.

Chapter 2

Climate and Indoor Comfort in Buildings in Saudi Arabia

2.1 Introduction

The Kingdom of Saudi Arabia is situated in the south west of the continent of Asia at latitude of 25º north and 45º east occupying most of the Arabian Peninsula with a total area of 2,149,690 km^2. It has one of the sunniest climates in the world with proximity to the circum-global latitudinal belt of generally high atmospheric pressure [10]. Its climate is dominated by the continental desert climate which is hot and dry, except in summer along the coasts where it is hot and humid. Figure 2.1 shows the geographical location of Saudi Arabia on the world map. In this chapter, the climate of the main cities of Saudi Arabia such will be reviewed and associated requirement for thermal comfort in buildings will presented.

Figure 2.1 Location of Saudi Arabia [11]

2.2 Climate

Climate is the “average weather” at different spatial and time scales, ranging from global changes over cycles lasting a number of years to local changes lasting a few minutes. A hot desert climate prevails over a large portion of Saudi Arabia and temperature distribution is controlled mainly by altitude, and to a lesser extent, its proximity to the sea. Figure 2.2 gives the different types of climates that can be found in Saudi Arabia, ranging from desert continental to coastal climates, represented on a psychometric chart. During summer the region can also experience patterns of extremely hot weather spells. The cities situated in the inner land such as Riyadh experience a desert continental climate which is hot and dry. Western and eastern coastal plains cites such as Jeddah and Dammam respectively represent a desert coastal climate whereas the temperatures of the mountain chain in the south of Saudi Arabia such as Abha are lower and more comfortable.

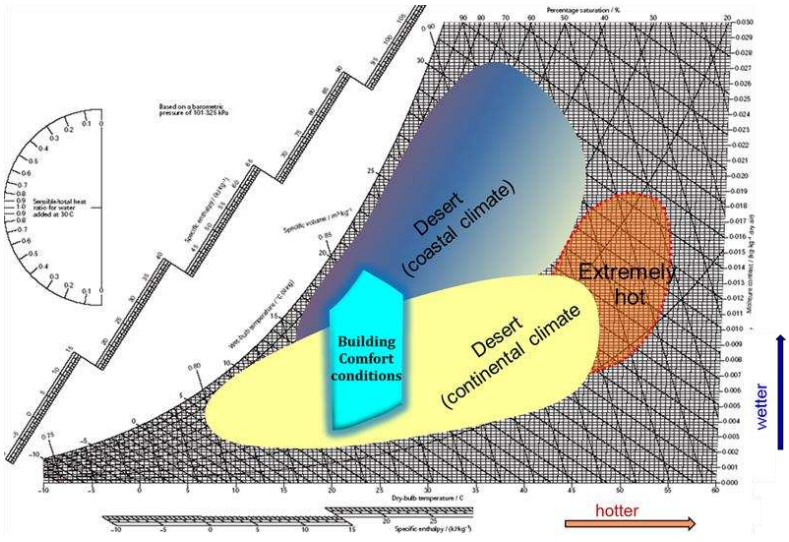

Figure 2.2 Climate and building comfort conditions for different regions of Saudi Arabia on psychrometric chart

2.2.1 Riyadh

Riyadh represents the central region's hot dry climate of the Kingdom, and it is 611m above sea level [12]. It can be seen from Figure 2.3 that the climate of Riyadh is characterised by extremely hot and dry summers with very large diurnal temperature ranges and moderately cold winters. In hot season of summer, which lasts from May to September, the temperature averages 39°C, whereas diurnal temperatures could fluctuate between 24 and 45°C. In winter season (November to February) the temperatures average 24°C, with the coldest temperatures recorded in December and January. The region is generally characterised by its low relative humidity which typically ranges from as low as 10% to 47% over the course of the year. In the remaining moths of the year (March, April, October and November), the climate of Riyadh is more comfortable with an average temperature between 20 and 30°C.

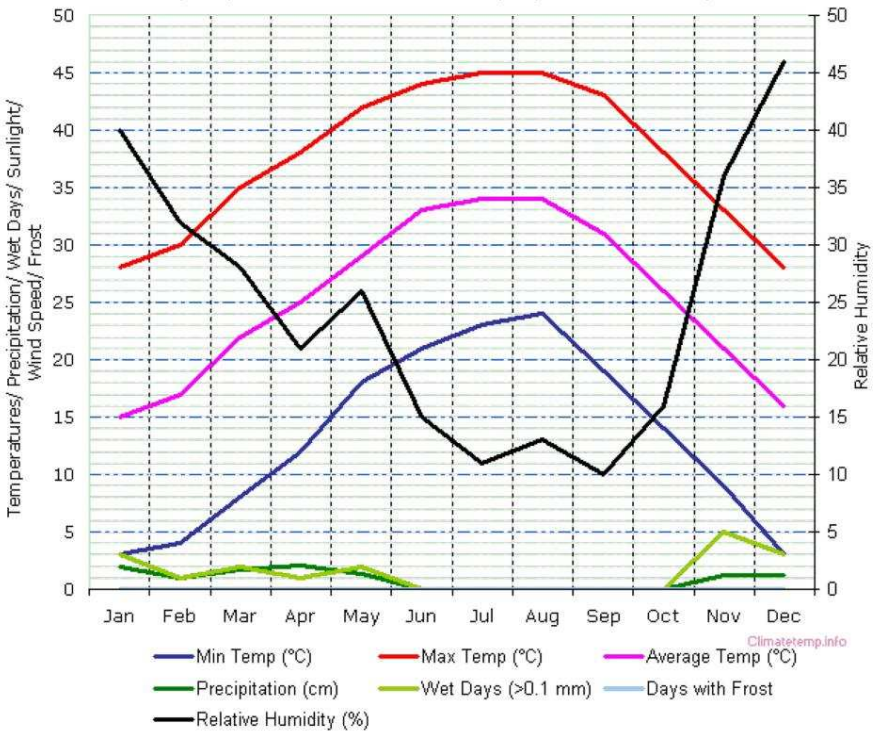

Figure 2.3 Riyadh climate graph [13]

2.2.2 Jeddah

Jeddah represents the western coastal hot-humid climate of the Kingdom, which is 17m above sea level [12]. It can be seen from Figure 2.4 and Figure 2.5 that the climate of Jeddah is characterised by long, hot and humid summers with an average daily high temperature above 37°C during the months of May, June, July, August, September and October, and the hottest days of the warm season are in July with an average high of 39°C and a low of 26°C. The cold season is short and mild from December to February with an average daily high temperature below 30°C and a comfortable temperature between 18°C and 24°C. On the other hand, the average of relative humidity shown in Figure 2.5 typically ranges from 30% to 89% over the course of the year. Figure 2.4 illustrates a monthly average of dry and wet-bulb temperatures, and the rather high solar radiation levels in Jeddah throughout the year.

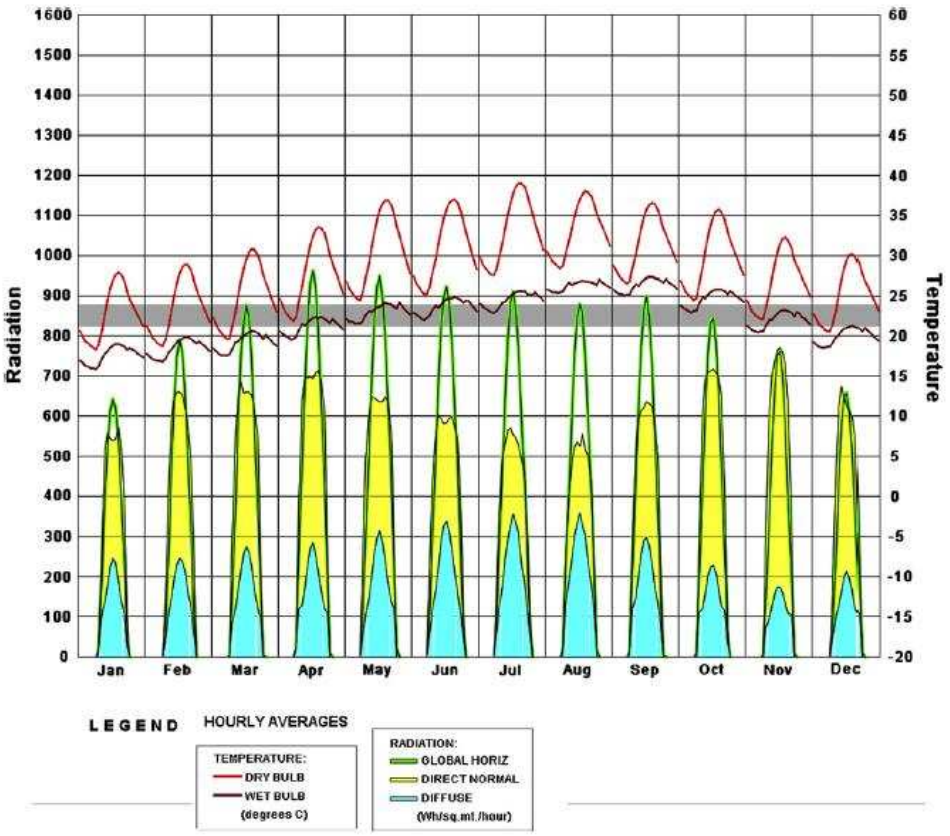

Figure 2.4 A monthly average of dry and wet-bulb temperatures, and the rather high solar radiation levels in Jeddah throughout the year [14]

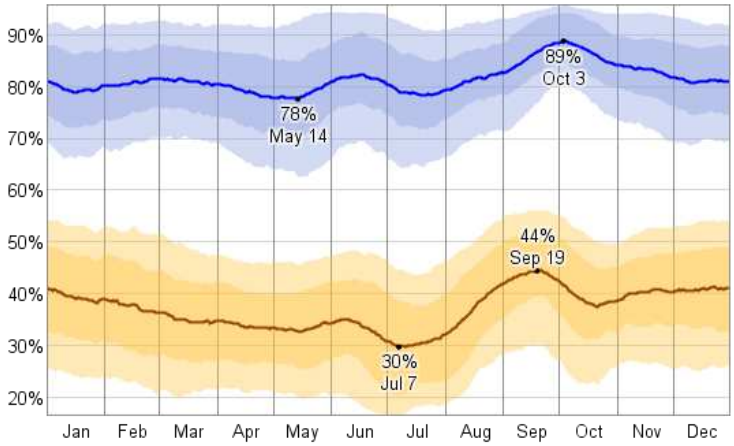

Figure 2.5 The daily average high (blue) and low (brown) relative humidity**[15]**

2.2.3 Abah

Abah is located in the mountains of south-western Saudi Arabia and at 2200 meters above sea level. The climate of Abah is known for its lower temperature and is more comfortable than others cities such as Riyadh and Jeddah. The warm season is between May and September with an average daily high temperature above 28°C. Yet the cold season is from December to February has an average daily high temperature below 21°C as shown in Figure 2.6.

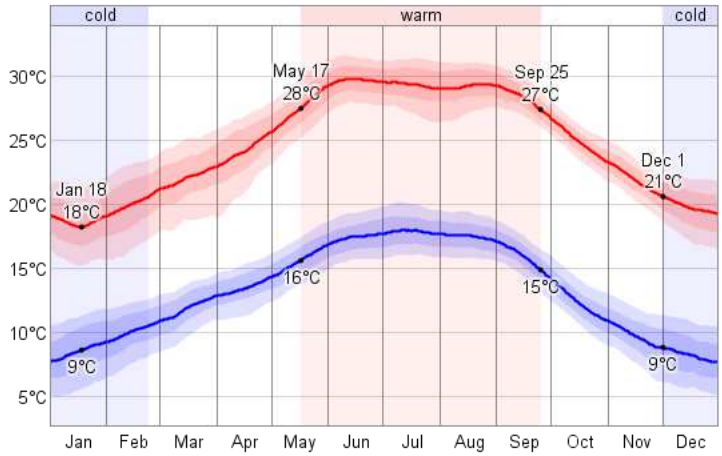

Figure 2.6 The daily average low (blue) and high (red) temperature **[15]**

2.3 Thermal comfort

Human thermal comfort is defined as "the state of mind which expresses satisfaction with the thermal environment" [16]. This is achieved when conditions of thermal neutrality are satisfied and the building occupant does not have a preference for a higher or lower ambient temperature. The thermal comfort is strongly influenced by the following [17]:

- Environmental parameters: such as surrounding air dry-bulb temperature, humidity, air velocity and radiation;
- Physical or personal parameters: such as human activity level or thermal insulation of clothing; and
- Organic parameters: such as age, sex and health.

The main purpose of a building structure is to create a physical boundary for an indoor environment that is comfortable and sheltered form the constant variation of the surrounding atmospheric conditions. The building structure should offer protection even under harsh environmental conditions such as those experienced in desert conditions. For example the building envelope in regions of Saudi Arabia such as Makkah experiences large temperature swing between day and night, with maximum temperature in summer exceeding 45^{o} C, as shown in Figure 2.7 [15].

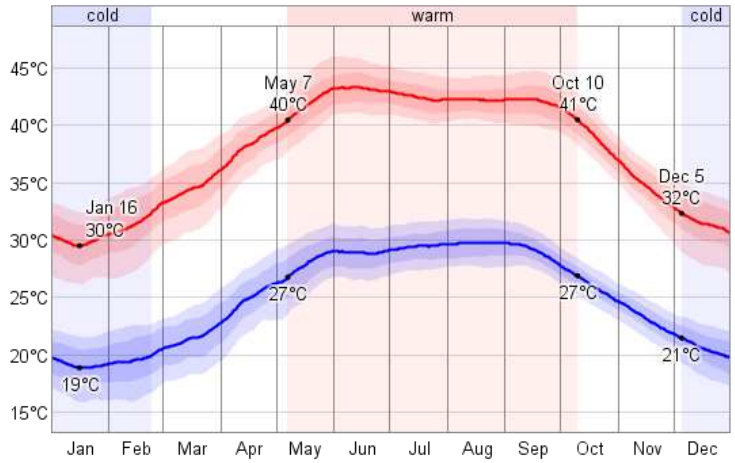

Figure 2.7 The daily average low (blue) and high (red) temperature profile in Makkah, Saudi Arabia **[15]**

2.3.1 Indoor air properties

To be able to provide the level of thermal comfort in buildings required by the building standards, understanding the operating states of the air at various environmental conditions is necessary. The properties that indoor air undergoes as it is conditioned in various building services equipment including heating, cooling, humidification and dehumidification are often determined using tables, charts and computer software.

2.3.2 Air properties on a psychrometric chart

The psychrometric chart is a graphical form of the important physical and thermodynamic properties of humid air. The chart provides a picture of how various properties relate to each other such as dry-bulb temperature, moisture and content, and relative humidity. The air properties that are considered to be required for occupants in buildings are referred to as “comfort zone” on the psychrometric chart. Figure 2.8 shows a comparison between an ASHRAE comfort zone for a mechanically air conditioned building space and that of evaporative cooling system. The evaporative air conditioning comfort zone takes into account the increased air flow that is modified

and compared with the ASHRAE comfort zone based on the vapour compression air conditioning [18].

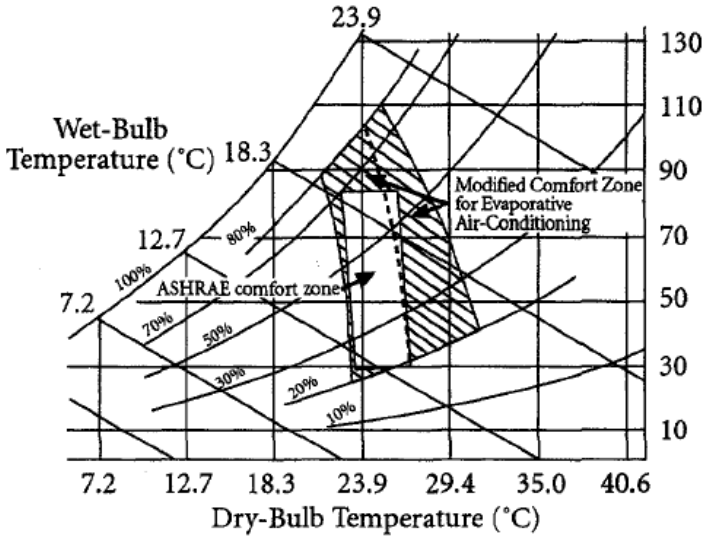

Figure 2.8 Modified evaporative air conditioning comfort zone taking into account increased airflow compared with ASHRAE comfort zone based on vapor compression air conditioning [18]

The operating conditions of air can be determined by locating their states on the chart, referred to as state points, the location of which at a given barometric pressure are fixed by any two of the following properties.

- Dry-bulb temperature, t (^{o}C)
- Wet-bulb temperature, t (^{o}C)
- Moisture content, g (kg of water vapour/kg dry air)
- Specific volume, v (m^3/kg dry air)
- Percentage saturation, % sat
- Specific enthalpy, h (kJ/kg dry air)

The most important properties of air are shown in Figure 2.9 as constant property lines on the psychrometric chart.

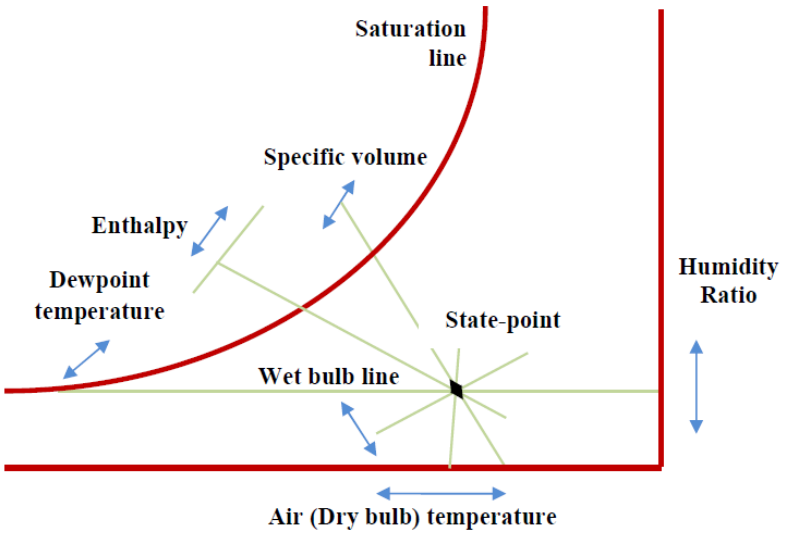

Figure 2.9 Constant air property lines[19]

i) Dry-bulb temperature

The dry-bulb temperature is the temperature of air measured by a thermometer shielded from radiation. The dry–bulb temperature indicates the degree of the sensible heat content of the air but it does not measure the amount of moisture in the air, so it does not give any information about latent heat content.

ii) Wet-bulb temperature

The wet-bulb temperature is measured using a thermometer whose bulb has been wrapped around a cloth and which is kept moist with water. It indicates the degree of the latent heat content of air but it does not give any information about the sensible heat content of the air.

iii) Dew Point Temperature (DPT)

When the air is cooled at the constant moisture content, the temperature of that air will reach the SVP curve. At this point, water vapour condensation will begin to take place. This point is known as the dew point temperature as shown in Figure 2.10 Hence, Dew Point Temperature is defined as “the temperature of saturated air, which has the same vapour pressure as the moist air under consideration” [20].

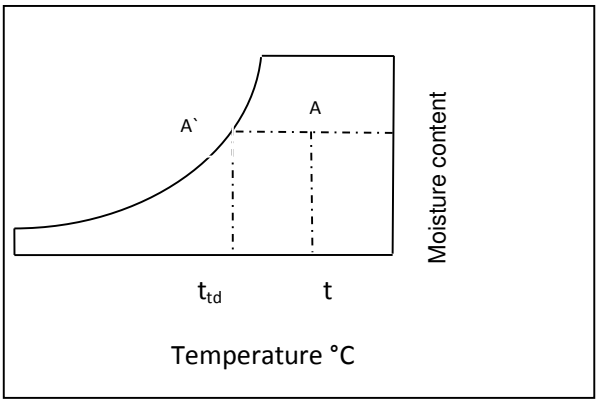

Figure 2.10 Representation of DPT on Psychrometric chart

iv) Humid air

Humid air is a gas mixture of dry air and water vapour. Both dry air and water vapour can be assumed to behave as ideal gases, and it is possible to describe that composition of gas mixture by giving the total mass of the mixture as a function of the number of moles of each component present as follows:

$$m = m_1 + m_2 + \ldots + m_n \tag{2-1}$$

And the total number of moles in the gas mixture can be expressed as:

$$n = n_1 + n_2 + \ldots + n_n \tag{2-2}$$

The average molecular weight of the mixture M can then be given as:

$$M = \frac{n_1 m_1 + n_2 m_2 + \ldots + m_n m_n}{n} \tag{2-3}$$

v) Relative humidity

The relative humidity of air is a property that gives the amount of water vapour in a mixture of air expressed in percentage (%). Commonly, relative humidity, ϕ, is defined as the ratio of vapour pressure of water vapour in the air, P_s, to the saturated vapour pressure at the same air temperature, P_{ss}. This is expressed as follows:

$$\phi = \frac{P_s}{P_{ss}} \times 100 \qquad (2\text{-}5)$$

Figure 2.11 gives a graphical representation of the operating state, A, and the saturated vapour state, SVP, of humid air on a psychrometric chart.

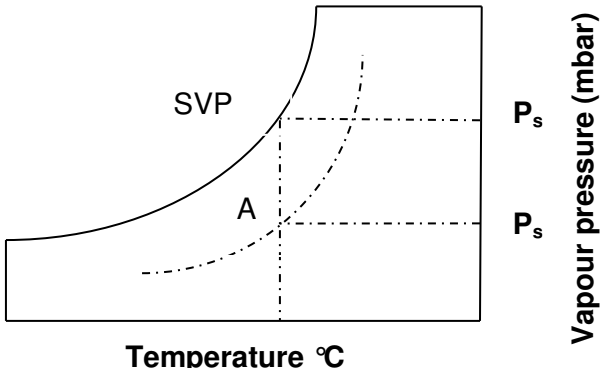

Figure 2.11 Relative humidity representation

vi) Moisture content

The moisture content of humid air, g, is defined as the mass of water vapour in 1 kg of dry air in an air/water vapour mixture. It is sometimes referred to as specific humidity or humidity ratio, which is expressed as:

$$g = \frac{m_s}{m_a} = \frac{kg\_of\_water\_vapour}{kg\_of\_dry\_air} \qquad (2\text{-}6)$$

vii) Specific enthalpy

The specific enthalpy of humid air is equal to the sum of the individual partial enthalpies of its constituents, dry air and water vapour. This is expressed as:

$$h = u + Pv \qquad (2\text{-}7)$$

Where u is the specific internal energy, P is the pressure and v is the specific volume.

viii) Specific volume

The specific volume is the volume of 1 kg of air in $1m^3$ associated with water vapour. The specific volume is given by v= V/m with the unit of m^3/kg of dry air.

2.4 Design Conditions

The local climatic changes are very important in air conditioning system design, particularly those elements of climate that influence the thermal environment such as radiation, dry-bulb temperature, humidity and wind speed [21].

2.4.1 External design condition for summer cooling

The establishment of external design conditions, both dry- and wet-bulb temperatures, is required for the sizing of air conditioning systems during summer cooling. For example, the dry- and wet-bulb temperatures of the summer design conditions for Riyadh in the Saudi Arabia are 43.9 20°C and 20°C respectively, with an average diurnal range of 18°C. Table 2-1 [22] presents the monthly air temperature, relative humidity and solar radiations for Riyadh, Jeddah and Abha.

Table 2-1 Average monthly air temperature, relative humidity and solar radiation for Riyadh, Jeddah and Abah for the year 2001[22]

Month	Air temperature (°C)			Relative humidity (%)			Solar radiation (W/m^2)		
	Riyadh	Jeddah	Abha	Riyadh	Jeddah	Abha	Riyadh	Jeddah	Abha
1	12.4 (4.7)	22.7 (3.8)	12 (4.3)	60.5 (4.7)	66.1 (23.1)	73.7 (24.9)	448	450	509
2	15.2 (4.6)	23.1 (3.7)	14.8 (4.2)	44.8 (16.1)	67.2 (18.5)	72 (24.5)	475	447	531
3	21.2 (4.4)	26.8 (4)	16.7 (3.2)	51.5 (24.5)	68.1 (20.2)	74 (21)	483	524	516
4	26.6 (4.8)	20.3 (4.1)	19.6 (4.1)	27.9 (13.9)	66.3 (19.4)	61 (23.5)	575	582	606
5	31.4 (4.8)	30.4 (4.6)	22 (4.3)	20.2 (9.2)	60 (30.6)	52 (23)	602	567	570
6	33.4 (4.6)	31.7 (4.9)	23.5 (2.2)	14.4 (4.4)	60.8 (25.3)	35 (15.8)	619	589	530
7	35.4 (4.9)	33.3 (4.3)	23.5 (3.8)	16.6 (4.3)	56.6 (23.7)	55 (27.7)	598	581	477
8	36 (4.7)	33.4 (2.6)	22.6 (4.3)	19 (7.1)	76.5 (14.9)	69.7 (29.3)	579	510	523
9	32.7 (4.7)	31.9 (2.7)	22.4 (4.6)	19.2 (7.3)	82.4 (13.4)	37.2 (23.8)	570	503	591
10	27.3 (4.9)	30 (3.7)	19.3 (4.3)	19.6 (9.7)	82.4 (18.1)	52.9 (29)	451	494	564
11	19.6 (5.2)	27.4 (3.5)	15.4 (4.3)	38.1 (15.9)	75.6 (18.4)	67 (28)	455	445	529
12	15.6 (4.8)	25.6 (2.9)	14.8 (4.3)	66.9 (23.3)	78.8 (13.5)	77 (23)	417	372	495

The climate of Riyadh was plotted and divided into four zones: comfort zone (1), passive cooling zone (2) , active cooling (3) and heating (4) based on the psychrometric chart as shown in Figure 2.12 [23] . The passive cooling zone is divided into three parts: 2a, 2b and 2c, and there are three strategies that could be used alone or in combination with each other to achieve comfortable conditions. These strategies are based on the use of thick walls or ventilation and/or evaporative cooling. Active cooling includes two parts (3a and 3b): for the first part, the heat must be removed to achieve a comfortable zone while the heat and humidity needs to be removed to achieve a comfortable zone. Mechanical vapour compression or an absorption system can be used for this zone to achieve comfortable conditions. The heating zone, which is characterised by low air temperature values, is divided into five parts (4a, 4b, 4c, 4d and 4e). The first part, 4a, requires little heat gain from active or passive solar heating to achieve comfortable conditions. For the other four parts, 4b, 4c, 4d, and 4e, they require active heating to achieve comfortable conditions.

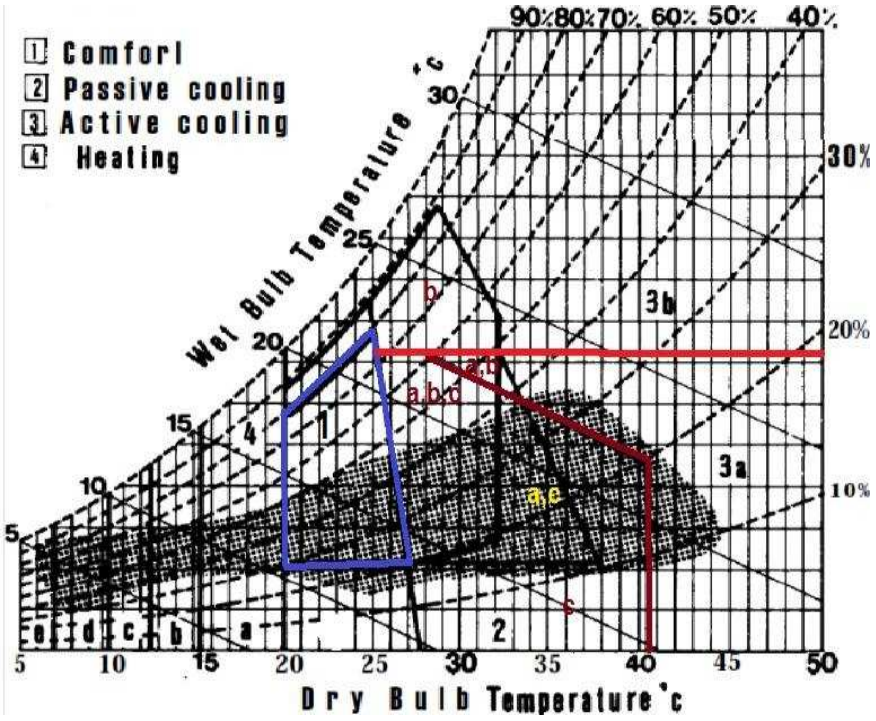

Figure 2.12 Comfort, passive cooling, and heating zones of Riyadh on psychrometric chart [23]

According to S. Abdul Rahim [23] the comfortable conditions for Riyadh occur for about 43.7% of the total hours of the year when the hot periods, which require active and/or passive cooling are at about 12.5% of the total hours of the year. However, the hot periods for which active cooling is essential are about 7% of the total hours of the year. On the other hand, the periods that require active and/or passive heating are 36.8% of the total hours of the year.

Al-Helal [22] evaluated the performance of direct evaporative cooling systems under different climatic conditions in Saudi Arabia. Air temperature, relative humidity and solar radiation for Riyadh, which represented an arid climate, Jeddah a humid climate and Abha a moderate climate were analysed. The average results of air temperature, relative humidity and humidity ratio for the air leaving the cooler, cooling efficiencies, temperature drop and cooling powers under different operations are shown in Table 2-2. This table shows that the cooling efficiencies were between 77% and 87% with an average of 82.4% for arid conditions, while it was between 65% and 84% with an average of 72.2% under humid conditions, and between 63% and 80.5% with an average of 75% for moderate conditions. Also, from Table 2-2 it can see that the highest temperature drop was in Riyadh, which is under arid conditions, ranging from 12°C to 23.5°C, and the averaging was at 18.2°C.

Table 2-2 Averages of temperature, relative humidity and humidity ratio for the air entering and leaving the cooler, cooling efficiency, temperature drop and cooling power [22]

Climatic conditions	Air entering the cooler			Air leaving the cooler			η (%)	D (°C)	q (W)
	T_{in}	RH_{in}	W_{in}	T_{out}	RH_{out}	W_{out}			
Arid	30.5	16	0.00432	18	70	0.00900	77	12.5	14595
	35.4	11	0.00391	20.1	63.1	0.00925	80.5	15.3	17581
	40	9	0.00411	22	59.4	0.00980	82.2	18	20379
	40	12	0.00549	22.6	66.4	0.01139	84	17.4	19700
	45	12	0.00715	24.5	69	0.01331	87	20.5	22845
	45	7.6	0.00451	24	59	0.01100	84.3	21	23402
	50	8.5	0.00651	26.5	65.4	0.01422	82	23.5	25783
Average	**40.8**	**10.9**	**0.00514**	**22.5**	**64.6**	**0.01114**	**82.4**	**18.2**	**20612**
Humid	30	42	0.01114	23.2	70	0.01247	71.6	6.8	8033
	31	67	0.01906	27.6	86	0.02014	67	3.4	3887
	30	71	0.01907	27.2	88	0.02013	65	2.8	3308
	35	58	0.02070	30	85	0.02297	68	5	5063
	38.8	46.2	0.02028	31	83	0.02378	75	7.8	7125
	40	45	0.02109	31.4	83	0.02435	74.5	8.6	7620
	40	56	0.02646	32.2	88	0.02713	84	7.8	6911
Average	**35**	**55**	**0.01969**	**28.9**	**83.3**	**0.02157**	**72.2**	**6**	**5992**
Moderate	28	19	0.00444	17	71	0.00856	80	11	13923
	29	43	0.01076	23	70	0.01232	63	6	7332
	30.5	16	0.00432	18	70	0.00900	77	12	14525
	30	25	0.00659	19.7	74	0.01061	78	10.3	12168
	30	42	0.01114	23.2	70	0.01247	71.6	6.8	8033
	35.4	11	0.00391	20.1	63.1	0.00925	80.5	15.3	15317
Average	**30.5**	**26**	**0.00686**	**20.2**	**69.7**	**0.01037**	**75**	**10.2**	**11883**

2.4.2 Internal design conditions for both summer and winter

A suitable indoor design condition depends on the type and general use of the building, thermal comfort considerations and economic considerations. Moreover, the internal design condition requires the specification of dry- and wet-bulb temperature, relative humidity and air velocity; in addition, they cannot be considered in isolation because all of them are affected on the thermal balance of the human body. For example, when a film of water is formed on the skin of the human body on a high relative humidity day, the higher air velocity will increase the evaporation rate from the body, and which will reduce skin temperature. Table 2-3 gives a general guide that can be used for a range of internal conditions for summer cooling and winter heating.

Table 2-3 General guide for internal design conditions [20]

RH (%)	Summer		Winter	
	Temperature Range (°C)	Air velocity Range (ms^{-1})	Temperature Range (°C)	Air velocity Range (ms^{-1})
40	23.0-26.5	0.20-0.40	20.5-24.0	0.13-0.28
50	22.5-26.0	0.19-0.35	20.0-23.5	0.13-0.23
70	22.0-25.5	0.17-0.35	20.0-23.0	0.13-0.21

Chapter 3

Review of Cooling Technologies in Traditional Buildings

3.1 Traditional Cooling Methods

Traditional buildings' architecture has been practised over a long period of time to create an adequate solution to a particular characteristic of the environment in which they were constructed. Traditional architecture integrates innovative elements that respond to the local climates such as convective cooling, carefully sized and positioned façade openings, adoption of windcatcher, mashrabiya and direct evaporative cooling system.

3.1.1 Natural convective and thermal mass cooling

In locations where there is a large swing between day and night temperatures, cooling of buildings using thermal mass is usually a viable alternative, a practice found in many desert constructions. In these buildings, the thermal mass of the dense materials is used as a heat sink-that can absorb and store the heat during the hot day and release heat through convection and radiation during the cool night. This process relies on the thermal inertia of the building materials (heavy masonry bricks, stones, earth blocks, etc.) to help moderate the temperature fluctuations over time within the occupied space [24]. For example, Figure 3.1 shows a wall construction with two different

thermal capacities [14]. Figure 3.1a shows a heavy masonry wall whereas Figure 3.1b shows a lightweight wall with high thermal insulation.

The thermal response of the two walls under the influence of ambient temperature fluctuation is shown in Figure 3.2. It can be seen that that the temperature variation experienced inside the building is smaller with the wall of heavy thermal mass than with one of a lower thermal mass, achieving a better thermal equilibrium.

Figure 3.1 Different wall structure a) heavy masonry B) light weight [25]

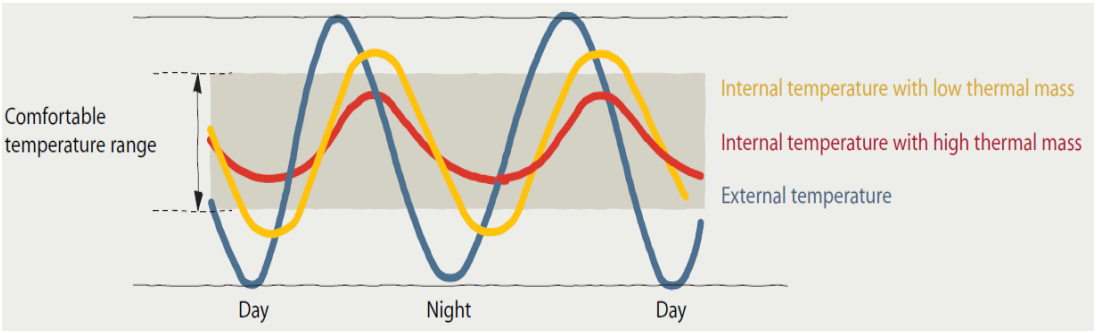

Figure 3.2 Temperature variation: (-) high thermal mass, (-) low thermal mass, (-) ambient temperature [25]

3.1.2 Openings

Natural airflows techniques appear in many places as a cooling method to provide thermal comfort for the occupants in building through various architectural forms. In dry regions, the elevation of outside openings or windows is reduced to diminish the daytime ventilation and the hot winds that carry sand and dust. There are, however, larger windows that look toward the patio. These windows include small upper

openings, usually made out of gypsum panels that allow warm air to escape, and lower openings, that include windows and doors [26]

For example, in Damascus, where the climate is hot and dry, the outside air enters to the house through the courtyard after being evaporatively cooled by water and plants as shown in Figure 3.3 a. The hot air stored in the house was driven to the outside by the cool air through the small upper openings above the doors. In areas where the humidity is high, such as some part of Algiers, the rooms are open on all sides to provide maximum cross ventilation as shown in Figure 3.3 b [26].

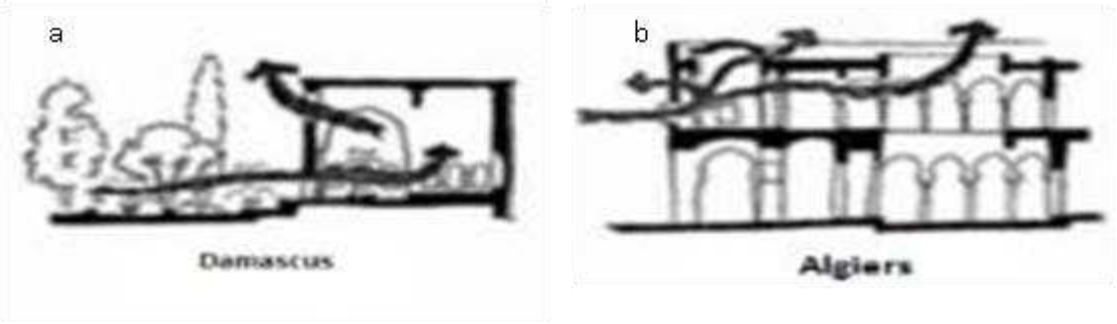

Figure 3.3 Some example of cross ventilation patterns throughout houses in different countries [26]

3.1.3 The Mashrabiya

It is an element of traditional Arabic architecture used since the middle ages up to the mid-twentieth century, and the word of ‘mashrabiya’ comes from an Arabic root meaning the ‘place of drinking’[27]. In fact, this concept is essentially a screened wooden device used instead of a window, which allows a good flow of breezes through the house. It is mostly used on the street side of the houses and residential places and also sometimes can be found it in commercial and public buildings. It also provides protection and shade for the ground floor windows that are flat and usually unprotected. Mashrabiya can be found in buildings in coastal areas of the Middle East,

such as where the weather is hot and humid [26]. Figure 3.4 shows an example of installed rows of mashrabiyas of a façade building in Jeddah, Saudi Arabia.

Figure 3.4 Rows of mashrabiya on the facade hotel in Jeddah

3.1.4 Wind Traps

i. Wind Scoops

A wind scoop is often located at a high point in the house and is made of bricks, timber or metal. It is designed with inclination so that the inlet pushes the prevailing wind downward toward the air shaft and directly to the rooms as shown in Figure 3.5. The wind scoop was traditionally found in Egyptian architecture and then extended to other parts of the Middle East, North Africa and as far to the east as Pakistan and Afghanistan. In the countries of the Gulf, it is known as ‘Badgir’, ‘serdab’, and ‘milqaf’ [26].

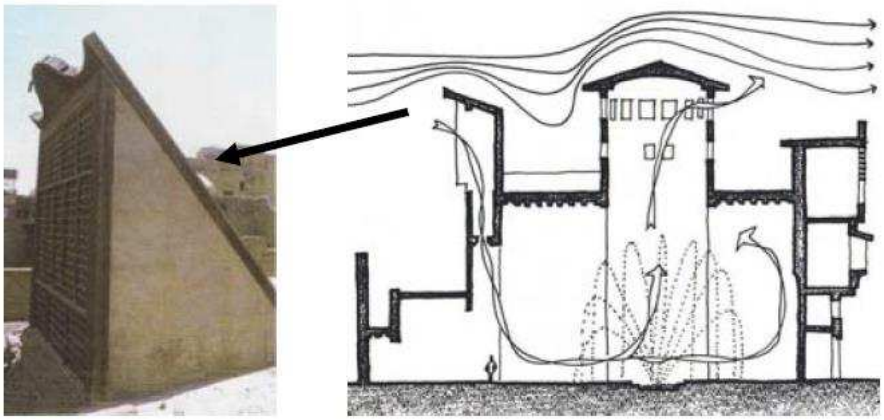

Figure 3.5 Example of wind scoop on Malqaf, a Cairane house, Egypt [28]

ii. Windcatcher towers

The windcatcher or cooling tower is used when there is no prevailing wind direction and differs from wind scoops in its shape and inner subdivisions. Cooling towers located on the roofs of buildings have several directional openings to capture wind movement above roof level from any direction and channel it to the room below for air ventilation through displacing stale air. Figure 3.6a and 3.6b show the process of air movement in the wind catcher and an illustration of a cooling tower in Qatar. The effectiveness of the cooling tower is highly dependent on the design of the building, the form of the building, the openings position and the wind-tower height.

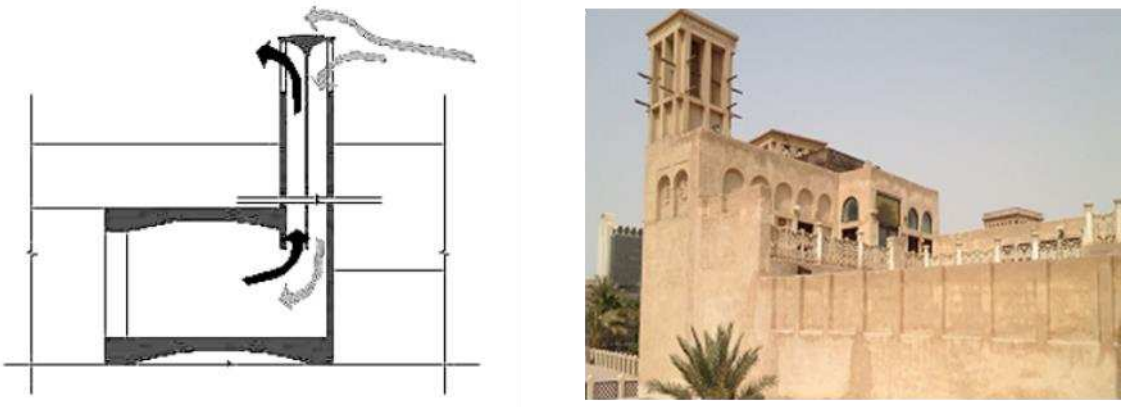

Figure 3.6 a) Air movement in the windcatcher [28] b) example of windcatcher, Qatar

Another technique that was used with cooling towers to reduce the inlet hot air below their ambient temperature is shown in Figure 3.7 [29]. The outside air penetrates the house through the access shaft after its temperature is being reducing by water evaporation available in the side `qanat,` as shown in Figure 3.7. After that, cold air pushes the warm air accumulated in the house through the cooling tower

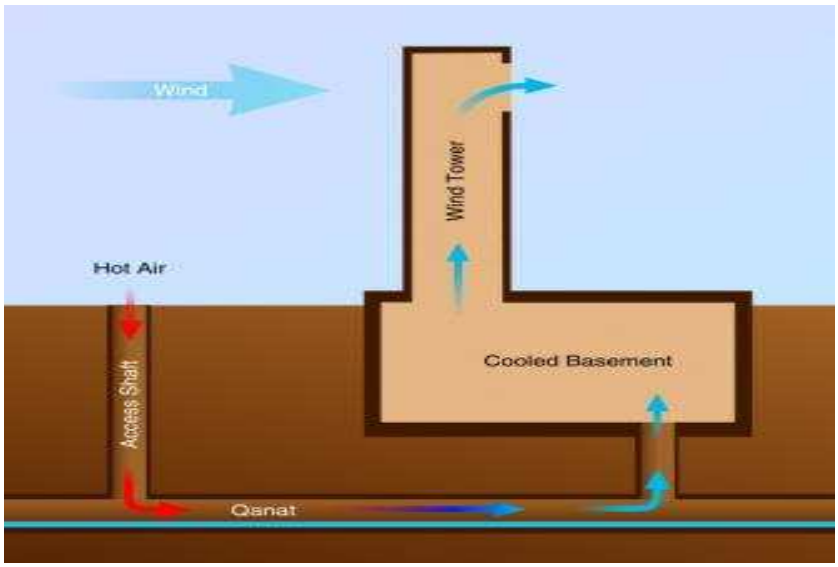

Figure 3.7 Diagram of building cooled by 'qanat' and wind tower [29]

3.1.5 Direct evaporative cooling (DEC)

The use of evaporative cooling for thermal comfort in buildings is not new, and several techniques were applied in building architecture for providing cooling and comfortable indoor conditions. The earliest use of evaporative cooling was in ancient Egypt and during the Roman Empire; the common people hung wet mats (cooling pads) over their doors and windows to cool the indoor air when wind blew through the mats [6-8].

Evaporative cooling with porous clay jars to cool air and water supply for home was found in the dry and harsh climate in Middle East countries. For example, this strategy applied in Egypt when large jars (maziara) were installed in windows as shown in Figure 3.8. When the water filled the maziara, the dry warm outside air flowing around it, sensible heat is transferred from the air into the jars' wet surfaces, causing water to evaporate. Hence the inlet air temperature and water temporary inside the maziara decreases.

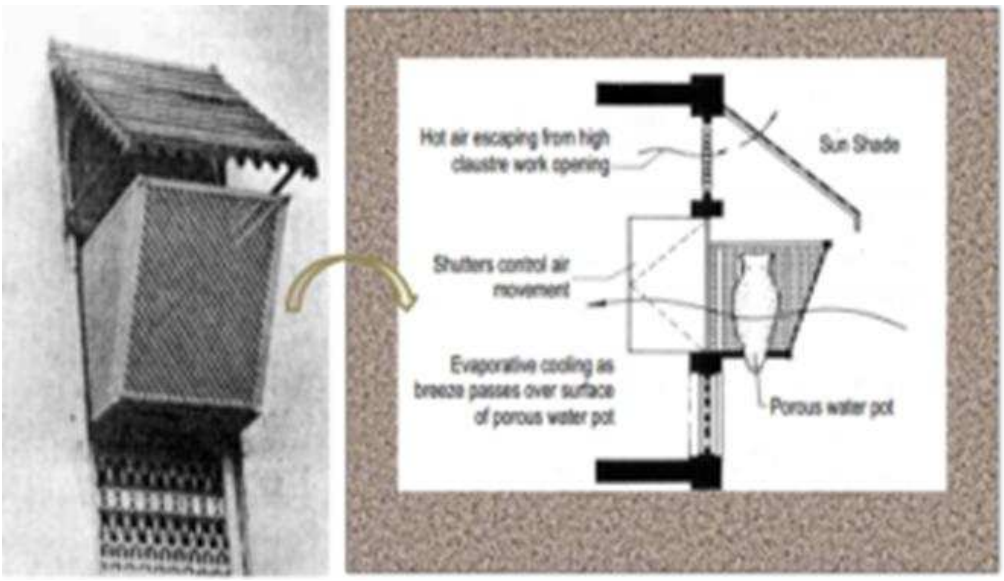

Figure 3.8 Musctese evaporative cooling window system [30]

3.2 Current Evaporative Cooling Technology

Evaporative cooling technology can be divided into two forms: direct evaporative cooling systems and indirect evaporative systems. In direct evaporative cooling systems, warm air is drawn through a wetted media. Figure 3.9 shows an example of current market direct evaporative cooler using fibre pad type as wet media.

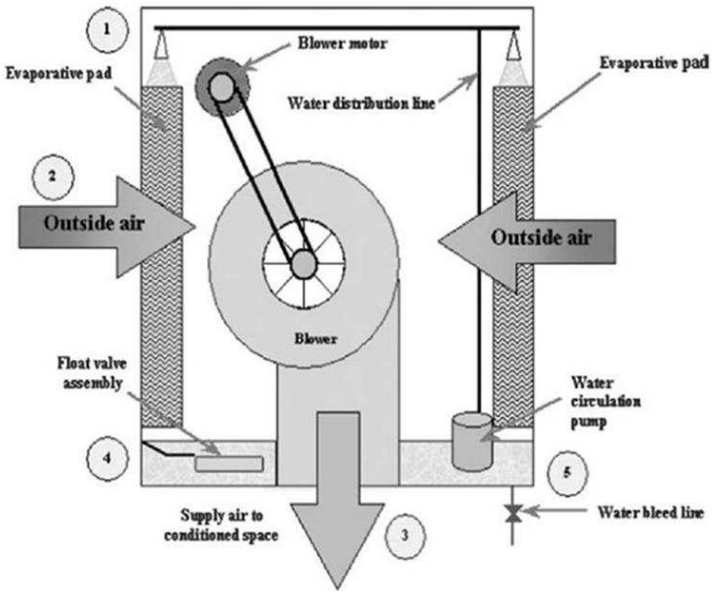

Figure 3.9 Direct evaporative cooling system (fibre pad type) [31]

Direct evaporative coolers are more effective in hot and dry climatic conditions and require venting through open windows or relief dampers, and water quality has a major impact upon the system performance and maintenance requirements [32-34]. The direct evaporative coolers' effectiveness could be as high as 70–95%. However, the drawbacks are potential mould growth due to increased supply of air relative to humidity, cooling temperature limited to air wet bulb and high humidity of intake air, which can lower the efficiency of the cooler.

Direct evaporative cooling technology is still widely practiced in hot and arid areas such as the Middle East, the South western part of the United States and the Indian subcontinent [35]. For example, 4 million evaporative air conditioning units in operation in the United States provide an estimated annual energy savings equivalent to 12 million barrels of oil and an annual reduction of 5.4 billion pounds of CO_2 emissions. They also avoid the need for 24 million pounds of refrigerant traditionally used in residential vapour air conditioning systems [36]. On the other hand, in Saudi Arabia there are over 48,000 rooftop-mounted evaporative air conditioning units

installed for air space for the purpose of building pilgrims' accommodation as shown in Figure 3.10. This will be the subject of a case study later on in this thesis.

Figure 3.10 Rooftop-mounted evaporative cooler for cooling in pilgrims' accommodations

3.3 Thermal Performance of DEC

Evaporative cooling is based on thermodynamics of the evaporation of water, which is a method of converting sensible heat into latent heat. The amount of absorbed heat from air that flows over a water surface depends on the evaporation rate. However, the vaporisation of one kilogram of water at 35^{o}C would require 2257 kJ of heat energy [37]. A schematic of a typical direct evaporative cooling process is shown on the psychometric chart of Figure 3.11. These systems are often known as "swamp coolers" where a fan is used to draw in outside air through a wet pad media and to circulate the cool air throughout the building.

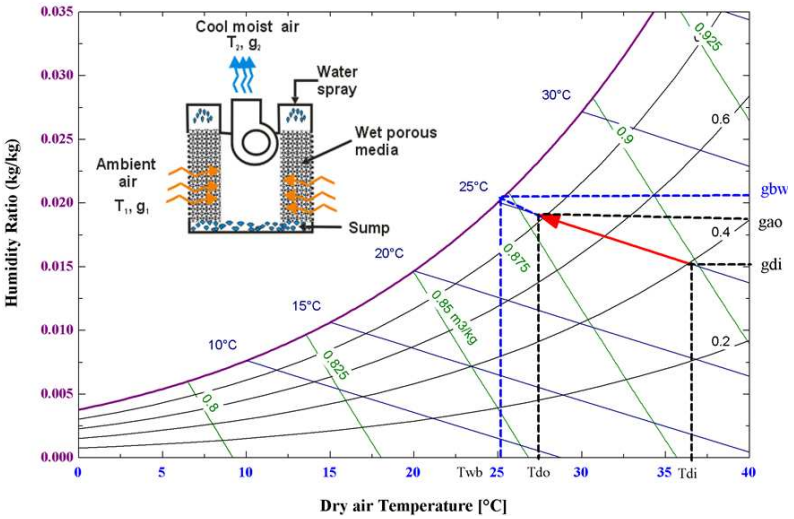

Figure 3.11 Direct evaporative cooling and air states on psychometric chart

The energy required to evaporate water in a direct evaporative cooler is supplied by the sensible heat content of the air to be cooled, hence lowering its temperature, albeit at the expense of increasing its moisture content. The heat and mass transfer between the warm dry air and water surface is an adiabatic process and can be expressed as follows [21] [38].

$$c_{pd}(T_{di} - T_{do}) + c_v g_1 (T_{di} - T_{do}) = (g_{ao} - g_{di})[(T_{do} - T_w) + h_{fg})] \quad (3.1)$$

where c_{pd}, T_{di} and T_{do} are dry air-specific heat, inlet and outlet temperature respectively; c_v g_{di} , g_{ao}, T_w and h_{fg} are the water vapour-specific heat, inlet moisture content, outlet moisture content, water temperature and water latent heat of evaporation respectively.

i) Cooling capacity

The cooling capacity of the evaporative cooler per unit area of the available wet surface can be calculated from the following:

$$q = m_s c_{pd} (T_{di} - T_{do}) \quad (3.2)$$

Where q is the specific cooling capacity (W/m^2), m_s is the supply air mass flow rate kg/s, C_{pd} is the specific heat capacity of the supply air, T_{di} is the inlet air temperature of the dry channel air flow and T_{do} is the outlet air temperature of the dry channel air flow.

ii) Coefficient of performance (COP)

The coefficient of performance is a common used term that refers to the efficiency of a thermodynamic cooling cycle or heat pump cycle and is defined as the ratio of the heat absorbed from the ambient to the total work input. The COP values are always positive and usually greater than one and can be calculated from the following:

$$COP = \frac{Qc}{P} \quad (3.3)$$

Where Q_c is cooling capacity and P is power consumption by driving fan motor.

iii) Wet bulb evocativeness

The wet bulb effectiveness is the ratio of the difference between intake and outlet air temperature to the difference between intake air temperature and its wet bulb temperature [39]. The mathematic expressions of the wet bulb effectiveness defined as follows

$$\varepsilon_{wb} = \frac{(Tdb,in - Tdb,out)}{(Tdb,in - Twb,in)} \quad (3.4)$$

vi) Water consumption

It is well established that the rate of evaporative cooling depends greatly on the air flow velocity; air temperature; and relative humidity, solar radiation and the properties of the evaporative materials and exposed surface area [40] [41]. From the following equation, the water evaporation rate can be calculated:

$$m_w = m_a (g_{ai} - g_{ao}) \quad (3.5)$$

Where m_w is water consumption, m_a is air mass flow rate; g_{ai} and g_{ao} are the inlet and outlet water content of the air flow respectively.

3.5 Modern Air Conditioning Technologies

Air conditioning system works by transferring heat between the inside and the outside of the building depending on whether heating or cooling is required. The modern air conditioning systems rely on a refrigeration cycle to perform the cooling and/or heating processes in a building. Clito F and Afonso [42] classified the refrigeration system into three main categories according to the final energy used to operate them: electrical systems, thermal system and hybrid systems, as shown in Figure 3.12.

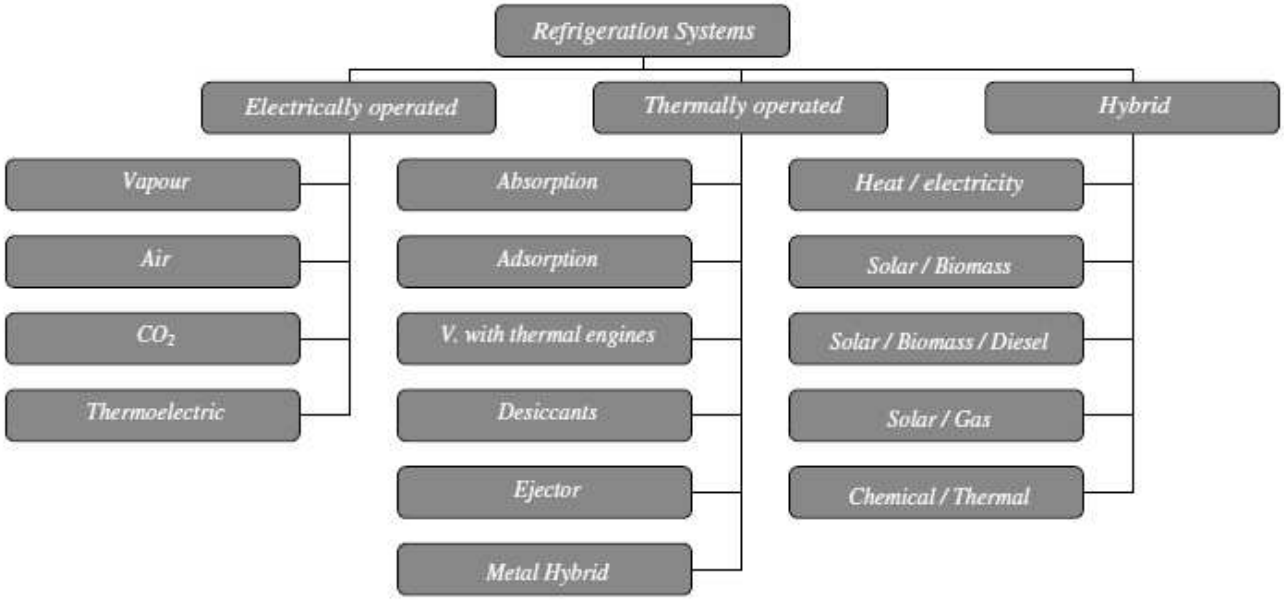

Figure 3.12 Classification systems according to the final energy used to operate them [42]

From Figure 3.12, it can be seen that each category contains several refrigeration systems. The driving force for operation refrigeration systems in the first category is electricity, as these systems operate on high-grade energy. The refrigeration systems in the second category operate on thermal energy, which can be supplied from low-grade heat sources. Finally, the third category which is an integration of more than one technology into a hybrid system uses several energy sources with one being a usually renewable source. Table 3-1 shows the typical values of coefficient of performance (COP) of different refrigeration systems presented in Figure 3.12. The vapour compression systems is the conventionally used method for refrigeration and air condition applications around the world [43] gives a higher COP value compared to others refrigeration systems. However, other cooling systems such as absorption and desiccant systems shown in the second category are receiving increasing interest from both the commercial market and research due to low CO_2 emissions compared to a vapour compression system [42]. The maximum COP values of absorption and

desiccant systems are often in the range of 1.3 and 1.5 respectively, as shown in Table 3-1.

Table 3-1 The typical values of (COP) of different refrigeration systems [42]

Refrigeration cycle	Vapour-compression	Absorption	Adsorption	Thermoelectric	Desiccant	Ejector	Hybrid
COP	0.3-5	0.6-1.3	0.2-0.8	0.5-1	0.5-1.5	0.25-0.8	0.5-3.5

3.5.1 Vapour compression cycle

Vapour compression cycle composed of four basic main components; the compressor, condenser, receiver expansion valve and evaporator, as shown in Figure 3.13. The refrigerant is compressed in compressor and then moves out as a high-pressure gas to the condenser. Here, the gas condenses into a liquid and gives off its heat to the outside air, and then the liquid moves to the expansion valve under high pressure. This valve restricts the flow of the fluid and lowers its pressure. After that, the low-pressure liquid moves to the evaporator, where heat from the inside air is absorbed and changes it from a liquid to a gas. Finally, the refrigerant moves to the compressor where the entire cycle is repeated.

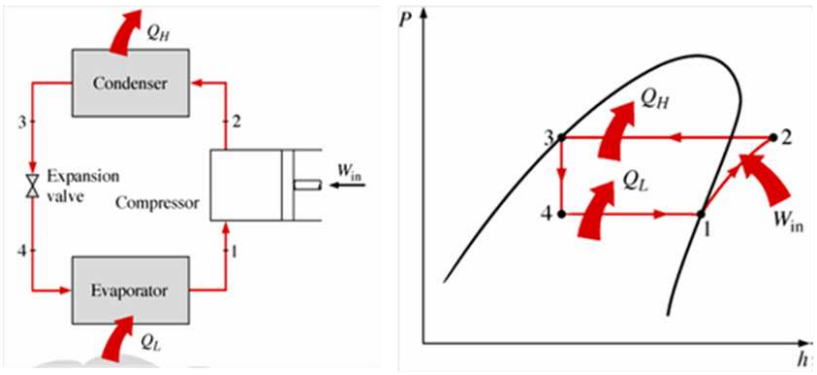

Figure 3.13 Vapour-compression refrigeration cycle [44]

Although the conventional vapour-compression refrigeration is suitable for hot arid or humid conditions, availability in various sizes and cooling capacities and the coefficient of performance is quite high. In addition, it has considerable disadvantages, such as a high specific power consumption, high CO_2 emission, high initial cost and use of chlorofluorocarbons (CFCs) as working fluids, which have harmful effects on the environment and contribute to the greenhouse effect that results in global warming and an increase in the ambient temperature.

Vapour-compression cycle is widely applied in buildings around the world, especially in hot-climate countries. For example, according to Proctor Engineering Group [45], the number of residential window air conditioners in Saudi Arabia is in excess of 10 million units with a replacement rate of over 1 million units per year. Figure 3.14 shows an example of window air conditioners installed in residential building in Saudi Arabia [46]

Figure 3.14 Air conditioning installed in residential building, Saudi Arabia [46]

3.5.2 Vapour Absorption Refrigeration

The vapour absorption system is driven by heat, and unlike the vapour compression system, it differs from vapour compression cycle in how the compression of refrigerant is carried out. Vapour absorption cycle consists of a heat-operated absorber-generator instead of a compressor in vapour absorption cycle, while having in common the other three components: the evaporator, the condenser and the expansion valve. Absorption cooling systems are classified into single effect, double effect and triple effect systems based on the number of times the heat is utilized within the absorption system. Figure 3.15 shows a schematic of a single-effect absorption refrigeration cycle. Vapour absorption cycle uses two working fluids; a refrigerant and a solution. Lithium bromide vapour is generated by the heat supplied to the generator. The water vapour is removed from the solution so that concentrated lithium bromide vapour is condensed in the condenser. The low temperature solution is returned to the evaporator. Heat is absorbed by the lot temperature refrigerant in the evaporator, which is turned into a saturated vapour. Low pressure vapour is absorbed by the weak solution and is sprayed into the absorber.

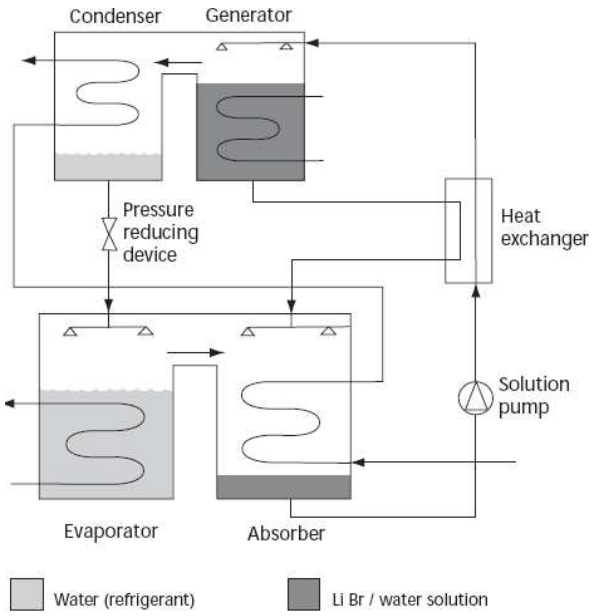

Figure 3.15 Single-effect absorption refrigeration [47]

3.5.3 Desiccants

Desiccant cooling systems are employed mainly to provide thermal comfort and good air conditioning in buildings through air humidity control and sensible cooling as alternative technology to vapour compression systems[48]. Desiccant cooling systems can be divided into solid desiccant system and liquid desiccant system. The differences between solid and liquid desiccant systems are in the equipment design when the principle work of both systems is similar [42]. For example, a solid desiccant system employs a rotary wheel with an integrated desiccant material allowing latent load removal through adsorption as shown in Figure 3.16. The liquid descant system uses a dehumidifier to dehumidify the air by storing liquid desiccant and a regenerator to regenerate the weak desiccant solution employing a heat input as shown in Figure 3.17. Although the liquid desiccant-based systems have higher operation flexibility and mobility, lower temperatures for regeneration and lower pressure drop on the airside. The system is still in the research and development phase with very few

products finding their way to the commercial market compared to solid desiccant system [48].

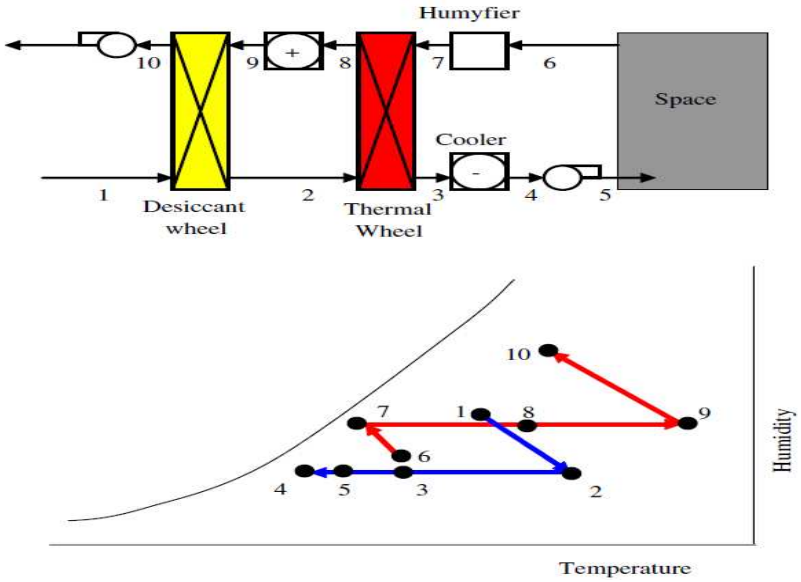

Figure 3.16 Solid desiccant [42]

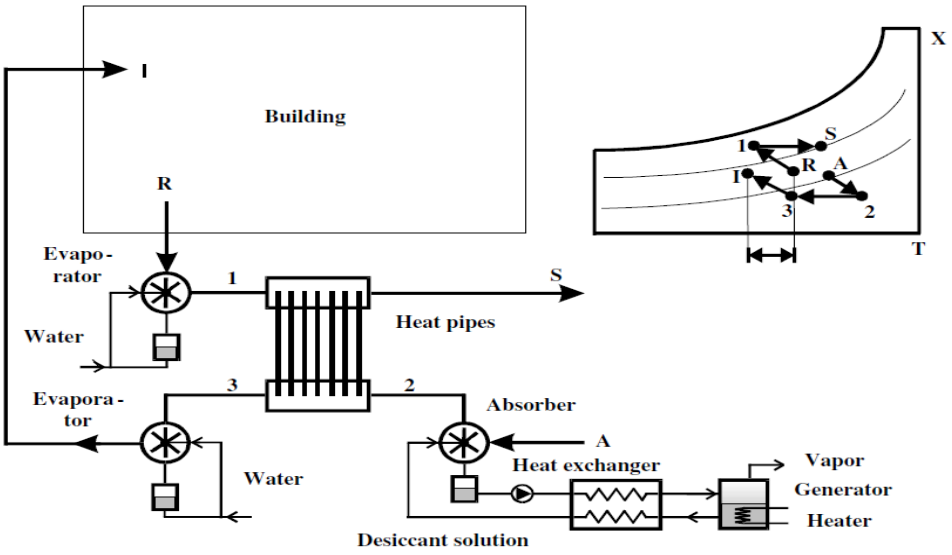

Figure 3.17 Liquid desiccant system [42]

3.6 Conclusion

Different traditional cooling systems used in hot, dry and humid Middle East countries were presented. Then, the examples of integration of cooling tower and evaporative cooling units in modern architectures were illustrated. On the other hand, the different types of modern air conditioning (refrigeration cycle) were introduced and advantages and disadvantage of the refrigeration cycle were addressed. From the above review, one can conclude that:

- The environmental benefits of evaporative cooling technology are impressive when compared to vapour compression in terms of low electrical power consumption, low noise from components and reduced CO_2 emission.

- Evaporative coolers also provide excellent ventilation as they use 100% fresh air from outside and could achieve up to 75% energy savings compared to all types of refrigeration cycles.

- Evaporative cooling technology for air conditioning is suitable for numerous applications such as buildings, urban environments, greenhouses and farms.

- The most important investment costs of evaporative cooling systems are simple. The energy efficiency increases with higher outdoor temperature, low capital and maintenance costs, compared to modern air conditioning systems.

Chapter 4

Indirect evaporative cooling technologies and the wet media materials

4.1 Introduction

The main proposal of this thesis is the development of an indirect evaporative cooler to supply air at sub-wet bulb temperature by using the porous ceramic materials as wet media for buildings in hot and dry climate. An indirect evaporative cooling system has the advantage of low energy consumption, being environmentally benign, and having low capital and maintenance costs compared to current vapour compression systems. According to Duan el at.[49], indirect evaporative cooling systems have the potential to be a viable alternative to conventional mechanical vapour compression refrigeration systems for air conditioning duties in buildings. Many research works have studied the heat and mass transfer, as well as the performance and optimisation geometries of indirect evaporative systems. Therefore, research, development and mathematical modelling algorithms of thermal performance of indirect evaporative cooling technology were investigated and reviewed. Furthermore, evaporative materials were investigated, particularly porous ceramics and heat pipes.

4.2 Principle of Indirect Evaporative Cooling (IEC)

Unlike direct evaporative cooling, in an indirect evaporative cooler the supply air is cooled without increasing its water content. This is accomplished by arranging the supply dry air and wet air in separate channels, as shown in Figure 4.1. The supply air is circulated in the dry channel and the wet airflow in the wet channel where evaporation takes place. A temperature difference necessary for sensible heat transfer between the two airflows is established by direct evaporation of water in the wet channel. The cool air in the dry channel is then supplied without increasing its moisture content; however, the lowest temperature that can be achieved.

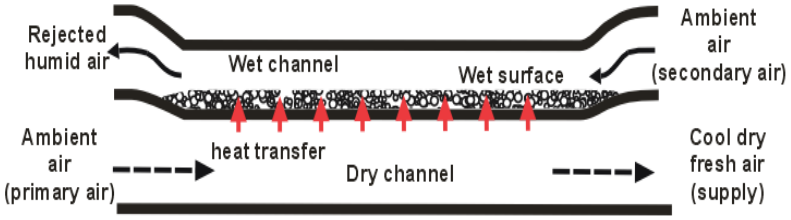

Figure 4.1 Simple schematic of an indirect evaporative cooling system

Figure 4.2 is a representation of the air states on a psychometric chart, where line (1-2) represents the evaporative cooling process on the psychometric chart. This line follows approximately the line of the moisture content of the air which remains constant between state 1 and state 2, whereas dry air temperature decreases from T_1 to T_2, without increasing its water content g_1 and g_2.

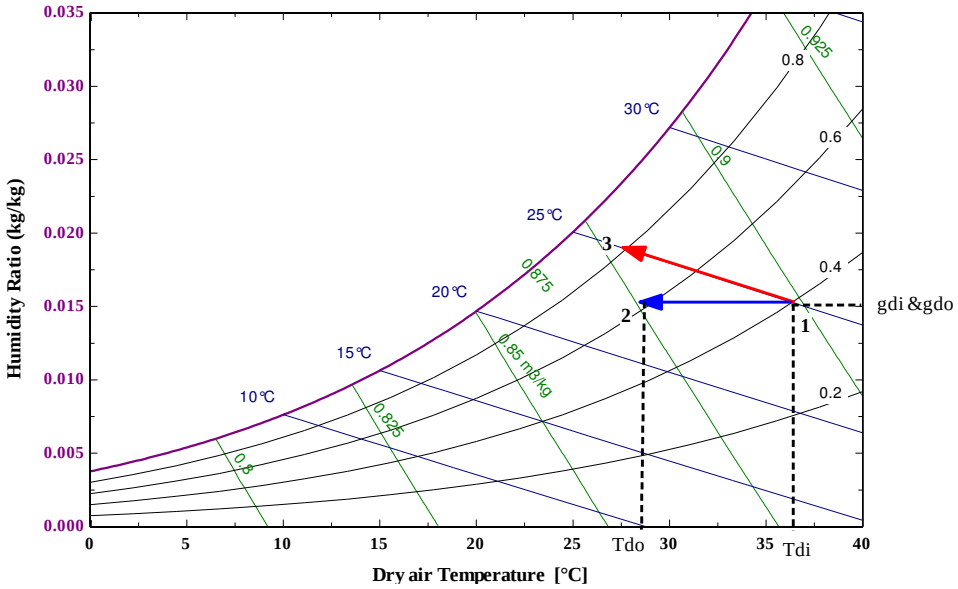

Figure 4.2 Psychometric representation of air states in an indirect evaporative cooling system

The thermal performance of an IEC is evaluated in the same way as the direct evaporative cooling in that the effectiveness of the system is given by its wet-bulb temperature effectiveness from Equation (3.4).

The effectiveness of IEC is lower than that of direct evaporative cooler and even in a well-designed indirect evaporative cooler, the supply air could be cooled to within 2 to 3^{o}C of the wet bulb temperature. This constitutes a severe thermodynamic limitation. According to ASHRAE, the effectiveness of indirect evaporative cooler may range from 40% to 80% [50]. This limitation of evaporative cooling processes has led several researchers to develop and modify the thermal process of indirect evaporative cooling system to achieving sub-wet bulb temperature, which is described later.

4.2.1 Application of Indirect Evaporative Cooling (IEC)

Heidarinejed G.[51] classified indirect evaporative cooling into two types based on heat and mass transfer occurring in the heat exchangers. The first type is dry surface indirect evaporative cooling, and the second type is wet surface evaporative cooling.

As shown in Figure 4.3a, in the first type the secondary air is cooled using direct evaporative cooling before entering the indirect heat exchanger. Then, this evaporatively cooled the secondary air through a conventional air-to-air heat exchanger. Whereas in the second type (Figure 4.3b), a wet surface heat exchanger is used where a non-adiabatic evaporation takes place. In this method, two streams of air are used; namely alternative wet and dry passages, which are separated from each other. Primary air is cooled in dry passages, which are separated from wet passages where secondary air and water flow.

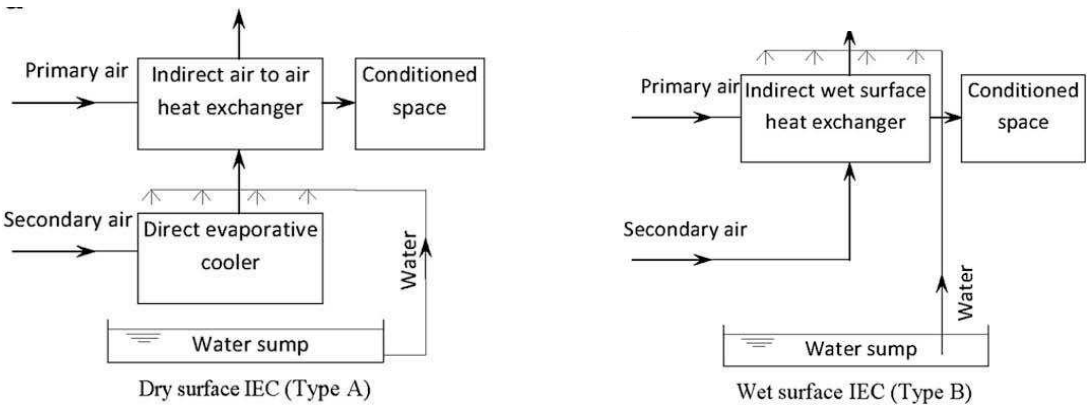

(a) (b)

Figure 4.3 Schematic diagram of IEC: (a) dry surface heat exchanger (b) wet surface heat exchanger [51]

Further work was carried out by El-Dessouky et al. [52] by evaluating the performance of an experimental unit of indirect evaporative cooling system followed by a direct evaporative system for indoor air conditioning in the hot and humid environment of Kuwait. The results of this experiment showed that the range of the efficiency for an indirect evaporative cooling system followed by a direct evaporative cooling system is 90–120%. The range of the efficiency for indirect evaporative cooling system is 20–40%. The range of the efficiency direct evaporative cooling system is 63–93%. Steeman et al. [53] used an Air Handled Unit (AHU) containing indirect evaporative cooling system (IEC) to measure the IEC- effectiveness and interaction between the

moisture balance and thermal comfort in buildings. The results found that the effectiveness of IEC is independent of the inlet conditions of the outdoor and return air, while increasing indoor moisture production and lowering the ventilation rate decreases the thermal comfort. Similarly, Kim et al. studied the heat exchange effectiveness of a dry coil indirect evaporation cooler under various operating conditions in hot and humid climate zones. For this study a pilot unit of Dry Coil IEC was built and a highly controlled lab environment was used to test the effectiveness. The test results showed that 20–60% effectiveness can be achieved even in hot and humid climates by using the dry coil IEC proposed.

In other applications, an evaporative cooling system can be used to pre-cool fresh air for air conditioned space for reduction in cooling capacity and seasonal energy savings, especially in hot climate countries. Maheshwari et al. [54] developed a methodology for energy saving potential of an Indirect Evaporative Cooling system to pre-cool fresh air to reduce cooling capacity of the conventional air conditioning equipment. This consists of using an IEC, which is made of vertical channels through which outdoor air flows with alternative channels providing humidification and sensible cooling of air, as shown in Figure 4.4. The wet channels, made of a highly water-absorbent coating, were continuously sprayed with water, hence humidifying outdoor air bringing down the surface temperature close to the wet bulb temperature. The air supplied to the building flows through alternate dry channels is cooled without addition of moisture. The humid air in the wet channels is exhausted to the atmosphere. The authors show that the indirect evaporative cooler when used in dry regions away from the coastal area reduced energy consumption of a conventional air conditioning system by nearly 30% and peak power demand by 40%, achieving nearly

100% more saving of electricity compared with the same system used in the coastal area.

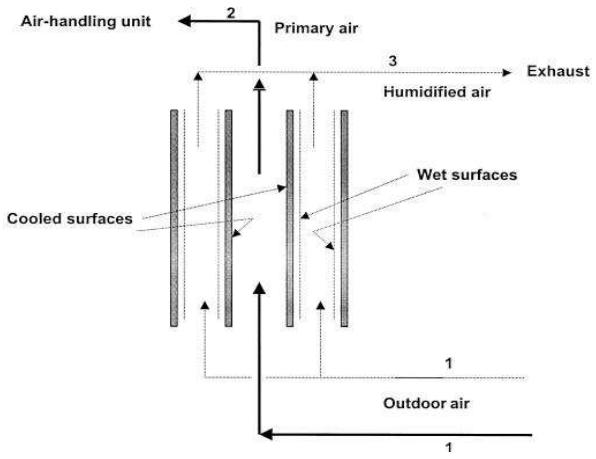

Figure 4.4 Configuration of indirect evaporative cooler for pre-cooling in A/C system

Delfani et al. [55] evaluated the performances of an indirect evaporative cooler as a pre-cooling unit for mechanical cooling systems in Iran. The results showed that about 75% of cooling load can be provided when using an evaporative cooling system before mechanical cooling systems. Furthermore, about 55% savings in electrical energy consumption can be obtained.

4.3 Sub-Wet bulb Evaporative Cooling Systems

Recent research efforts have been focused on improving the cooling process of indirect evaporative cooling system to achieve air temperatures below the ambient air wet bulb temperature. This is usually referred to as dew point or Sub-wet bulb temperature evaporative cooling [6]. A sub-wet bulb temperature evaporative cooler arrangement consists of a dry and wet channel; however, to achieve sub-wet bulb temperature, part of the cool air in the dry channel is redirected to accomplish the

evaporation process in the wet channel, as shown in Figure 4.5. The advantage of this arrangement is that the moisture content of the supply air remains unchanged.

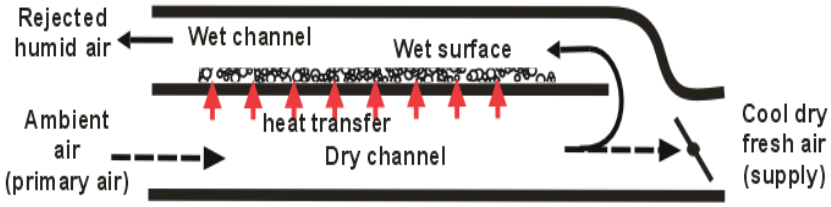

Figure 4.5 Simple schematic of sub-wet bulb temperature evaporative cooling

Dry and wet channels of configuration shown in Figure 4.5 were separated by panels to form narrow ducts with air flowing. In the dry channel side, a thin non-permeable membrane was used to seal the panel surface, while on the wet channel side the air flow contacted directly with water. The direct evaporation of the water in the wet channel cools the panel and the bulk of its water content, which in turn creates a temperature gradient with the air in the dry channel. This allows primary air in the dry channel to be cooled by transferring its heat to the panel through the thin water-proof membrane without increasing its moisture content. On the other hand, the evaporation of water in the wet channel carries away the heat-added panels from the dry channel airflow and is ultimately rejected as a saturated state (humid air). By redirecting part of the airflow at the outlet of the dry channel to the wet channel, sub-wet bulb temperature conditions are made possible.

Figure 4.6 shows the air states in the sub-wet bulb temperature evaporative cooler on a psychometric chart. Line (1-2) in Figure 4.6 represents the evaporative cooling process on the psychometric chart of dry channel. This line follows approximately the line of the moisture content of the air, which remains constant like the indirect evaporative

cooler, but the supply air (T_{d2}) will be cooled below their wet bulb temperature without increasing its water content ($g_1 = g_2$).

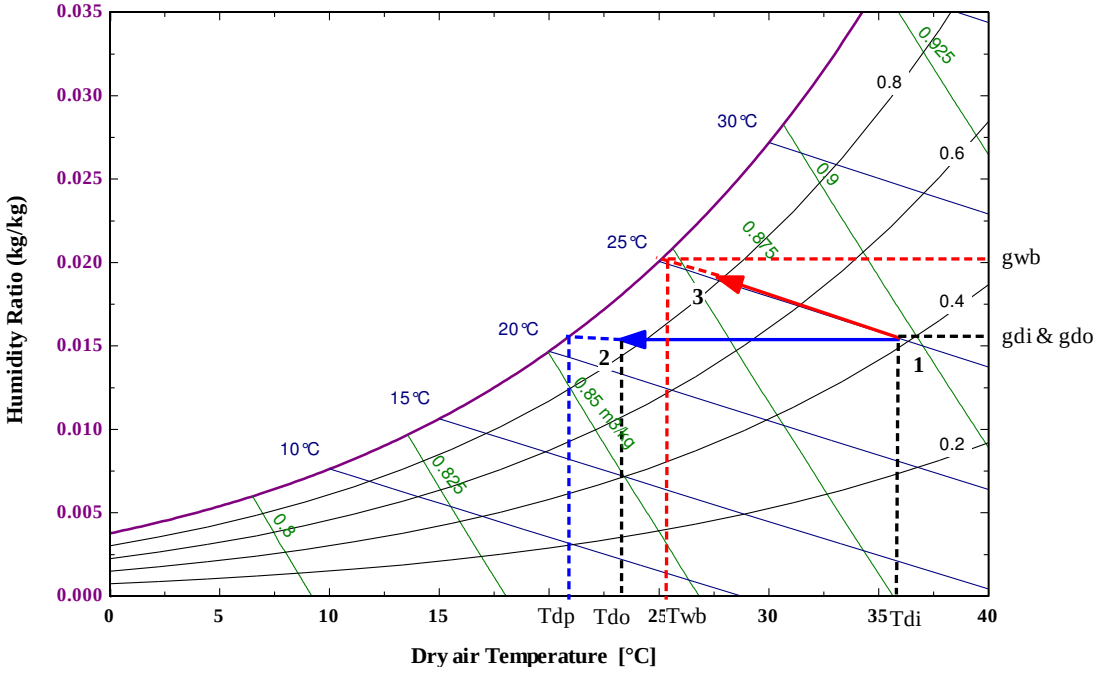

Figure 4.6 Psychometric chart of sub-wet operative cooling

The dew point effectiveness is the ratio of the difference between intake air temperature to the difference between intake air temperature and its dew point temperature [39]. The mathematic expressions of the dew point effectiveness are defined as follows.

$$\varepsilon_{db} = \frac{(Tdb,in - Tdb,out)}{(Tdb,in - Tdp)} \tag{4.1}$$

4.3.2 Review of previous research and developed work of sub-wet bulb temperature indirect evaporative cooling system

4.3.2.1 Theoretical studied of sub-wet bulb temperature

S. Tzer Hasu et al. [56] analysed wet-surface heat exchangers in order to determine the configuration that optimizes the performance. The objective of this work is to cool a stream of air to a lower-than-the inlet wet-bulb temperature by the evaporation of water. Three types of wet-surface heat exchangers were investigated: unidirectional flow, counter flow and two closed-loop flow configurations with extraction. Analysed results found that the inlet dew point temperature can be approached with moderate flow rates and simple geometries.

Hasan [57, 58] presented a thorough computer modelling of four combinations of product and working air. For instance, he considered two-stage counter flow and parallel flow, single stage regenerative and a mixture of parallel flow for first stage and regenerative flow for second-stage arrangements. The specification of the indirect evaporative cooler used in his computer model are summarised in Table 4-1.

Table 4-1 Indirect evaporative cooler speciation

Height of the dry& wet passages (y_1=y_2)	0.0035m	Total working air	0.00098 kg/s
Passage length & width (L=Z)	0.5m	Total product air	0.00042 kg/s
Water film thickness	1mm	Inlet dry bulb temperature	30c
Wall thickness	0.5mm	T_{wb}	18.8c
Dry side (d)	0.0015m	T_{db}	12.5c
Total inlet air	0.0014 kg/s	Relative humidity	34%

He concluded that the combined regenerative parallel flow arrangement yields the lowest product air temperature possible as it makes good use of the high cooling effectiveness of the parallel stage at the beginning and that of the regenerative at the final part of the cooling process, as shown in Figure 4.7.

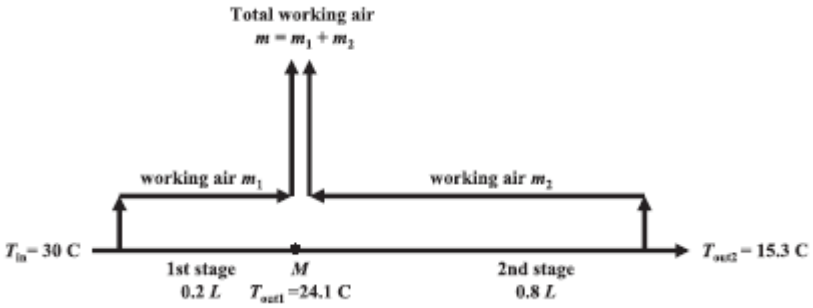

Figure 4.7 Combined parallel-regenerative flow arrangement

The product and working air properties presented on a psychometric chart is given in Figure 4.8 where it can be seen that sub-wet bulb temperature could be achieved. He also computed the wet bulb and dew point effectiveness of this arrangement to be 1.31 and 0.84 respectively.

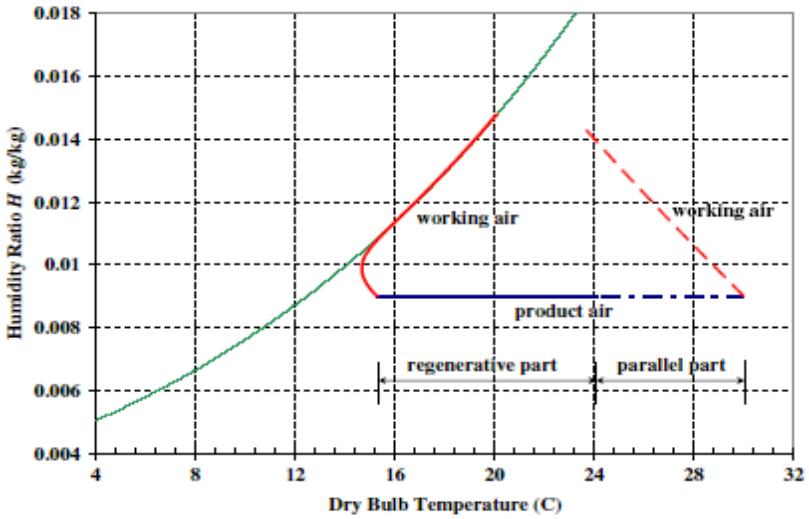

Figure 4.8 Product air and working air condition in the psychometric chart for combined parallel-regenerative flow

An experimental study of a novel dew point evaporative cooling system carried out by Riangvilaikul and Kumar [59, 60] to investigate the outlet air conditioning and the system effectiveness at different inlet air conditions; temperature, humidity and velocity. The results showed that the wet bulb effectiveness ranged between 92 and

114% whereas the dew point effectiveness ranged between 58 and 84%. The velocity of intake air should be kept below 2.5 m/s when inlet air temperature more than 30^{o}C to obtain wet bulb effectiveness greater than 100%. Furthermore, the authors developed a computer model of a dew point evaporative cooling system to simulate the heat and mass transfer processes[59]. In their work, the length of air flow path within dew point evaporative cooling is divided into an identical differential control volume as shown in Figure 4.9 to analyse the heat and mass transfer mechanism. The results of this simulation are compared with experimental findings for various inlet air conditions. A good agreement between simulation values and experimental results is achieved within 5 and 10% discrepancies of the outlet air temperature and effectiveness, respectively.

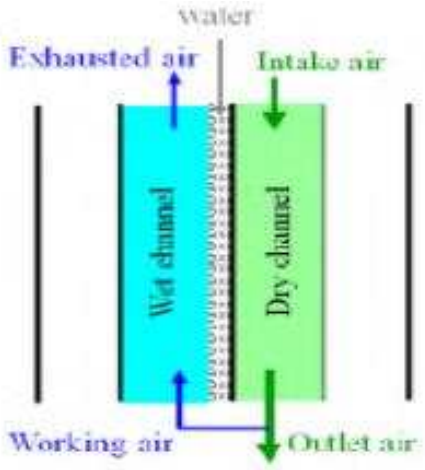

Figure 4.9 Schematic of dew point evaporative cooling (a) unit configuration (b) a differential volume

Anisimov and Pandelidis [61] studied theoretical energy analyses of the novel plate-fin heat exchanger based on M-cycle and used for indirect evaporative cooling in air conditioning system. The results found that the heat and mass transfer performance M-cycle cooler strongly depends on inlet parameter such as air temperature, relative

humidity and intake air velocity and also geometrical size of the channels, type of plate-fin surface, which is secondary to primary air mass flow ratio but depends less on the conductive conductance through the fin. Moreover, the dew point effectiveness increases with increasing relative humidity while the specific cooling capacity rate of the heat and mass exchanger became lower. Regarding these results, the authors indicated that wet bulb and dew point effectiveness is not an adequate indicator for indirect evaporative air cooler performance, and it's considered only an efficiency factor. Finally, the authors recommended for a future work a comprehensive analyses of the M-Cycle based on different air and water film flow arrangements.

Cui et al. [62] theoretically investigated the thermal performance of a counter-flow closed-loop flat-plate-stacked heat exchanger of a dew-point evaporative cooler under varying inlet conditions. The results showed that the wet bulb effectiveness spanned from 122% to 132% and dew-point effectiveness ranged from 81%–93%. Additionally, it was found that the effectiveness could be effectively increased by 10–20%, if the room return air was used as working air, and also when roughness of channels surface were applied with inlet air velocity higher than 1.5 m/s.

Rogdakis et al. [63] theoretically and experimentally evaluated the performance characteristics of an M-cycle-based IEC system at Greek climate condition. It was found that the Maisotsenko cycle can be applied for most Greek cities without intensive consuming of electricity and water, the effectiveness ranged between 97% and 115%, while water consumption was in the range of 2.5 kg_w/kWh and 3.0 kg_w/kWh.

X. Zhao et al. [64, 65] developed the counter-flow heat and mass exchanger for dew point evaporative cooling. The results of the numerical study found that cooling effectiveness and energy efficiency for dew point and wet bulb temperature are largely

dependent on the dimensions of the airflow passages, air velocity and working air to intake air ratio and are less dependent on the feed water temperature. Furthermore, the authors compared the performance of counter-flow heat and mass exchanger with M-cycle cross-flow heat exchangers[66] as shown in Figure 4.10. The results of a comparative study showed that the counter-flow arrangement achieved around 20% higher cooling capacity and 15–23% higher dew-point and wet-bulb effectiveness respectively under the same geometrical sizes and operational conditions. Contradictorily, the cross-flow exchanger has 10% higher performance which is due to an increase in power consumption of counter-flow heat exchanger.

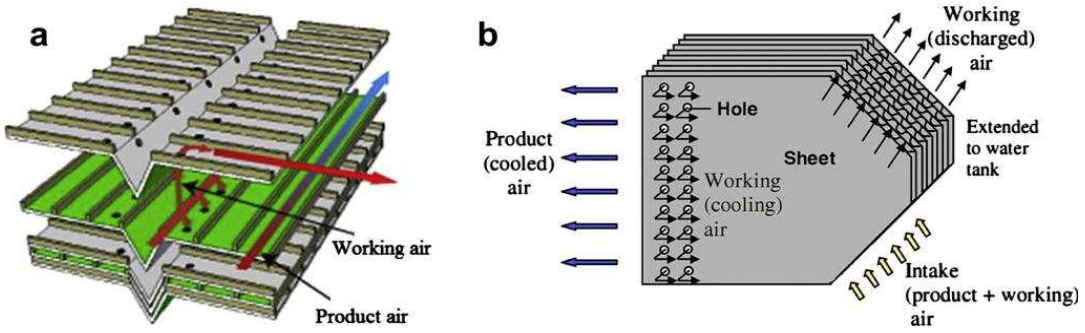

Figure 4.10 Schematic of the cross and counter flow heat exchanger for dew point cooling (a) cross-flow; (b) counter-flow

Xudong Zhao et al. [64, 65] investigated the feasibility of a novel dew point evaporative cooling for air conditioning of system for China building application. As a result of the work, dew point evaporative cooling system is suitable for most of regions of China, particularly where the climate is hot and dry during the summer season.

Z. Duan's [67] investigation of novel dew point indirect evaporative air conditioning system for building indicates that the dew point cooler can achieve a higher

performance of effectiveness and energy efficiency than the typical indirect evaporative coolers without adding too much cost.

4.3.2.2 Application of sub-wet bulb temperature

Maisotsenko [7] introduced the (M-cycle) which is a new design of the heat exchanger of IEC system to overcome some of the disadvantages of DEC systems and enhance the effectiveness of wet-bulb temperature IEC. The heat and mass transfer process of this heat exchanger are shown in Figure 4.11.

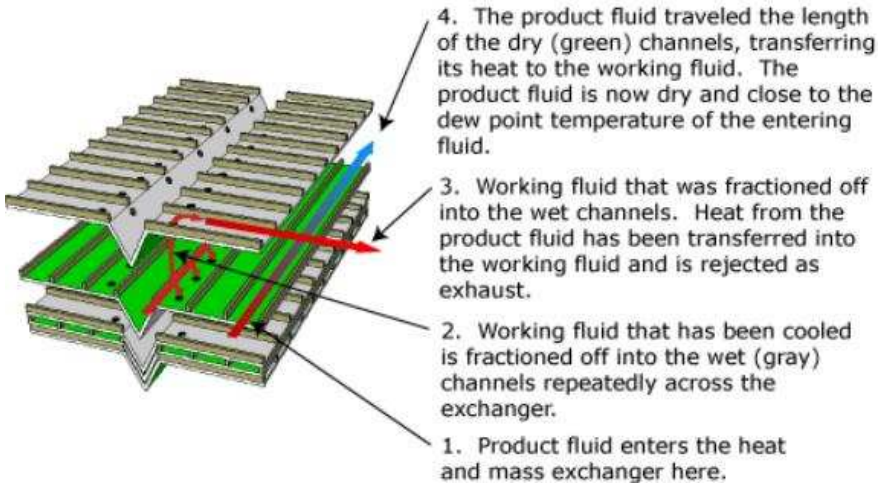

Figure 4.11 The heat and mass transfer process of heat exchanger, (M-cycle)

The performance of an early-2005 model Coolarado Cooler indirect evaporative cooling unit shown in Figure 4.12 was evaluated by Elberling (2006) [68]. The author indicated that, although theoretically the wet bulb effectiveness of this unit can be greater than 100%, the wet-bulb effectiveness over the test conditions ranged from 81% to 91% .

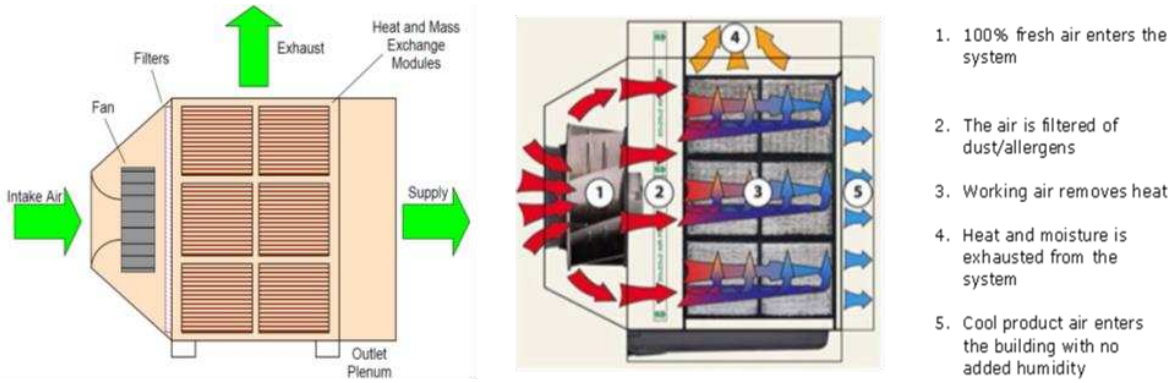

Figure 4.12 A cross section of Coolerado Cooler and heat and mass exchanger[68] [69]

Frank Bruno [39] evaluated the performance of counterblow dew point cooler installed in a residential building shown in Figure 4.13. The results of a performance characteristic of this cooler in regards to its outlet temperatures and electrical energy efficiency, as shown in Figures 4.14 and 4.15, show that the highest differential between inlet and outlet air temperature can be achieved in the midday when the air temperature is reduced from 40 to 15 ^{o}C as shown in Figure 4.14. While the average cooling capacity was 10.5 kW and the average of EER was 8.0 as given in Figure 4.15. The author also determines the energy saving when using the dew point evaporative cooler in buildings in comparison to a packaged unity refrigeration air conditioner. Table 4-2 shows the results of energy savings for each year from 2001 to 2005 and the annual energy saving associated with cooling the outside fresh air between 52 to 56%.

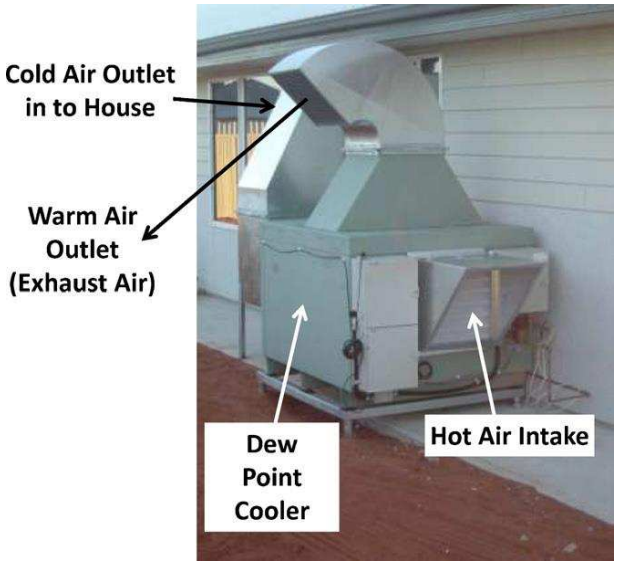

Figure 4.13 The dew point cooler installation in residential building

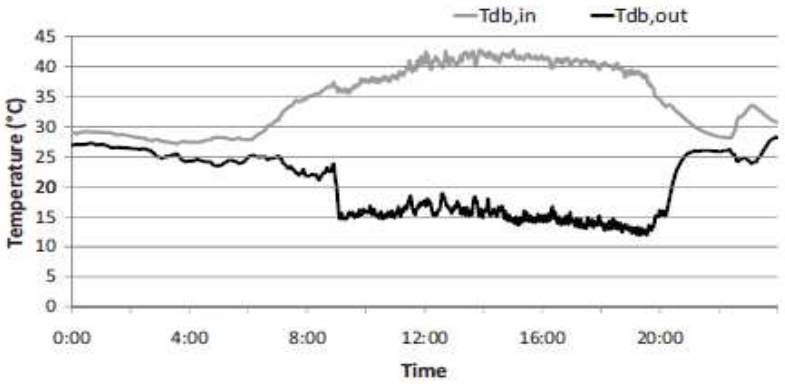

Figure 4.14 Inlet and outlet dry bulb air temperatures on a hot day (for residential building)

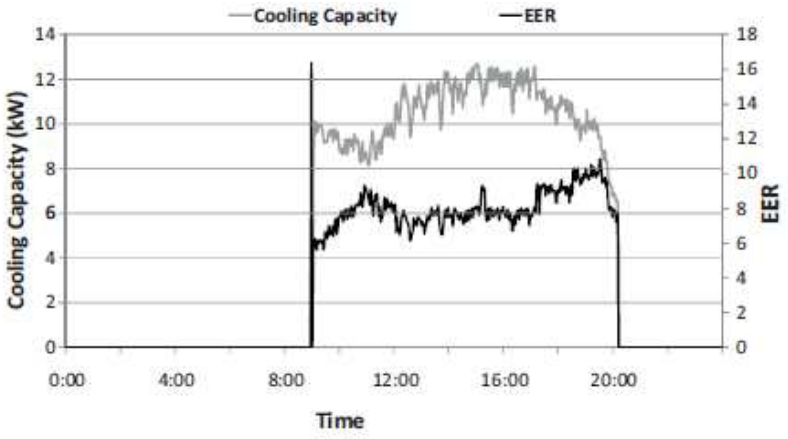

Figure 4.15 Cooler cooling capacity and EER (for residential building)

Table 4-2 Energy saving when using the dew point cooler to cool outdoor air for ventilation

Year	Total hours fresh air to be cooled (h)	Cooling produced by dew point cooler (kW h)	Average EER of dew point cooler	Energy used by dew point cooler (kW h)	Average EER of packaged unit air conditioner	Energy used by packaged unit air conditioner (kW h)	Energy saving (%)
2001	427	5706	7.7	738	3.4	1673	56
2002	413	5392	7.6	714	3.6	1533	53
2003	524	6562	7.2	907	3.5	1882	52
2004	516	6981	7.8	893	3.5	1996	55
2005	468	6229	7.7	809	3.5	1784	55

4.4 Porous materials used in evaporative cooling systems

The wet media used in evaporative coolers is an essential component of an evaporative cooler. It is usually made of a porous material with a large microscopic surface area and capacity to hold liquid water. The selection of the wet media materials would depend on the application, effectiveness, availability, cost, safety, and environment factors [70].

Numerous research works were published on investigation of wet media materials using in evaporative cooling technology. For example, Fouda and Melikyan [71] used synthetic wet pad as evaporative materials on an indirect evaporative cooler. The use of wet special durable paper and GIASdek as pad material was studied by Wu et al. [72, 73] . Velasco et al. [74] and Naticchia et al. [75] used hollow bricks in their research. Dai [76] study a cross-flow direct evaporative cooler using honeycomb paper as packing material.

Zhao [77] investigated several types of materials including metals, fibres, ceramics, zeolite and carbon for their potential to be used as heat and mass transfer medium in the evaporative cooling systems. Table 4-3 presents the thermal characteristics of the selected fibres.

Table 4-3Thermal characteristics of selected fibres

Fibres	Thermal conductivity (W/m K)	Porosity (%)
Wood fibres	0.012–0.654	54.7–63.6 (very high water penetrability)
Latex with cement	0.28–0.52	1.10–2.32 (±0.02)
Methylcellulose with cement	0.32–0.42	2.07–2.12 (±0.02)
Silica fume	0.33–0.36	2.97–3.14 (±0.02)
Methylcellulose + fibre + cement	0.28–0.44	3.33–3.97 (±0.02)
Silica fume + methylcellulose	0.28–0.36	3.14–4.36 (±0.02)
Natural random fibrous materials (porosity = 10–58%)	0.02–0.13	Porosity = 10–58%
Cotton fibre (Sisal, Ramie and Jute)	0.176–0.351	40
Glass fibre	0.277	2.05–2.3 (±0.02)

4.4.1 Synthetic pad materials

Figure 4.16 shows a sample section of rigid media (a) and Aspen pad (b) respectively, which are used with evaporative cooling system such as air cooler [78].

(a) (b)

Figure 4.16 A simple section of rigid media (A) an aspen pad (B)

Figure 4.17 shows a cooling pad for evaporative cooler. According to Muse [78], the Aspen pads materials were common because of their low cost.

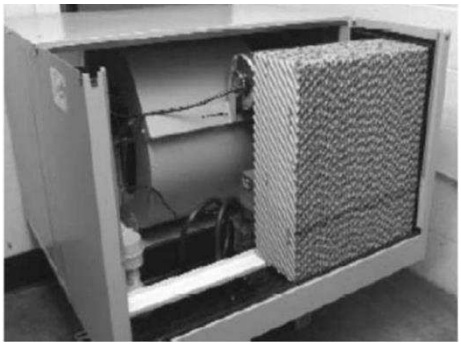

Figure 4.17 Direct evaporative cooler with rigid sheet pads[31]

4.4.2 Organic pad materials

Application of indigenously grown organic materials as wet cooling pads for evaporative cooling systems were also attempted by a few researchers using, for example, Luffa sponge and palm dates fibres, as shown in Figure 4.18 [79] [80].

Figure 4.18 a) Luffa aegypatiaca sponge b) Palm dates fibres

4.4.3 Metal pad materials

Furthermore Figure 4.19 shows metal foams and metal wools materials respectively.

Figure 4.19 Metal foams and metal wools [77]

The metal foams are high strength, low density, low thermal conductivity and good caustic absorption. Moreover its can be produced in different type such as powders, melts, sputtering and deposition with porosity ranging 30-80% .While metal wools mainly made from copper, aluminium and steel. The porosities are various based on the metal fibre length, fibre diameter, and the density, ranging 30–95%. [77]

Today, there is a wide range of synthetic porous materials used in evaporative cooling system. Table 4-4 presents several of current porous materials for evaporative cooling technology [67].

Table 4-4 Various of current porous materials for evaporative cooling technology [67]

Category	System type	Medium
DEC	Random media air coolers	Aspen, Plastic, Fibre and Foam
	Rigid media air coolers	Cellulose (Cardboard box/kraft paper) and Fibreglass
	Slinger packaged air coolers	Latex coated fibre, Fibreglass and Coated nonferrous metal
	Packaged rotary air coolers	Latex coated fibre, Fibreglass and Coated nonferrous metal
	Remote pad evaporative system	Standard random media and Rigid media
IEC	Air-to-air heat exchanger	Cellulous fibre, Porous ceramic and Cotton or other moisture retaining cloths
	Cooling tower and coil system	Film fill (water to spread into a spread into a thin film usually PVC) and Splash fill (interrupts water flow)

4.4.3 Porous ceramic materials

Wet materials such as porous ceramic structures are also being developed that combine various chemical elements and binders such as alumina (Al_2O_3), silicon oxides (SiO_2), nitrides (Si_3N_4) and non-silicate glasses, which are widely used in evaporative cooling applications.

Ceramics offer many advantages compared to other materials, including those that are corrosion-resistant, lightweight, widely available and inexpensive [81]. Moreover, they have an accurately controlled pore size/porosity, elevated temperature capability, a capability of being produced in a variety of shapes and sizes to specific requirements and an extension of the useful life under harsh conditions [82]. These were mainly designed to be a fully integrated and functional building element. Figure 4.20 shows some examples of these materials.

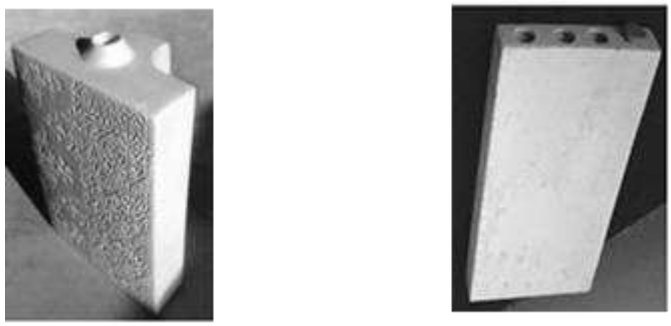

Figure 4.20 Porous ceramic samples for evaporative cooling [7] [8]

Figure 4.20a shows a ceramic container used by Schiano-Phan [8], who evaluated its cooling properties as an integral part of a building's fabric. Similarly, Ibrahim et al. [7] used a ceramic evaporative cooler from Figure 4.20b for direct evaporative cooling in buildings. Furthermore, both authors Schiano-Phan [8] and Ibrahim et al [7] have measured the porosity of ceramic container prototypes by using the following mathematical expression.

$$P = \frac{(W - D)}{(W - I)} \tag{4.2}$$

where W is the wetted weight, D is the dry weight of each prototype, and I is the immersed weight of each prototype. Table 4-5 shows an example of a high porosity ceramic container sample [7].

Table 4-5 High porosity prototype-fired at 1110 C [7]

No.	*D* (dry (g))	*W* (wetted (g))	*I* (immersed (g))	P_o (porosity (%))
1	1516	1646	901	17.4
4	1301	1415	775	17.8
5	1335	1456	796	18.3
6	1683	1829	990	17.4

The availability of porous ceramic materials, which occur naturally, allowed for wide use in evaporative cooling applications. Al-Koheji [40] used ceramic container materials as wet media with heat pipes in indirect evaporative cooling systems as shown in Figure 4.21. The constituents of the ceramic container used in this experiment are given in Table 4-6.

Table 4-6 Ceramic main chemical components [40]

SiO_2	Al_2O_3	Fe_2O_3	TiO_2	MgO	CaO	K_2O	Na_2O	LOI
69.4%	19.2%	0.47%	0.26%	0.18%	0.84%	1.62%	0.36%	6.91%

The ceramic containers in this work were used as wet media to cool the end of the heat pipes (condensers) while the heat pipes were used to transfer heat from the dry airflow channel (supply) to the ceramic container in the wet channel as shown in Figure 4.21. The results of the effect of the inlet air relative humidity on the cooling power and efficiency for the simulation and experiment for the system are presented in Figure 4.22. It can be seen that both the cooling power and efficiency of the system decreased with increasing inlet relative humidity.

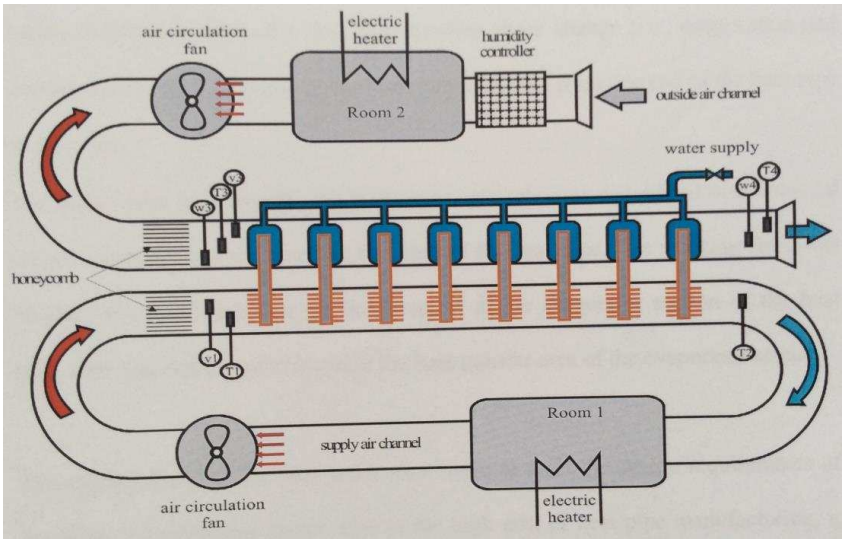

Figure 4.21 Indirect evaporative cooler using porous ceramic with heat pipes [40]

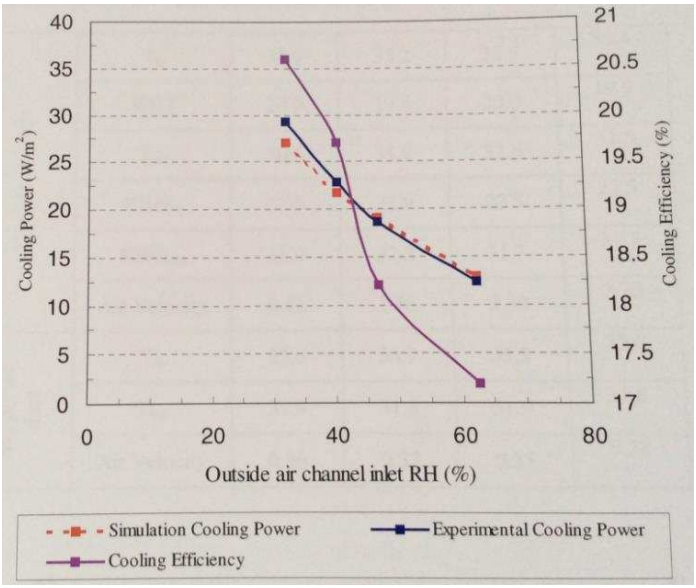

Figure 4.22 The effect of the air relative humidity on the cooling power and efficiency[40]

Ibrahim et al [7] evaluated the effect of porosity on the cooling performance of the ceramic evaporative cooler. It was found that high porosity materials achieve superior cooling capacities as presented in Figure 4.23

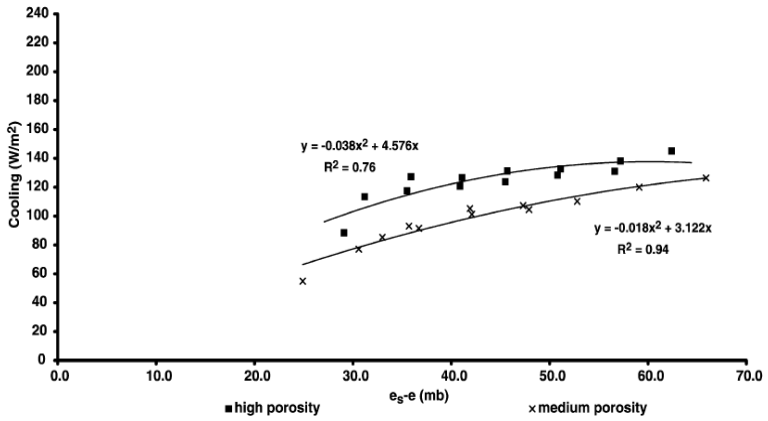

Figure 4.23 Effect of porosity on cooling performance of ceramic [7]

Musa [78]investigated the porous ceramic direct evaporative cooling systems . The author used two different shapes of "stacking" rectangular porous ceramic shown in Figure 4.24 as wet media. The general air flow pattern across the porous ceramic evaporators was in accordance with the system integration into the building as illustrated in Figure 4.25.

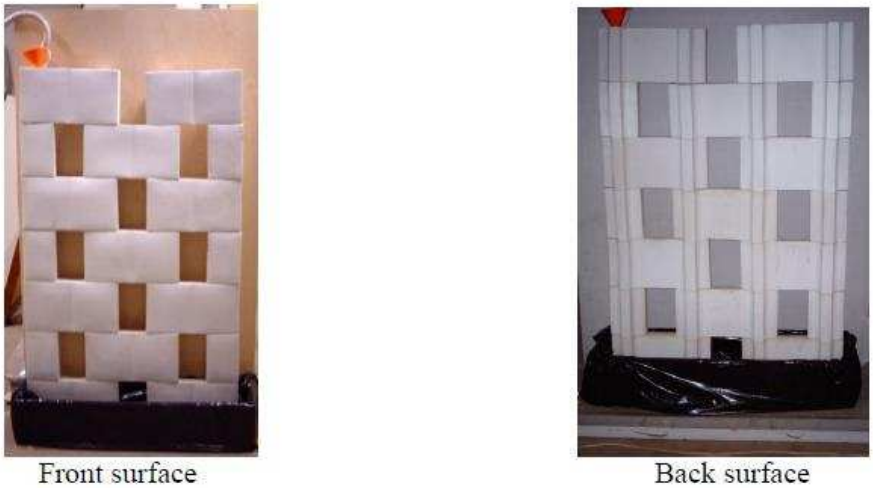

Figure 4.24 The front and back evaporative cooling surfaces of stacked system in condensate tank [78]

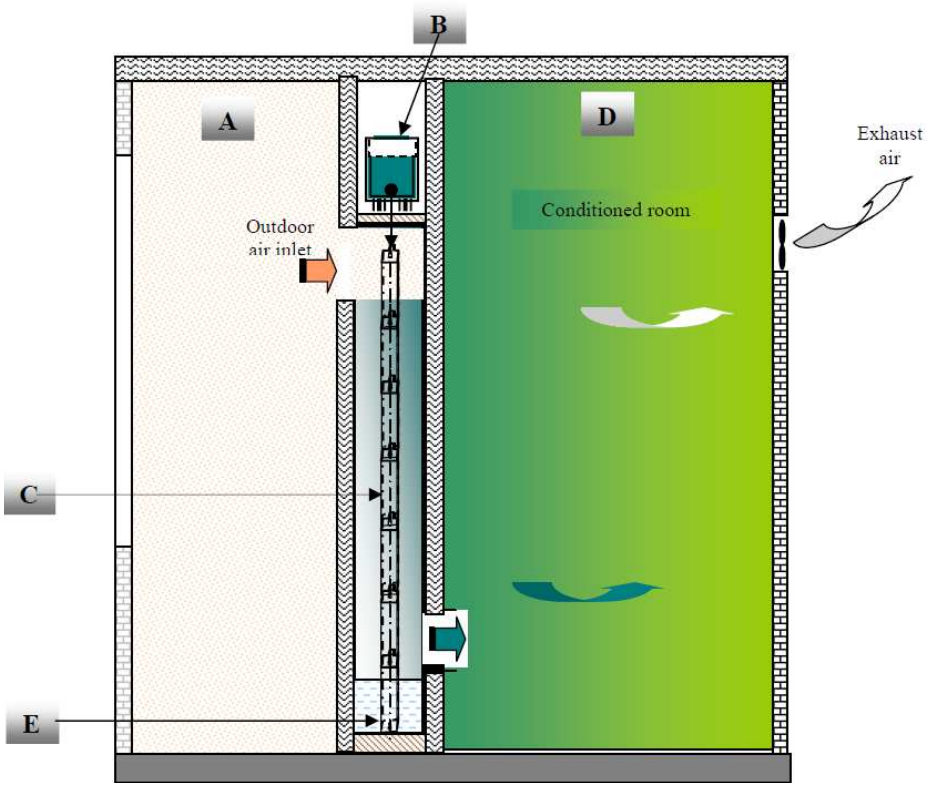

Figure 4.25 Stacking system configurations (A-environmental chamber set conditions, B-water supply tank to porous ceramics, C- stacked evaporators in evaporation chamber, D-room space cooled[78]

The author observed the temperature drop across the ceramic's evaporative cooling chamber, with the air volume flow rate set at 140 m3/h before the steady state tests, and which indicated that the difference between inlet and outlet temperatures increases with an increase in the inlet temperature values as shown in Figure 4.26. The highest value of temperature drop was 9.2°C when the inlet temperature was 43.8°C.

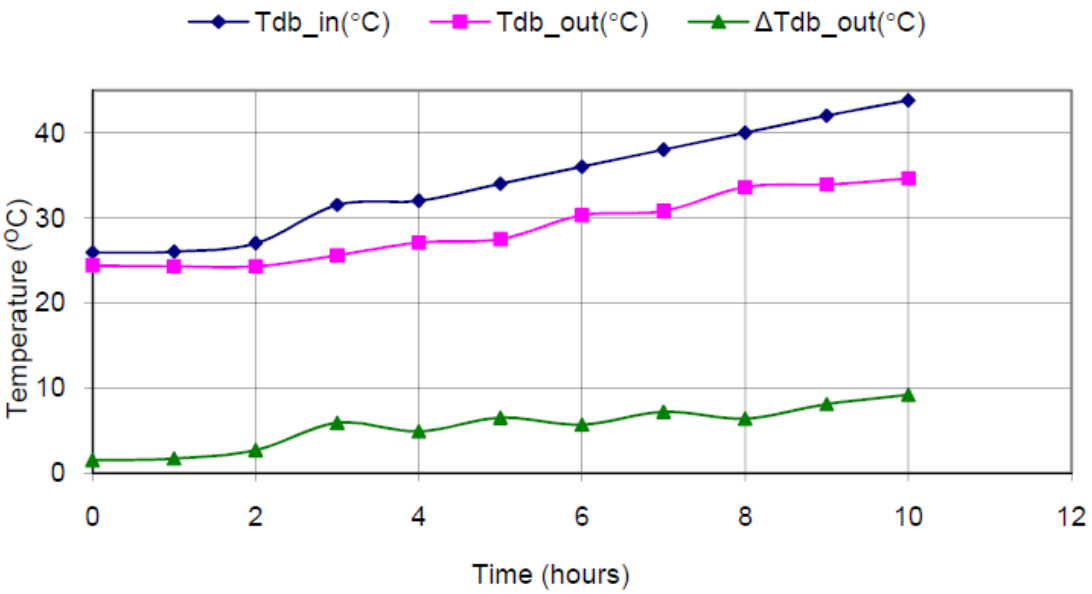

Figure 4.26 Inlet and outlet dry bulb temperature variation [78]

For an inlet air temperature of 35°C and a relative humidity of 35%, the steady state measured the outlet air temperature of 27.3°C, with a drop of 7.7°C, and at a mass flow rate of 140 m^3/hr as shown in Figure 4.27.

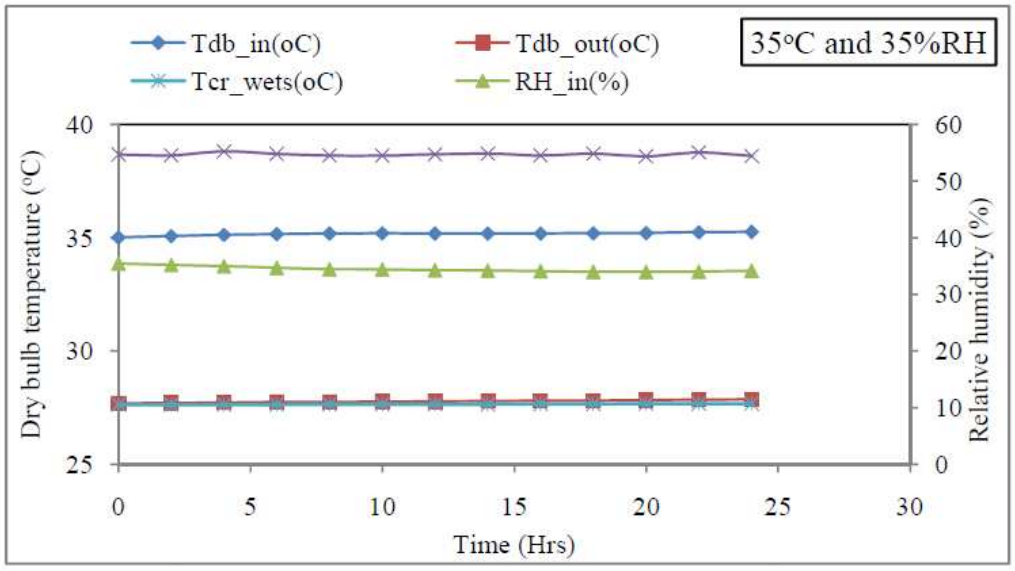

Figure 4.27 Variation of inlet and outlet dry bulb temperature under 35 ^{0}C and 35% constant inlet ambient conditions [78]

Riffat and Zhu [83] carried out the experiments to examine the effects of various ceramic properties, such as porosity, wall thickness and outside diameter under similar

environmental conditions for a chilled ceiling cooler that consists of a porous ceramic and a heat pipe as shown in Figure 4.28. The authors indicated that the cooling capacity increased about 9 W/m^2 when the ceramic porosity increased from 32.8% to 34.6%. However, the cooling capacity decreased with an increase of the ceramic wall thickness and outside diameter. The average decreasing rate of cooling capacity was 1.03 (W/m^2)/mm as the ceramic wall thickness increased, and the cooling capacity decreased from 65.65 W/m^2 to 28.17 when the outside diameter of the ceramic increased from 60mm to 240 mm.

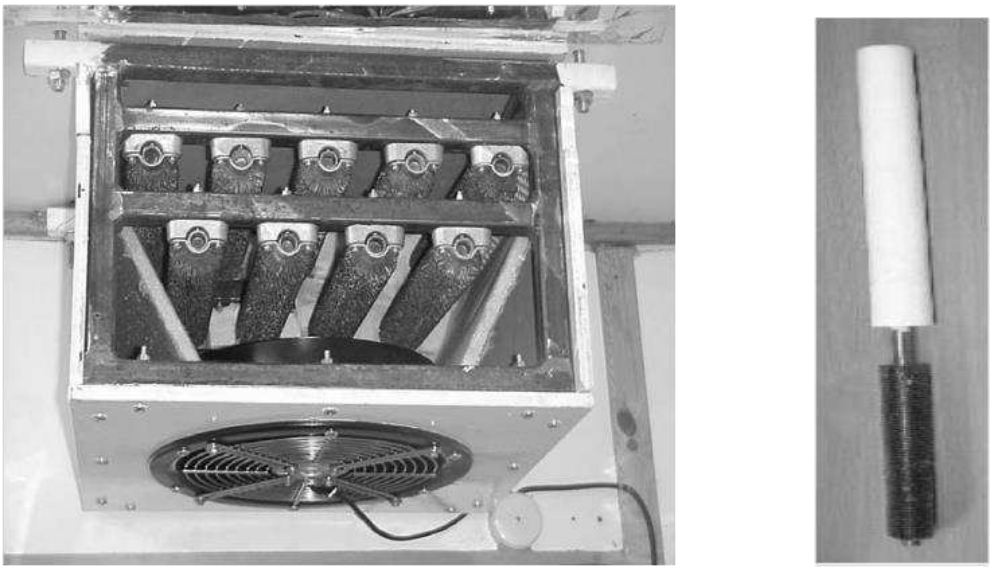

a b

Figure 4.28 Chilled ceiling (a) and cooler with heat pipe embedded in porous ceramic (b)

The authors indicated that the cooling capacity increased to about 9 W/m^2 when the ceramic porosity increased from 32.8% to 34.6%. However, the cooling capacity decreased with an increase of the ceramic wall thickness and outside diameter. The average decreasing rate of the cooling capacity was 1.03 (W/m^2)/mm as the ceramic wall thickness increased, and the cooling capacity decreased from 65.65 W/m^2 to 28.17 when the outside diameter of the ceramic increased from 60mm to 240 mm.

Lomas et al. [84] focused on the conceptual design of the passive downdraught evaporative cooling systems (PDEC) for a multi-storey office building to be located in the middle of Seville in Southern Spain. The authors indicated that the PDEC system must be carefully controlled in order to ensure that there is a flow of cool air to every space and to every floor of the building when applied to a multi-storey building, and which must meet contemporary standards of indoor climate quality.

He and Hoyano [85, 86] used a ceramic bundle of ceramic material tubes as a passive evaporative cooling wall. The ceramic material is highly water absorbent, and its properties are shown in Figure 4.29.

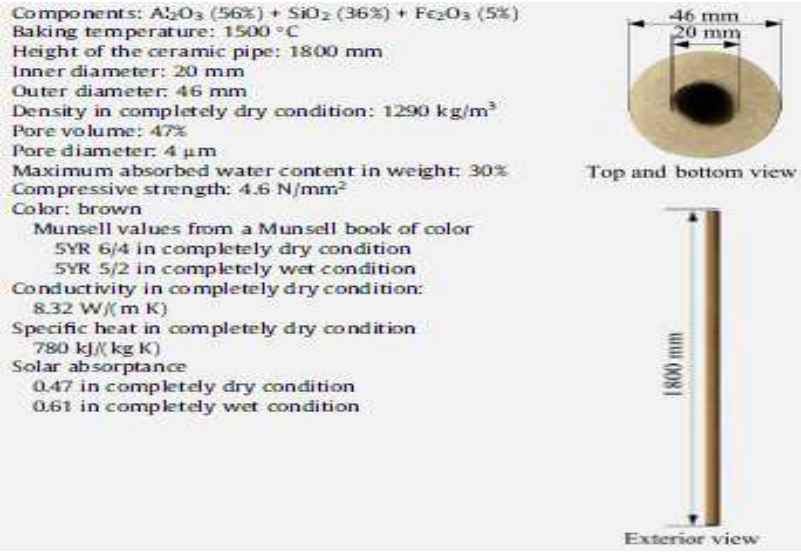

Figure 4.29 Specifications of the ceramic pipe used in the PECW

E. Velasco Gomez et al. [74, 87, 88], F.J Rey Martinez and R. Herrero [88] used porous ceramic materials for a semi-indirect ceramic evaporative cooler. Figure 4.30 shows the heat and mass exchange in ceramic pipes, and Table 4-7 shows the properties of the solid porous material.

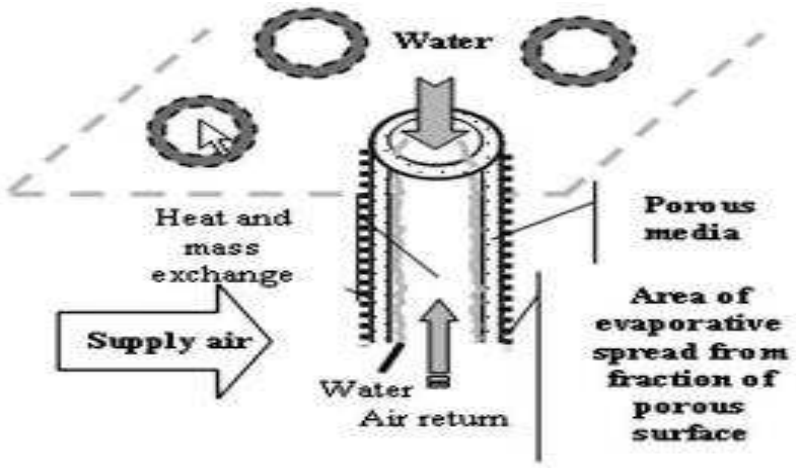

Figure 4.30 Heat and mass exchange in ceramic pipes

Table 4-7 Properties of solid porous material

Chemical analysis	
SiO_2	Below 19%
Al_2O_3	Above 79%
TiO_2	Below 0.3%
Fe_2O_3	Below 0.5%
CaO	Below 0.2%
MgO	Below 0.1%
K_2O	Below 0.5%
Na_2O	Below 0.2%
Physical properties	
Density	2.5–2.55 g/cm^3
Absorption in water	9–10%
Porosity	22–25%
Bending	350–400 kg/cm^2
Dilation coefficient	5.5–5.9 × 10^{-6} °C^{-1}
Max. work temperature	Max. 1300 °C

Direct evaporative cooling systems can also be used to create cooler urban environments in summer when applied in public areas such as parks or pedestrian areas. He and Hoyano [85] [89] developed a passive evaporative cooling wall (PECW) constructed of porous ceramics with high water permeability. As shown in Figure 4.31, the PECW consists of rows of pipe-shaped porous ceramics with the lower ends immersed in a water pool. The air flow through the PECW is cooled by the effect of water evaporation from the surfaces of the ceramic pipes.

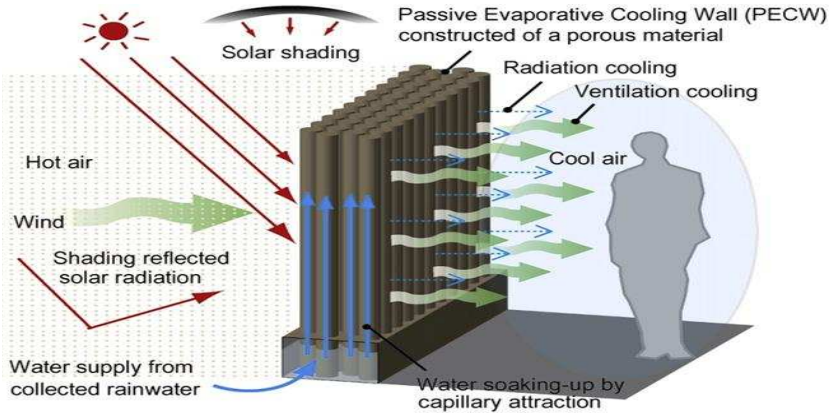

Figure 4.31 Passive evaporative cooling wall using ceramic pipes

The capillary forces of the porous ceramics, acting against gravity, permit the circulation of water upward along the ceramics to replenish the water evaporated from the surfaces. It was indicated that the absorbed water could reach heights of 1m when the maximum height of the water absorbency in common porous material is 30–40 cm. The porous ceramics used in this experiment were baked at a temperature of 1250°C, achieving a bulk porosity of 47%. Table 4-8 gives the main design parameters of the ceramic pipes.

Table 4-8 Specification of the ceramic pipes

Ceramic materials (chemical reaction)	$MgCO_3$, AI_2SiO_s, SiO_2
Baking temperature	1250^oC
Physical dimensions of the ceramic pipes	
Height	1200 mm
Inner diameter	28mm
Outer diameter	48 mm
Outer external surfaces area	0.18 m^2
Pore volume	47%
Pore diameter	5-50um
Maximum absorbed water content in weight	30%
Compressive strength	23 N/mm^2

The experimental result showed that when the clean water (city water) was used as supply water for evaporation, there was no significant change in the wet surface condition of the ceramic pipes over one year, but when the collected rainwater was used as supply water, the change in the surface condition of the ceramic pipes was observed.

Extensive design and development of passive downdraught evaporative cooling systems (PDEC) were carried out by Ford et al. [90]. It was found that the PDEC system could make a significant contribution to reducing the energy consumption in new and existing buildings in many European countries and throughout the hot dry regions of the world. The results of the Theoretical Models of this project showed that, in buoyancy-driven conditions and for highly porous ceramic, the direct system can achieve a specific cooling power of 100 W/m^2 of ceramic surface area. However, the results of the Laboratory Scale Measurement indicated a specific cooling power of 100–200W/m of the ceramic surface area of the direct system, but with very low air velocities [7].

The development of passive downdraught evaporative cooling systems (PDEC), using porous ceramic evaporators and their application in residential buildings, was also a subject of a PhD thesis by Schiano-Phan [91]. The aim of this work was to analyse the performance of a building in winter and summer and the cooling loads in the different rooms. The author also gives the principle idea to the components' different shape for the porous ceramic. Figure 4.32 and Figure 4.33 illustrate the assembly options to component stacked ceramic, hang ceramic and cantilevered ceramic, which were used as wet media for the direct evaporative cooling system by Musa, Ford et al. [90] and E. Ibrahim respectively.

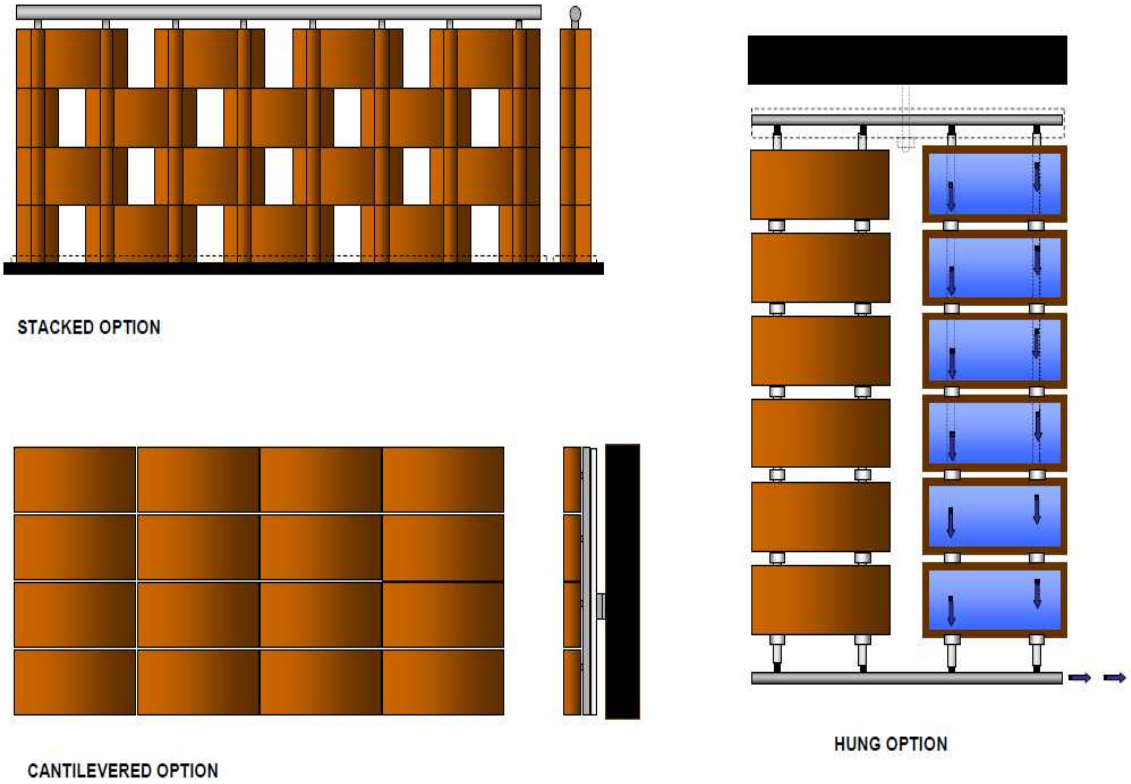

Figure 4.32 Assembly options to component stacked ceramic, hang ceramic and cantilevered ceramic **[8]**

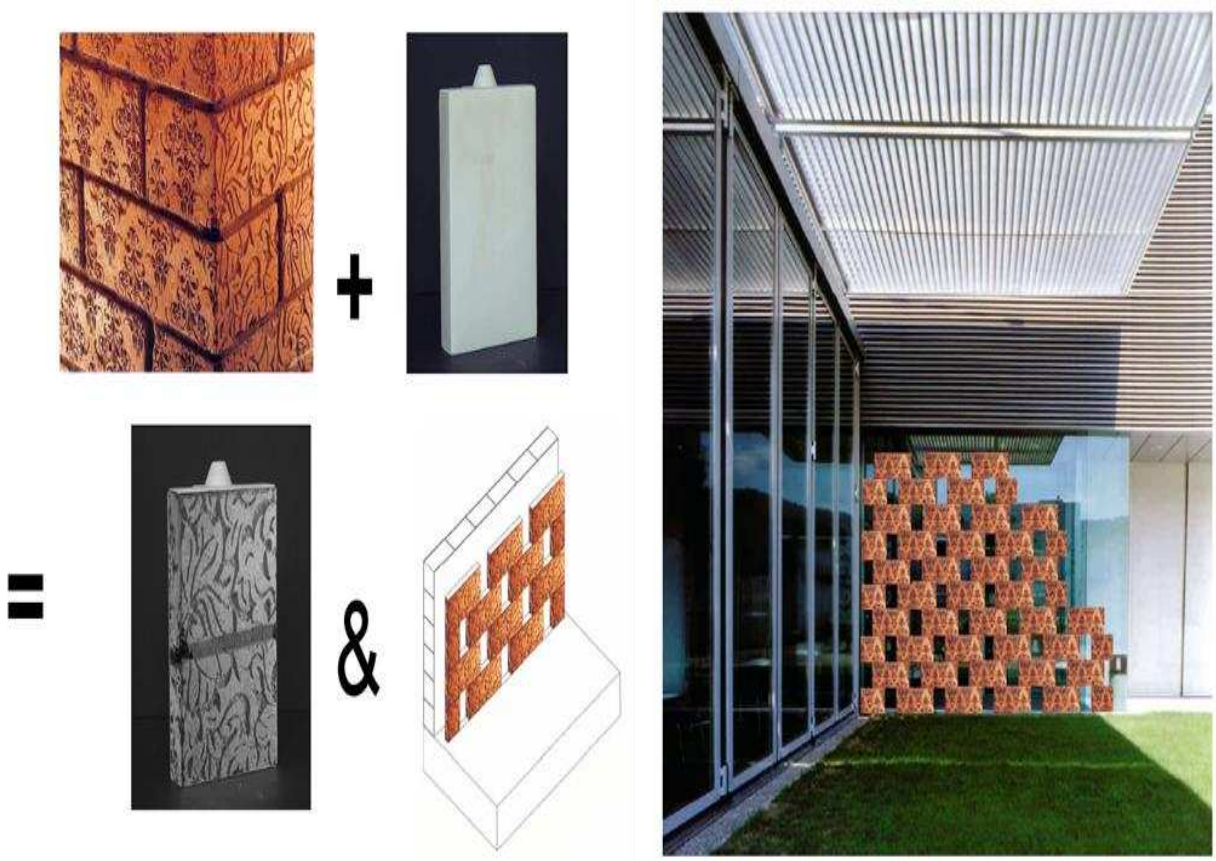

Figure 4.33 Cool wall idea **[8]**

4.4.4 Heat pipe application for cooling

The heat pipe is a “closed evaporator-condenser” device consisting of a metal container (pipe or tube), working fluid (e.g., water) and wick or capillary structure as shown in Figure 4.34 [92]. When heat is applied to one end of the heat pipe evaporative section, the liquid working fluid heats and evaporates. The fluid vapour travels along through the heat pipe hollow centre to the condenser section where the temperature is lower than the evaporator section. Due to this, the vapour condenses and changes into a liquid phase then returns to the evaporator section through the wick.

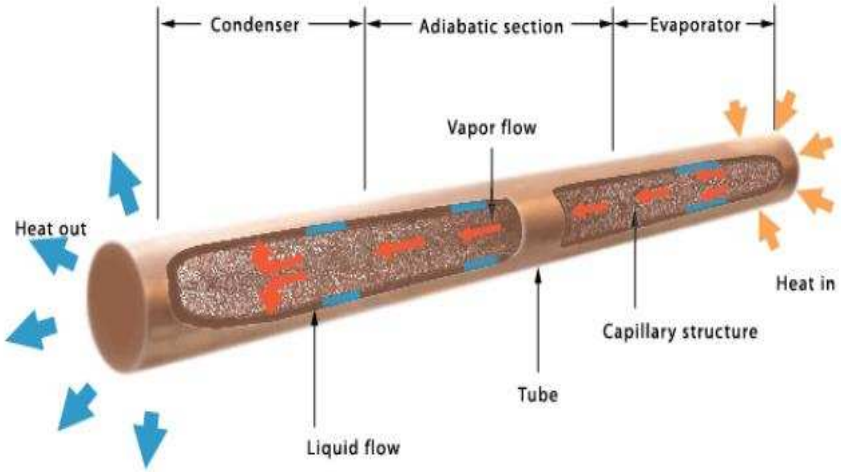

Figure 4.34 Heat pipe structure[92]

A heat pipe has a highly effective thermal conductance, and heat is transported with a small temperature difference between the evaporator and the condenser [93]. Figure 4.35 shows a cross section of a heat pipe and temperature drops in different parts

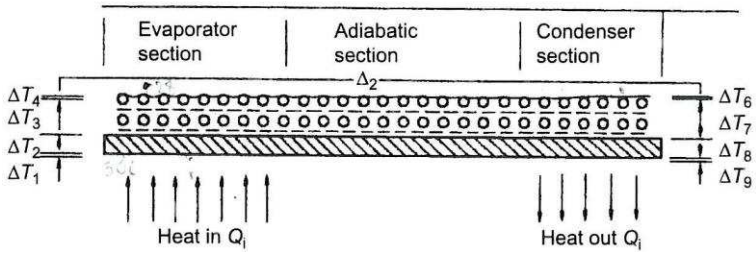

Figure 4.35Temperature drop and equivalent thermal resistance in a heat pipe [93]

The equivalent thermal resistance network of a heat pipe is given in Figure 4.36.

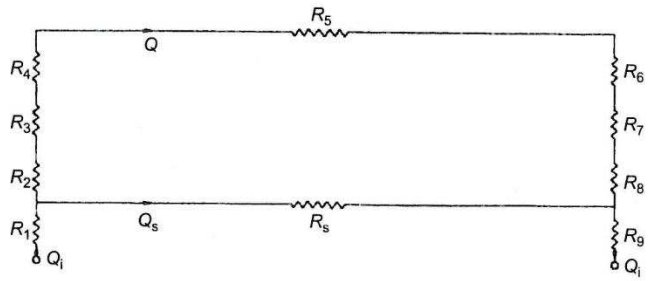

Figure 4.36 Equivalent thermal resistance network of a heat pipe [93]

Where R_1 and R_9 are external surface resistance of evaporator and condenser section respectively, R_2 and R_8 are wall resistance of evaporator and condenser section respectively, R_3 and R_7 are wick resistance of evaporator and condenser section respectively and R_4 and R_6 are liquid vapour interface resistances of evaporator and condenser section respectively. Typical values of the thermal resistance in the heat pipe are given in Table 4-9.

Table 4-9 Representative values of thermal resistances [93]

Resistance	°C cm²/W
R_1	10^3–10
R_2	10^{-1}
R_3	10
R_4	10^{-5}
R_5	10^{-8}
R_6	10^{-5}
R_7	10
R_8	10^{-1}
R_9	10^3–10

The application of heat pipes in building cooling include HVAC systems[94], heat recovery systems [95] and dehumidification enhancement of air conditioning system [96]. However, there is limited research work on the applications of heat pipes in indirect evaporative cooling systems for building cooling. Published work include that of Riffat and Zhu [9] who developed an indirect evaporative cooling system that combines a porous ceramic container with a passive heat pipe for heat exchange between the air in the dry channel and air in the wet channel. Figure 4.37 shows a cross section of the system. The wet channel encloses a porous ceramic container, which is filled with water, and as air flows over its exposed surface, water permeates through the pores and siphon to the surface and evaporates, creating a cooling effect. A heat pipe is used to transfer heat from the air in the dry channel to the air in the wet channel. The mathematical model developed by the authors show that the thermal conductivity between the heat pipe and the ceramic cooler was improved to achieve better performance. Also, Huang et al. [37] and Wang et al. [38] used the same configuration proposed by [24], apart from the use of water sprayers on the heat pipe condensation section, which was wrapped with a thin layer of water absorption material instead of using ceramic container, as shown in Figure 4.38. According to the findings by [37], an effectiveness of 70% was achieved, which crested an average of 10^{o}C temperature difference between the heat pipe and airstreams

Moreover, four configurations were tested for heat elimination from an IEC system incorporating heat pipes, which are: (1) the outdoor air is used for cooling heat pipe condensation section (Figure 4.38-a), (2) the outdoor air is precooled by air washer before being passed through the condensation section of the heat pipe (figure 4.38-b), (3) the outdoor air is precooled by DEC unit then flowed through the heat pipe condensation section (Figure 4.38-c), (4) the outdoor air is flowed through the heat

pipe condensation section and water is sprayed on the top of condensation section surface (Figure 4.38-d). It was found that configuration 4 had best cooling capacity and higher efficiency than other configurations of 7-16 % [39].

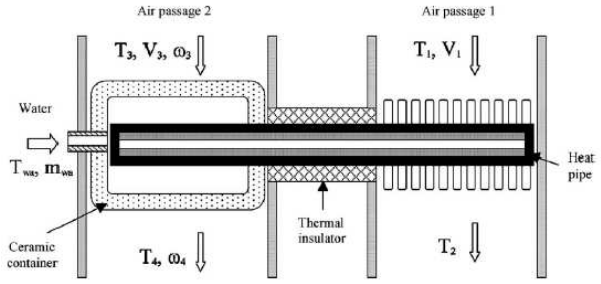

Figure 4.37 Indirect evaporative cooling using ceramic container and heat pipes

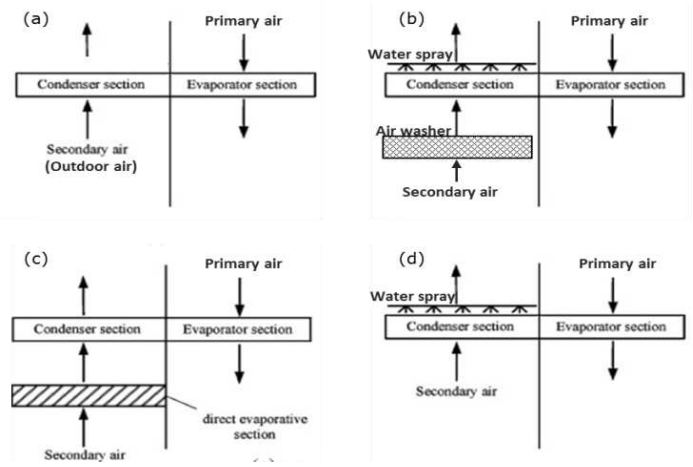

Figure 4.38 Schematic of different configuration of heat-pipe-based IEC [97]

4.5 Conclusions

The previously published research works of evaporative cooling technology for air conditioning in buildings were reviewed. The review covered the concept of evaporative cooling technology and reporting the findings of relevant studies. In addition, the indirect evaporative cooling systems and the materials used for wet media were explained. In conclusion:

- Indirect evaporative cooling can achieve high thermal efficiencies comparable to vapour compression machine without increasing supply air humidity.

- The sub-wet bulb temperature system breaks the limitation of wet bulb temperature and can supply air temperatures below the wet bulb temperature.

- The sub-wet bulb method could be used for the cooling of buildings if air is at a relative humidity of 70% or below because it can lower incoming air temperatures without adding moisture [98].

- The effectiveness of the indirect evaporative cooler depends on type and characteristics of wet media material.

- Different materials such as plastic can be used as wet media for the sub-wet bulb temperature method, but most of previous works tested cellulose materials as wet media materials with this method.

Chapter 5

Theoretical Analysis and Computer Modelling of directly integrated sub-wet bulb temperature evaporative cooler using porous ceramic materials

5.1 Physical description of the cooling system

In this work, porous ceramic panels in the form of hollow flat containers were used as wet media for evaluation in a sub-wet bulb temperature evaporative cooler. Figure 5.1 shows a cross section of the proposed ceramic container. The panel is made of a thin porous ceramic wall material that contains water and a water inlet and outlet.

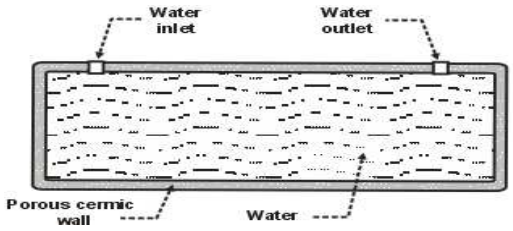

Figure 5.1 Cross section of the porous ceramic panel

In this design, the porous ceramic panels were placed between the dry and wet air channels to form narrow ducts with air flowing at low velocity. To eliminate water ingress to the dry channel side from the porous ceramic panel, a thin non-permeable membrane was used to seal the panel surface while on the wet channel side, it is directly exposed to air flow so that the sips through the micro-pores to form a thin water film on its surface. The system arrangement is shown in Figure 5.2. The direct

evaporation of the water film in the wet channel cools the ceramic panel and the bulk of its water content, which in turn crates a temperature gradient with the air in the dry channel. This allows air in the dry channel to be cooled by transferring its heat to the ceramic panel through the thin water-proof membrane without increasing its moisture content. On the other hand, the evaporation of water from the porous ceramic panel surface in the wet channel carries away the heat added to the ceramic panels from the dry channel airflow and is ultimately rejected as at saturated state. By redirecting part of the airflow at the outlet of the dry channel to the wet channel, sub-wet bulb temperature conditions are made possible.

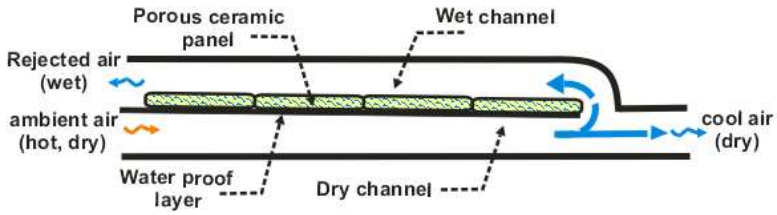

Figure 5.2 A schematic of the arrangement of the porous ceramic panels

5.2 Mathematical Model Formulation

To study the design parameters and thermal performance of the cooling system, a mathematical model was developed by solving common energy and mass conservation laws. The mathematical model was formulated by considering the finite volume method where the physical system was divided into small finite boundaries. These include the hard surfaces of the ceramic panel, the water film on the ceramic panel, and the airflow in the dry and wet channels. Figure 5.3 illustrates the main mathematical model parameters related to air flow temperature, humidity, enthalpy, mass flow rate, etc. for an i^{th} control volume.

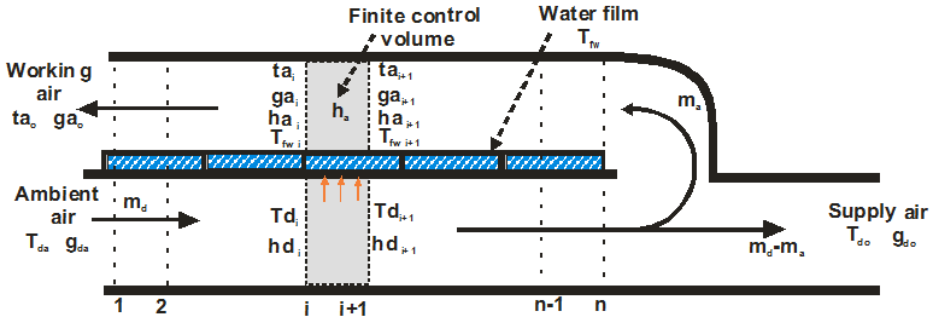

Figure 5.3 Air flow parameters modelling

However, the complexity of formulating the exact physical phenomena of heat and mass transfer in different parts of the system meant that some preliminary assumptions have to be made to simplify the modelling process. These include the following:

i) The air properties and heat and mass transfer coefficients are constant in each finite control volume.
ii) The height to length ratio of the dry and wet channels is very small, leading to improved heat and mass transfer [45, 49].
iii) The airflow velocity in both channels is low and laminar.
iv) The heat transfer to the surroundings is negligible.
v) The air-water interface temperature is assumed to be identical with the water film temperature

5.2.1 Energy conservation in the dry channel

Intake ambient air at high temperature and low humidity is drawn in the dry channel, where it is cooled indirectly by transferring its sensible heat to the wet channel through the porous ceramic panel. The energy balance in a control volume can be expressed as follows [99].

$$\frac{\dot{m}_d \partial h_d}{\partial A} = -k_s (T_d - T_{fw}) \tag{5.1}$$

where, m_d is the air mass flow rate in the dry channel, h_d is the enthalpy of air, A is the heat transfer area, k_s is the overall heat transfer coefficient between the two air channels, T_d is the average temperature of the control volume in the dry channel, and T_{fw} is the average temperature of the control volume of the water film. The overall heat transfer coefficient, Ks, between the dry and wet channel air flows can be written as:

$$k_s = \frac{1}{\frac{1}{\alpha_d} + \frac{At_c}{\lambda_{csw}} + \frac{At_w}{\lambda_w} + \frac{1}{\alpha_a}} \tag{5.2}$$

Where α_d is the convective heat transfer coefficient in the dry channel, A is the heat transfer area, t_c is the thickness of the ceramic panel wall, t_w is the water layer thickness in the ceramic panel, λ_{csw} is the thermal conductivity of the ceramic panel, λ_w is the thermal conductivity of the water, and α_a is the convective heat transfer in the wet channel. The porous ceramic wall is saturated with water and its thermal conductivity should take into account both the dry ceramic and water thermal conductivities. This is computed as follows [9]:

$$\lambda_{csw} = \frac{\lambda_w[\lambda_w + \lambda_c - (1-\phi)(\lambda_w - \lambda_c)]}{\lambda_w + \lambda_c + (1-\phi)(\lambda_w - \lambda_c)} \tag{5.3}$$

λ_c is the thermal conductivity of the dry ceramic container and ϕ is the ceramic container's porosity.

5.2.2 Energy conservation in the wet channel

The heat transfer mechanism in the wet channel is more complicated than in the dry channels, as sensible and latent heat is exchanged between the wet airflow and the

water film on the surface of the porous ceramics. The energy balance of the control volume can be written as follows [99]:

$$\frac{\dot{m}_a \partial h_a}{\partial A} = \alpha_a (T_{fw} - t_a) + \sigma(g_{fw} - g_a) h_{fg} \quad (5.4)$$

where, m_a is the air mass flow rate in the wet channel, h_a is the enthalpy of air, A is the heat transfer area, α_a is the convective heat transfer coefficient, t_a is the average temperature of the control volume in the wet channel, T_{fw} is the average temperature of the control volume of the water film, σ is the mass transfer coefficient, g_{fw} is the moisture content at saturation, g_a is the average moisture content of air in the wet channel, h_{fg} is the latent heat of vaporisation of water.

It assumed that the air flow in the narrow channels is in laminar regime and heat and mass transfer are correlated by Lewis number formula as follows [99]:

$$\mathbf{Le} = \frac{\alpha_a}{\sigma \mathbf{c}_p} \quad (5.5)$$

where, Lewis number is often taken in the range of 0.9 to 1.15 and to simplify the model, it is considered in this work to be unity.

5.2.3 Mass conservation in the wet channel

The evaporation of water from the ceramic panel surface appears as an increase of the air moisture content along the length of the wet channel. Therefore, the mass balance for the water vapour in the control volume of the wet channel can be written as:

$$\frac{m_a \partial g_a}{\partial A} = \sigma(g_{fw} - g_a) \quad (5.6)$$

5.2.4 Overall energy balance

The overall energy balance at the water film interface can be seen as the heat transferred from the airflow in the dry channel, the sensible heat and removal and latent heat addition to the airflow in the wet channel. This is given as follows:

$$\frac{\dot{m}_{fw} C_{pfw} \partial T_{fw}}{\partial A} = Ks(T_d - T_{fw}) - \sigma(g_{fw} - g_a) h_{fg} - \alpha_a (T_{fw} - t_a) \quad (5.7)$$

where m_{fw} is the water film mass flow and C_{pfw} specific heat of water.

To solve governing equations of heat and mass transfer (5.1), (5.4), (5.6), and (5.7), the boundary conditions need to be added to obtain a closed form solution.

The equation of energy conservation in the dry channel (5.1) was then simplified to the following:

$$\frac{\partial T_d}{\partial U} = -KCX_o (T_d - T_{fw}) \quad (5.8)$$

Where constant coefficients U, K, C and X_o are given as:

$$U = \frac{x}{L}, \; K = \frac{k_s}{\alpha}, \; C = \frac{m_a . c_p}{m_d . c_{pa}} \text{ and } Xo = \frac{\alpha . A_s}{m_a . c_p}$$

The equation of energy and mass conservation in the wet channel (5.4) and (5.6) are simplified to:

$$\frac{\partial t_a}{\partial U_a} = -X_o (t_a - T_{fw}) \quad (5.9)$$

$$\frac{\partial g_a}{\partial U_a} = -X_o Le(g_a - LeBT_{fw}) \quad (5.10)$$

Where, Lewis number Le was defined in Chapter 4.

Finally, the overall energy balance of the system is given by:

$$\frac{\partial T_{fw}}{\partial U_{fw}} = \frac{X_o}{W} [KT_{fw} + t_a + g_a - (K + 1 + LeB) T_{fw}] \quad (5.11)$$

Where coefficient, W, is given as: $W = \frac{m_{fw}.c_{pw}}{m_a.c_p}$ and B can be read from a chart given in Appendixes A1 if the temperature of water and air wet bulb temperature are known.

5.2.5 Boundary conditions

In this system the main boundary conditions consist of the following:

i) Dry channel inlet airflow properties: this including known dry bulb temperature, wet-bulb temperature, moisture content or relative humidity

$$T_d|_{x=0} = T_o \text{ and } g_d|_{x=0} = g_o \quad (5.12)$$

ii) Wet channel inlet airflow conditions: in this case the dry bulb temperature is set equal to the outlet temperature of the dry channel and the moisture content equal to the airflow inlet moisture content.

$$t_a|_{x=L} = T_d|_{x=L} \text{ and } g_a|_{x=L} = g_o \quad (5.13)$$

iii) Heat transfer at the outside boundary: it is assumed that all outside boundaries are Adiabatic and no heat is transferred through.

$$\dot{q} = 0 \quad (5.14)$$

5.3 Computer Codes

The equations described in the mathematical model of previous section were discretised and applied to each finite volume element of Figure 5.3 along the dry channel, water film and wet channel length using implicit finite method. The computer codes are given in Appendixes 2, 3, 4 and 5

The computer algorithm used to develop the codes is shown in Figure 5.4. The operating parameters including airflow temperature profiles along the air channels

length, moisture content, water film temperature were performed iteratively until converging conditions were satisfied, giving a temperature difference between two consecutive iterations less than 0.01^{o}C. The computer codes were written using Matlab© Software. Matlab is a high level programming language and interactive environment for numerical computation, visualization, and programming.

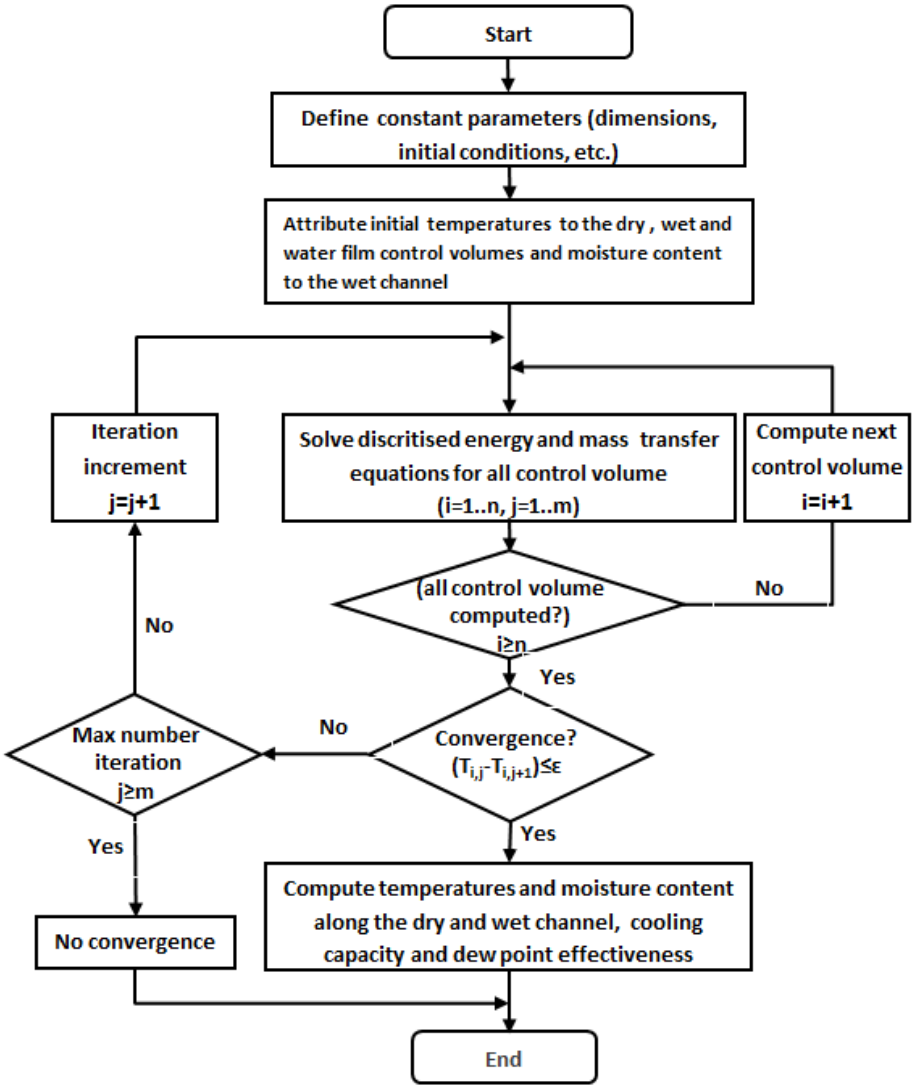

Figure 5.4 The computer model flow chart

5.4 Mathematical model results and validation

The thermal performance of the porous ceramic evaporator cooler shown in Figure 5.5 was evaluated at temperature of 30 and 35^{o}C and corresponding relative humidity of 35% to 55%, weather conditions that prevail in dry and hot climates such as in the Middle East region.

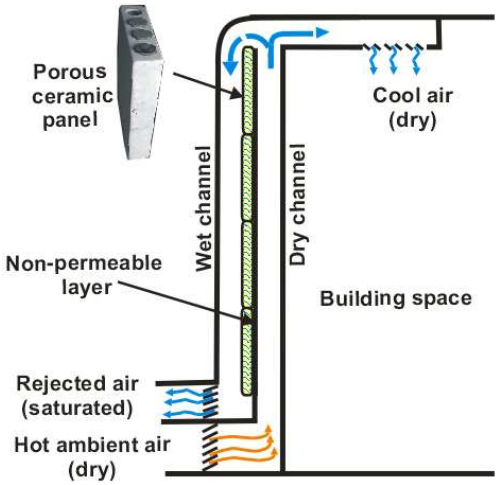

Figure 5.5 Schematic of the sub-wet evaporative cooler

The effect of intake channel air velocity on wet bulb effectiveness and product air temperature and also the effect of the ratio of air in the wet channel to the total air in the dry channel on cooler effectiveness were modelled to determine the appropriate inlet air velocity and the ratio of working to intake air of this cooler. After that, temperature profiles of air along the dry and wet channels, air moisture content along the wet channel, and temperature profile of the water film on the ceramic panel surface were further modelled. Furthermore, the effect of relative humidity on the cooling capacity and the wet bulb and dew point effectiveness of the cooler were calculated and analysed. The model was defined by the parameters given in Table 5-1

Table 5-1 Main prototype characteristics

Design parameters	
Porous ceramic panel length	0.64 m (20 cm x 3 ceramic panels)
Porous ceramic panel width	0.93 m (40cm x 2 ceramic panels)
Dry and wet channel air gap	0.005 m
Mass flow rate in the dry channel	0.03 (kg/s)
Mass flow rate in the wet channel	0.012 (kg/s)
Water supply temperature	23 (^oC)
Nusselt number	4.861[100]
Porous Ceramic properties	
Materials composition	Al_2O_3, SiO_2, Si_3N_4
Porosity	17%
Density	2300 kg/m^3
Thermal conductivity	1.5 W/mK

5.4.1 The effect of inlet air velocity on the effectiveness and product air temperature

The effect of varying intake air velocity on the wet bulb effectiveness and product air temperature were modelled and the results are shown in Figure 5.6. Two inlet air temperatures are considered at 30^o C, 35^o C, with relative humidity set at 35% (i.e., wet bulb temperature, $T_{wbi,}$ of 18.9 ^{o}C and 23^{o}C respectively) and air velocity are 1, 1.5, 2, 2.5 and 3 m/s. From figure 5.6 it can be seen that the wet bulb effectiveness of both inlet air temperatures steadily decreased when the intake air velocity increased from 1 to 2 m/s. Then the wet bulb effectiveness for air temperature at 30 and 35 ^{o}C decreased gradually when the intake air velocity increased from 2 to 3 m/s. Moreover, it can be observed that the wet bulb effectiveness can be more than 100% when the intake air velocity is less than 2 m/s for both inlet air temperatures.

On the other hand, the product air temperature for both 35 ^{o}C and 30 ^{o}C inlet temperatures increased linearly with increasing intake air velocity, whereas the dew point temperature can be achieved in this cooler when the intake air velocity is also

less than 2 m/s. This is due to the decreased evaporation rate with increasing intake air channel velocity, because when the working air velocity increases, the time of contact between the working air and wet surfaces will be reduced, which results in decreased capacity of moisture absorbed by working air in the wet channel. Therefore, to decrease the product air temperature for both inlet air temperatures below their wet bulb temperature and achieve wet bulb effectiveness of more than 100%, the velocity should be set between 1 to 2 m/s for this cooler.

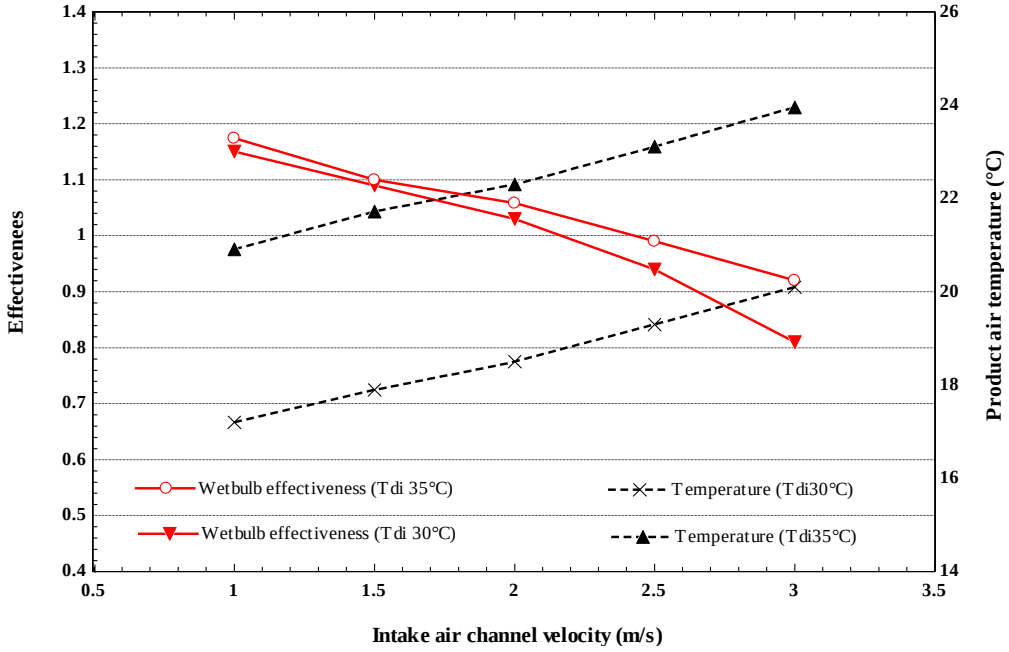

Figure 5.6 Effect of inlet air velocity

5.4.2 The effect of working to intake air ratio

The effect of working to intake air ratio on the cooler's effectiveness is further modelled for 30 ^{o}C and 35 ^{o}C inlet air temperatures and intake air velocity of 2 m/s as shown in Figure 5.7. It shows that the wet bulb effectiveness of both inlet air temperatures rose steadily when the working to intake air ratio increased from 0.1 to 0.3 kg/kg$_{d}$, then they gradually increased with the increasing working to intake air ratio. Furthermore, it can be observes that the wet bulb effectiveness is higher than 1

when the working to intake air ratio is between 0.5 and 0.9. However, the dew point effectiveness for inlet air temperatures (T_{di} 35 ^{o}C and T_{di} 30 ^{o}C) gradually increased from 0.298 to 1.348 and from 0.279 to 1.33 respectively when the working to intake air ratio (kg/kg$_d$) varied from 0.1 to 0.9. From this finding it can be noted that higher working to intake air ratio (kg/kg) gives higher effectiveness, therefore the cooled supply air should be reduced to increase the effectiveness of this cooler and to achieve wet bulb effectiveness greater than 100% for this cooler, the working to intake air ratio should be set from 0.5 to 0.9 (Kg/kg)

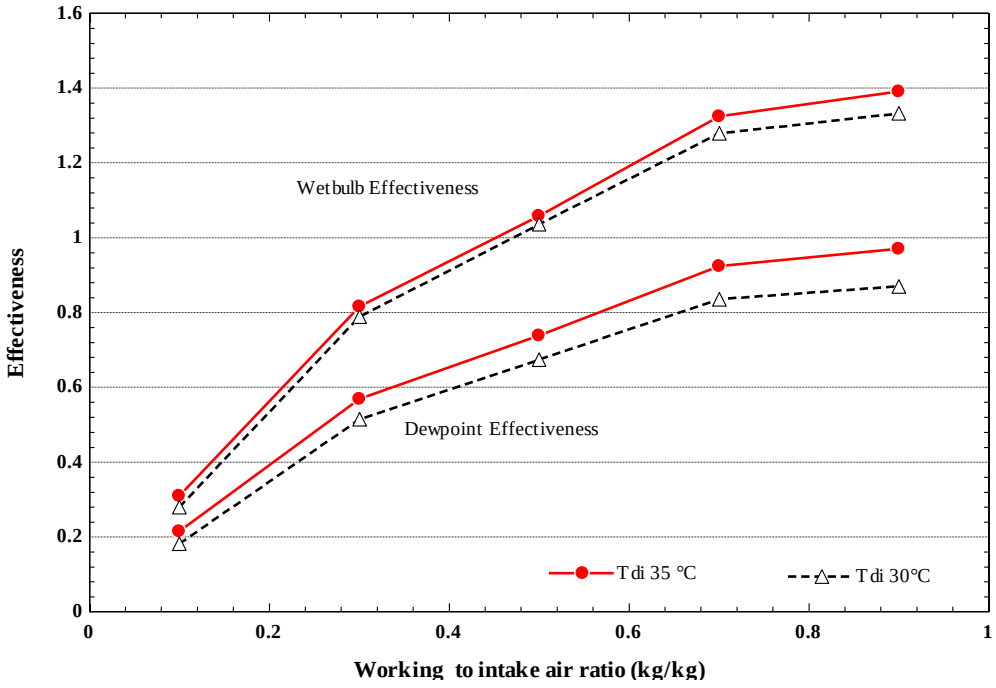

Figure 5.7 Effect of working air ratio

5.4.3 Temperature profile in the air ducts

For an initial inlet air (atmospheric air) temperature, T_{dbi}, of 35^{o}C and relative humidity of 35% (i.e., wet bulb temperature, $T_{wbi,}$ of 23^{o}C and dew point of 17.9^{o}C), supply water temperature of 23 ^{o}C and mass flow rate of 0.03kg/s, Figure 5.8 shows

the computer model results of product air temperature distribution (T_{do}), working air (t_{ao}) and film of water (T_{fw}) in the sub-wet bulb temperature indirect evaporative cooling systems. It can be seen that the temperature of the air in the dry channel decreases from 35^{o} C to 22.2^{o} C, which is below the wet bulb temperature (T_{wbi}), showing that the evaporative cooler would perform adequately in such climatic conditions. Another important property is that the water film temperature increases from 20.5 ^{o}C to 27.2^{o} C along the duct as the balance between heat gain from the air in the dry channel and heat loss by evaporation to the air in the wet channel is positive. The heat loss through evaporation of water to the air in the wet channel is reflected by the increase in both the airflow temperature and water content profiles along the channel. It can also be noticed that the working air temperature, t_{ao}, at the turning point of the airflow is higher than that of the water film and drops from 22.2^{o}C to 20.9^{o}C, which is below that of the water film, before resuming the normal trend and then being rejected at a temperature of 26.3^{o}C. The point at which the water film and wet air temperature profiles intersect depends on the design parameters of the evaporative cooler.

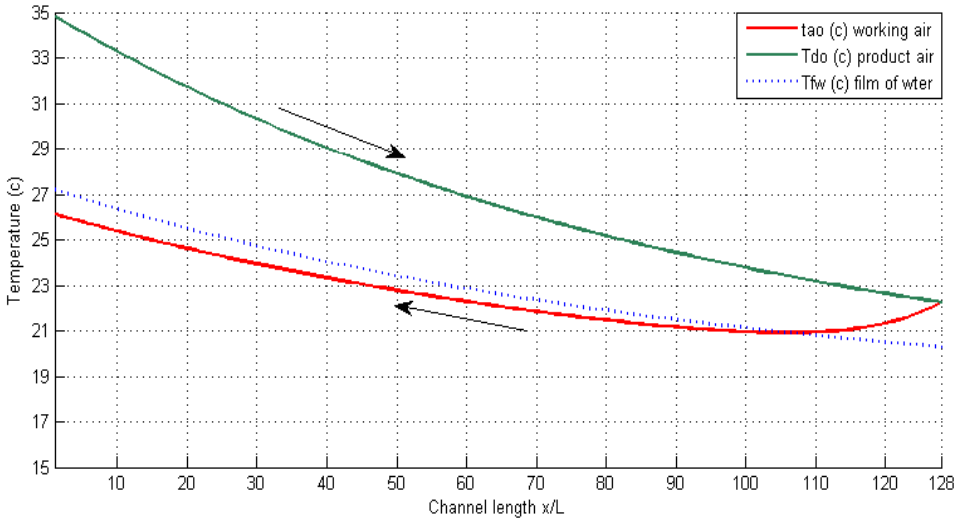

Figure 5.8 Modelling results of temperature profile along the air ducts

(T_{di} = 35 ^{o}C, RH= 35%, T_{w}= 23 ^{o}C)

5.4.4 The effect of cooler configuration on humidity ratio

The operating properties of the conditioned air in the sub-wet bulb temperature evaporative cooler are further shown on a psychometric chart of Figure 5.9. It can be seen that at design conditions of T_{di}=35^{o} C and relative humidity of 35%, the conditioned air supply has a constant water vapour content of 12.3 g/kg$_{d}$ and a temperature lower than the wet bulb temperature, with the ultimate cooling temperature that can be achieved equal to the dew point temperature of 17.7^{o} C. This led to the dry channel side of the porous ceramic panel being sealed with a thin non-permeable membrane so no latent heat transferred from the porous ceramic panel to the intake air dry channel; heat only transferred from the intake air to the porous ceramic panel. However, the working air circulated in the wet channel is rejected at saturation conditions when its characteristic coincides with that of the saturation line on the psychometric chart and exits the evaporative cooler at 26.3^{o}C and water vapour content increases from 12.3 g/kg$_{d}$ to 22 (g/kg$_{d}$) because of the direct contact between the working air and the ceramic panel.

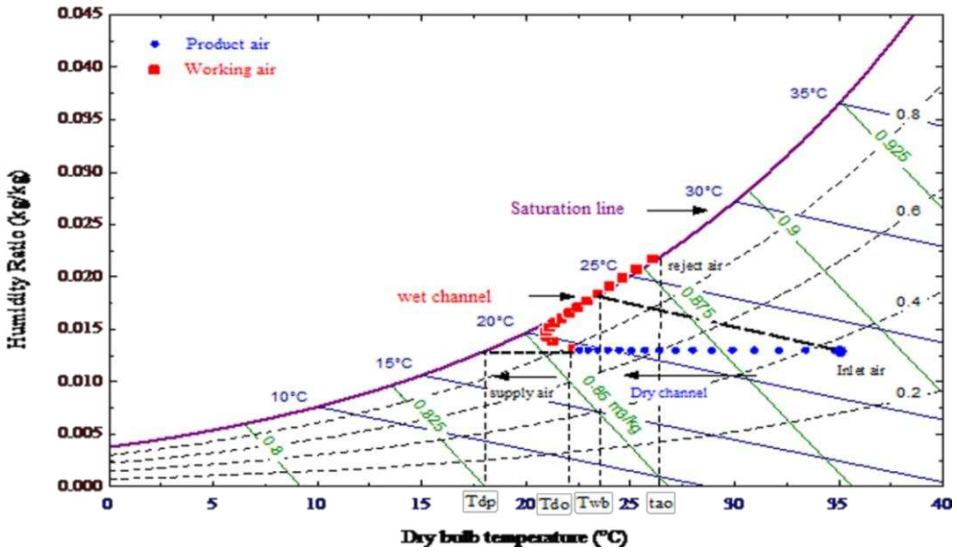

Figure 5.9 Presentation of modelled air properties on a psychometric cart (blue line: product air temperature, Tdo and (red line: working air temperature tao)

5.4.5 The effect of intake air channel velocity and relative humidity water consumption

The effect of varying intake air velocity and inlet relative humidity on water consumption was also considered. Three air inlet relative humidities were considered: 35%, 45% and 55% with inlet dry air temperature set at 35 ^{o}C set and air velocity ranged from 1 to 2 (m/s). The results of the model are shown in Figure 5.10 where it can be seen that the highest water consummation rate by the cooler was achieved when the relative humidity was 35%. Moreover, the water consumption increases with increasing of intake air channel velocity.

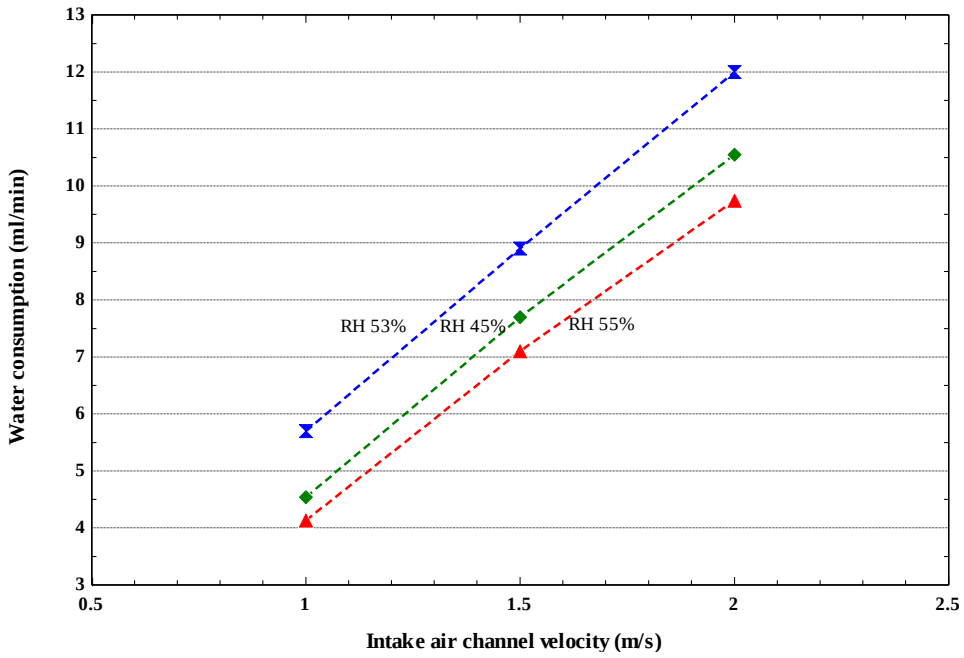

Figure 5.10 Effect of intake air channel and relative humidity in water consumption

5.4.6 The effect of relative humidity

The cooling capacity of the evaporative cooler per unit area of the available wet surface can be calculated from Equation (3.2).The lowest supply air temperature T_{do} that can be achieved depends on the design of the evaporative cooler (wet area

available, porous materials properties, air mass flow rates, etc.) and prevailing climatic conditions, particularly relative humidity.

The effect of varying inlet air relative humidity on the cooling capacity is further modelled and the results are shown in Figure 5.11. Three inlet air temperatures are considered: 30^{o} C, 35^{o} C, and 40^{o} C with relative humidity set at 35%, 40%, 45%, 50%, and 55%, with supply air mass flow rate remaining constant at 0.03 kg/s. Figure 5.11 shows that the cooling capacity and COP are strongly influenced by relative humidity; with both of them the cooling capacity and COP are inversely proportional to relative humidity. The lower the relative humidity level of the inlet air, the higher the cooling capacity and COP that can be obtained from the cooler system. This lead to diverted lower level of inlet air humidity into wet channel more moisture will absorb, since the larger driving force of mass transfer results from the greater vapour pressure difference between the air and the water interface when the inlet air humidity is lower.

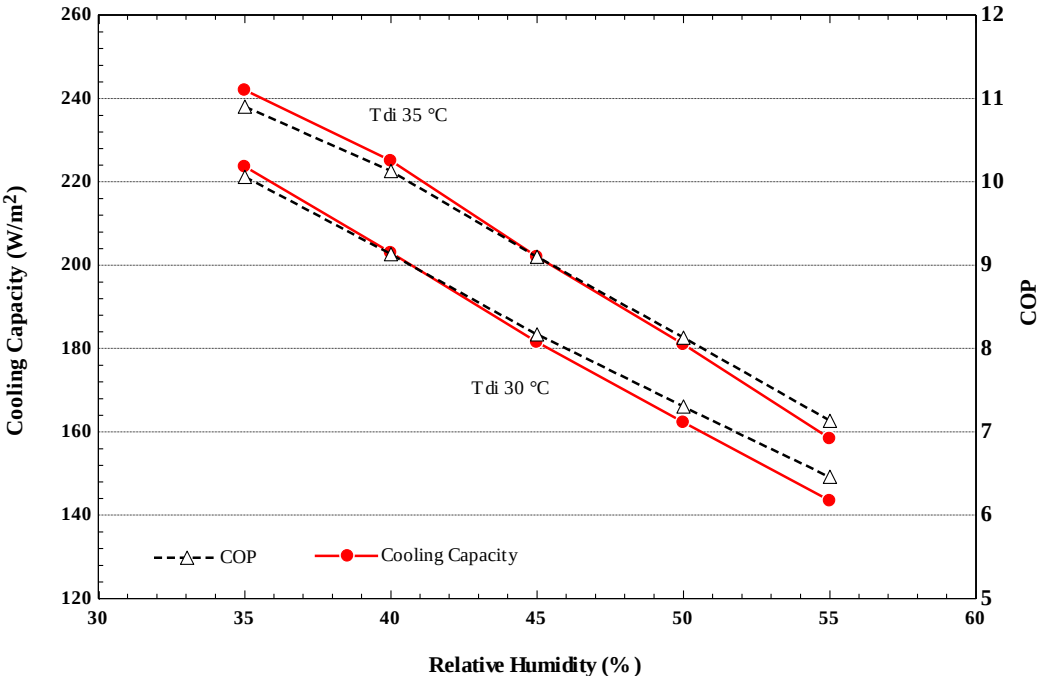

Figure 5.11 Effect of relative humidity on cooling capacity and COP

Furthermore, the effect of relative humidity on the wet bulb and dew point effectiveness was modelled for the same design inlet air conditions. Figure 5.12 shows that the wet bulb effectiveness at T_{di} of 35 ^{o}C inlet air temperature decreased from 1.058 to 1.0533 when relative humidity increased from 35to 55%, whereas the wet bulb effectiveness at T_{di} 30 ^{o}C inlet air temperature varied from 1.056 to 1.053 with increasing of the relative humidity. However, the dew point effectiveness steadily increased with the increase of relative humidity for both inlet air temperatures. From the above analysis it can be noted that a higher inlet air temperature gives a higher wet bulb and dew point effectiveness. Moreover, by increasing inlet relative humidity, higher dew point effectiveness can be achieved due to increasing of product air temperature.

The sub wet bulb temperature evaporator cooler would achieve a high thermal performance with wet bulb effectiveness higher than unity (which is the maximum effectiveness a direct evaporative cooler could achieve), reducing overall energy consumption of air conditioning in buildings.

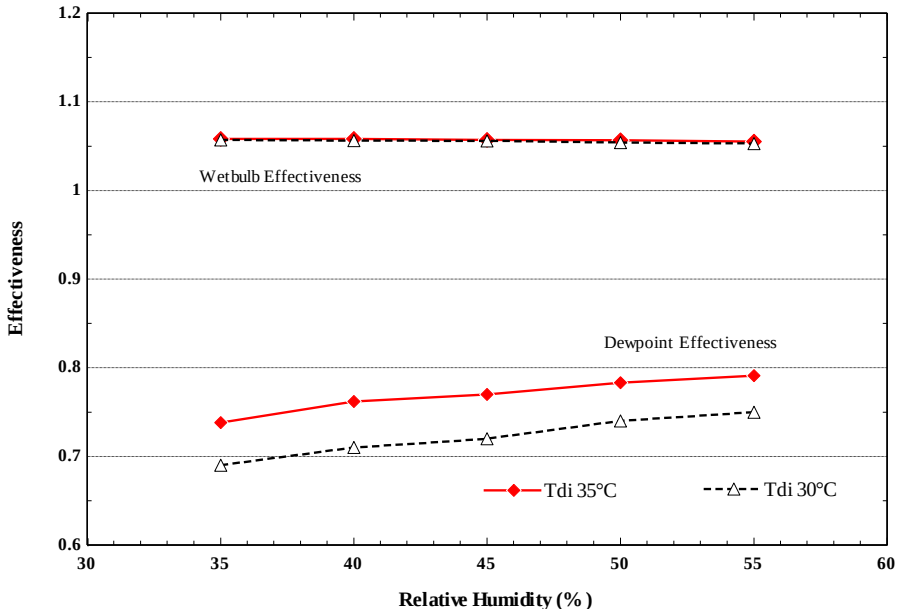

Figure 5.12 Effect of relative humidity on wet bulb and dew point effectiveness

Chapter 6

Design and testing of a porous Ceramic Sub-Wet Bulb Temperature Evaporative Cooler

6.1 Description of the experimental set-up

A laboratory test rig experiment was built to test the porous ceramic sub-wet bulb temperature evaporative cooler. The prototype consists of 15 porous flat ceramic containers which form a hollow wall structure, as shown in Figure 6.1.

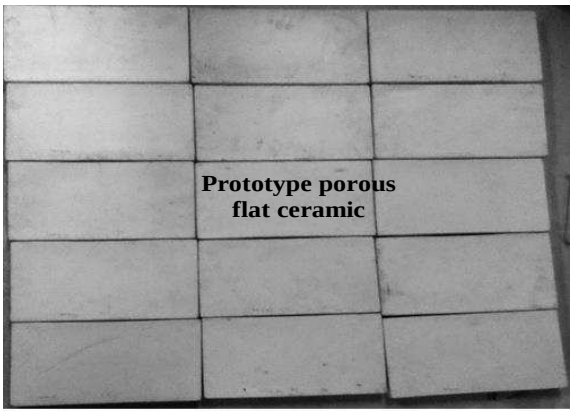

Figure 6.1 Ceramic panels

The porous ceramic panels were mounted on a frame in the form of a wall and filled with water through a water feed hose from an overhead tank, as shown in Figure 6.2 (a, b). The porous ceramic wall was sandwiched between two Perspex flat sheets forming two narrow air gaps to the front and back of the ceramic wall: the dry channel

and the wet channel. The dry channel side of the ceramic wall was sealed using a thin membrane as shown in Figure 6.2 b.

a) b)

Figure 6.2 Prototype porous flat ceramic and laboratory test rig experiment

The airflow in the dry and wet channel was circulated by a fan with a controlled mass flow rate, temperature, and relative humidity. The inlet air temperature and water content were controlled using an environmental chamber. The intake air velocity was adjusted by using a variable power supply to drive a DC powered rated between 16-24 Volts, shown in Figure 6.3.

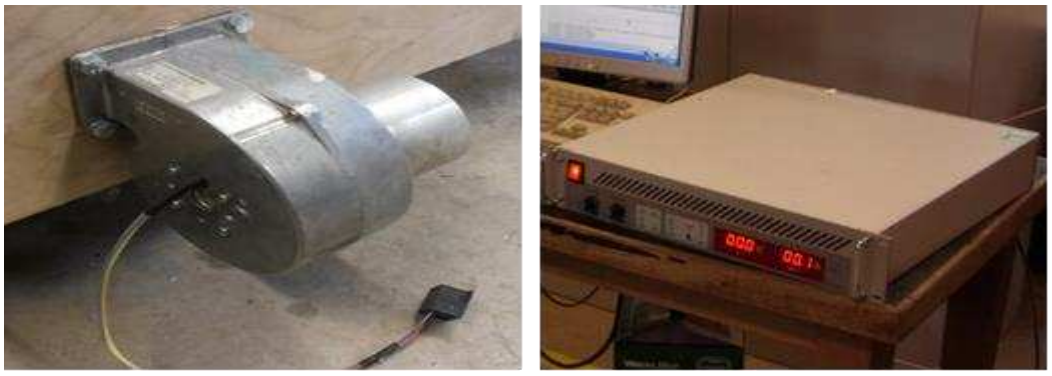

Fan power rating 16-24 Volts Transformer type LAB/SM 270

Figure 6.3 Fan and electrical power supply using to adjust the intake air velocity

6.2 Porous ceramic materials

The wet media material used in evaporative coolers is an essential component of an evaporative cooler. It is usually made of a porous material with large surface area and capacity to hold liquid water. Materials such as porous ceramic structures are also being developed combining various chemical elements and binders such as alumina (AL_2O_3), silicon oxides (SiO_2), nitrides (Si_3N_4) and non-silicate glasses are wide used in evaporative cooling applications.

Ceramics offer many advantages compared to other materials, including corrosion resistance, light weight, wide availability, and inexpensive price [81] in addition to accurately controlled pore size/porosity, elevated temperature capabilities, and capability of being produced in a variety of shapes and sizes to specific requirements and extension of its useful life under harsh conditions [82].

Figure 6.4 shows the chemical composition of the prototype porous ceramic materials that were used as the wet media in this design of a sub-wet bulb temperature evaporative cooler analysis to determine the chemical content and measure the porous size. The analysis was carried out as follows:

a. The ceramic sample was first washed with industrial methylated liquid
b. A carbon evaporation device was used to add a carbon layer on the surface of the porous ceramic sample.
c. SEM&EDS equipment was used to measure porous size and analyse chemical content.

a) Industrial methylated

b) Carbon evaporation

Sample after adding carbon

c) SEM & EDS

Figure 6.4 The process of investigation of chemical composition of the prototype porous ceramic materials

The results of the chemical analysis show that the chemical composition of the prototype porous ceramic materials is predominantly silica and alumina is shown in Table 6-1. Figure 6.5 illustrates the porous size and distribution of prototype porous ceramic materials when magnified.

Table 6-1 Chemical content of prototype porous ceramic container

SiO_2	Al_2O_3	Albite	MAD-10 Feldspar	Fe	Wollastonite	MgO	KCI
66.85%	25.68%	4.03%	2.07%	0.54%	0.42%	0.29%	0.11%

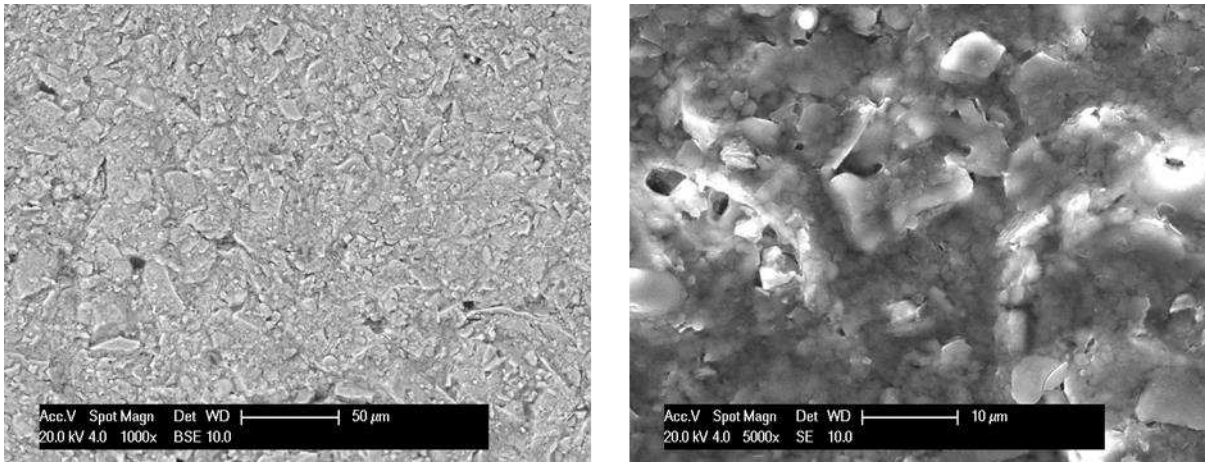

Figure 6.5 The porous size of prototype porous ceramic materials

6.3 Measurements and instruments

The rig was fully instrumented to measure the air temperature, relative humidity, and flow rates along the dry and wet channels. All thermocouples and humidity sensors were connected through a data logger device to a computer. Table 6-2 gives the main design parameters and measurement instruments used in the experiment and Figure 6.6 show date logger and airflow

Table 6-2 Parameters and measurement instruments used in the experiment

Parameters	Sensor type
Dry-bulb temperature of inlet air	K-type thermocouple range (-50 to +250 ^{0}c)
Relative humidity of inlet air	HygroClib S3 range (0-100 % rh)
Intake air, product air and working air velocity	Airflow TSI incorporated velocity rang (0-25 m/s)
Dry-bulb temperature of product air	K-type thermocouple range (-50 to +250 ^{0}c)
Relative humidity of product air	HygroClib S3 range (0-100 % rh)
Dry-bulb temperature of working air	K-type thermocouple range (-50 to +250 ^{0}c)
Relative humidity of working air	HygroClib S3 range (0-100 % rh)
Water supply ant water film temperature	K-type thermocouple range (-50 to +250 ^{0}c)

Data Logger series 2

Airflow TSI incorporated velocity

Figure 6.6 Data Logger and Airflow velocity

6.4 Laboratory rig testing procedure

i. The environmental chamber was first switched on and the temperature and relative humidity of the air established.

ii. The overhead water tank of the system was filled with water.

iii. The date logger and computer switched on, and all thermocouples were checked to ensure correct readings.

iv. The fan was started to circulate air from the environmental chambers and through the evaporative cooler until the system was stable.

v. The air temperature in the dry and wet channels was recorded using the data logger as well as water consumption.

6.5 Experimental results

The thermal performance of the laboratory porous ceramic evaporator was evaluated at temperatures of 30 and 35^{o}C and corresponding relative humidity of 35, 40, 45, 50, and 55(%).

6.5.1 The effect of inlet air velocity on effectiveness and product air temperature

The test rig results of the effect of varying intake air velocity on the wet bulb effectiveness and product air temperature are shown in Figure 6.7. The intake air velocity considered ranged between 1 m/s to 3 m/s with two inlet air temperatures at 30^{o} C, 35^{o} C, (i.e., wet bulb temperature $T_{wbi,}$ of 18.9 ^{o}C and 23^{o}C respectively and relative humidity set at 35%). From Figure 6.7 it can be seen that the wet bulb effectiveness decreased with increasing of velocity of intake air channel whereas the product air temperature increased almost linearly with increasing air velocity. This is due to the decreased evaporation rate with increasing intake air channel velocity, because when the working air velocity increases the time of contact between the working air and wet surfaces will be reduced, which results in a decreased capacity of moisture absorbed by working air in the wet channel .

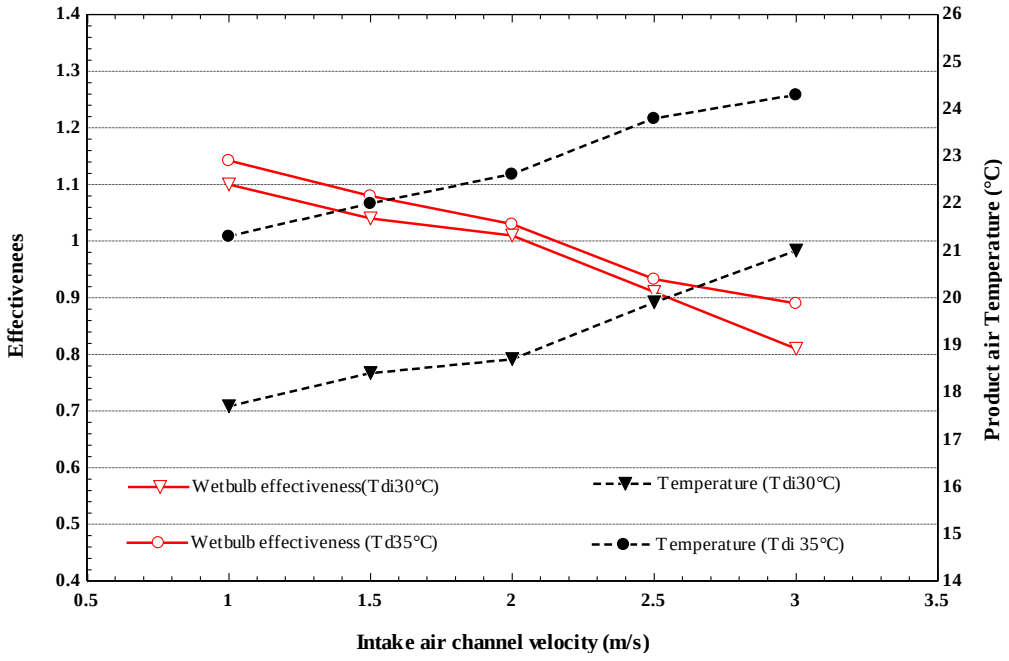

Figure 6.7 Effect of intake air channel velocity on effectiveness and product air temperature

6.5.2 Cooling performance

For an inlet air temperature of 35°C and relative humidity of 35% (i.e., wet bulb temperature, $T_{wb,}$ of 23°C and dew point of 17.9°C), the steady state measured supply air temperature (airflow temperature at the exit of the dry channel) was 22.7 °C, a drop of 12.2 °C, at a mass flow rate of 0.03kg/s, as shown in Figure 6.8.

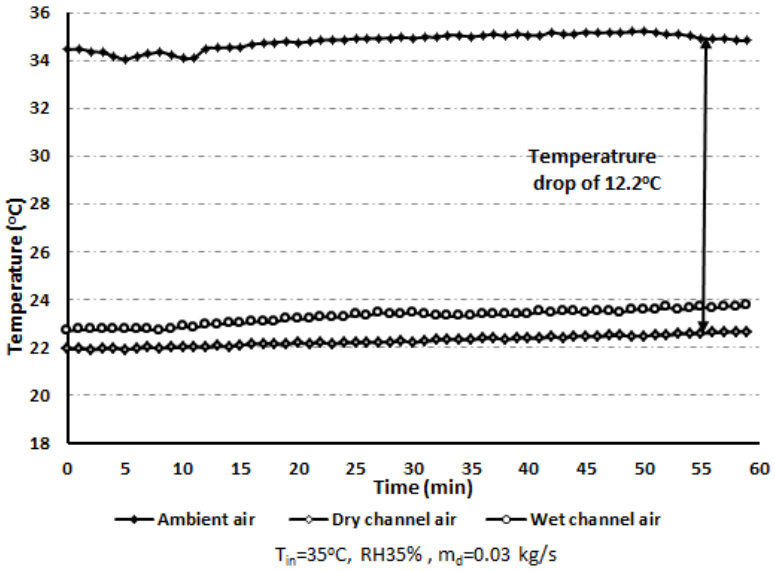

Figure 6.8 Recorded temperature profile in the wet and dry channel

6.5.3 The effect of intake air channel and relative humidity on water consumption

Figure 6.9 compares the amount of water consumption collected from the water drain of the cooler and the water consumption of the cooler by using Equation (3.5). The air inlet relative humidity considered was 35% and 55% with inlet dry air temperature set at 35 °C and air velocity ranged from 1 to 2 m/s. The results of this comparison indicated that the differential between them is small and the highest values can be achieved when inlet relative humidity is low. In addition, water consumption for both of them increases with increasing intake air channel velocity.

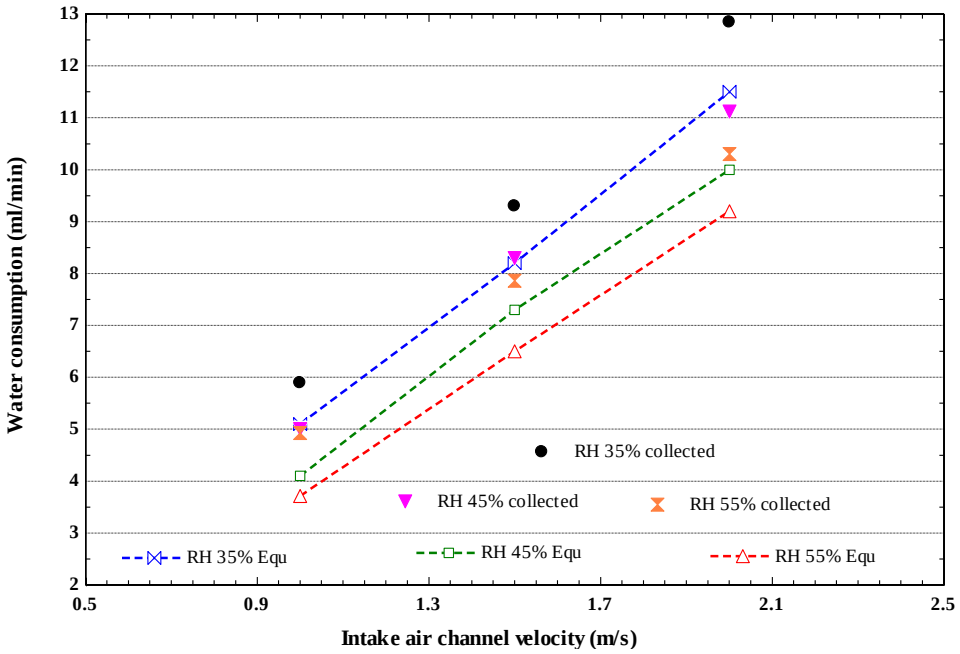

Figure 6.9 Effect of intake air channel velocity and relative humidity on water consumption

6.5.4 The effect of relative humidity on cooling capacity, COP and wet bulb and dew point effectiveness

The effect of varying inlet air relative humidity on cooling capacity and COP is shown in Figures 6.10 for two inlet air temperatures held at 30 ^{o}C and 35 ^{o}C with relative humidity set at 35%, 40%, 45%, 50%, and 55%, while the supply air flow rate remains constant at 0.0031 kg/s. It was shown that the cooling capacity and COP are strongly influenced by relative humidity when both of them are inversely proportional to relative humidity. The lower the relative humidity level of the inlet air, the higher the cooling capacity and COP that can be obtained from the cooler system. This led to diverted lower level of inlet air humidity into wet channel more moisture will absorb, since the larger driving force of mass transfer results from the greater vapour pressure difference between the air and the water interface when the inlet air humidity is lower.

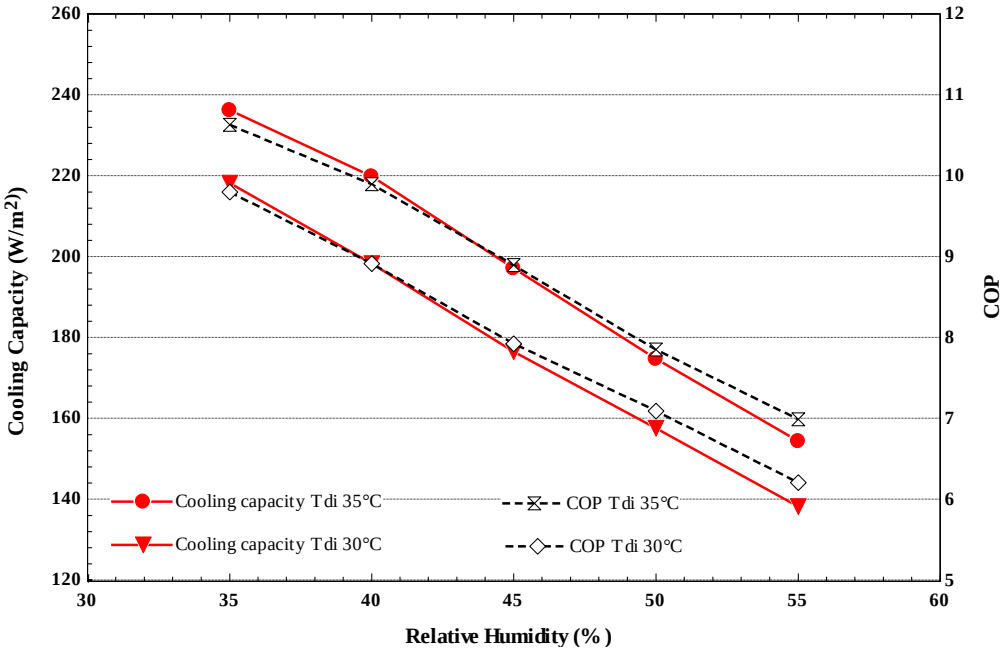

Figure 6.10 Effect of relative humidity on cooling capacity and COP

For the same test conditions, the effectiveness of the cooling system was shown in Figure 6.11. It can be seen that unlike the wet bulb effectiveness, which remains overall constant, the dew point effectiveness increases slightly as the relative air humidity is increased.

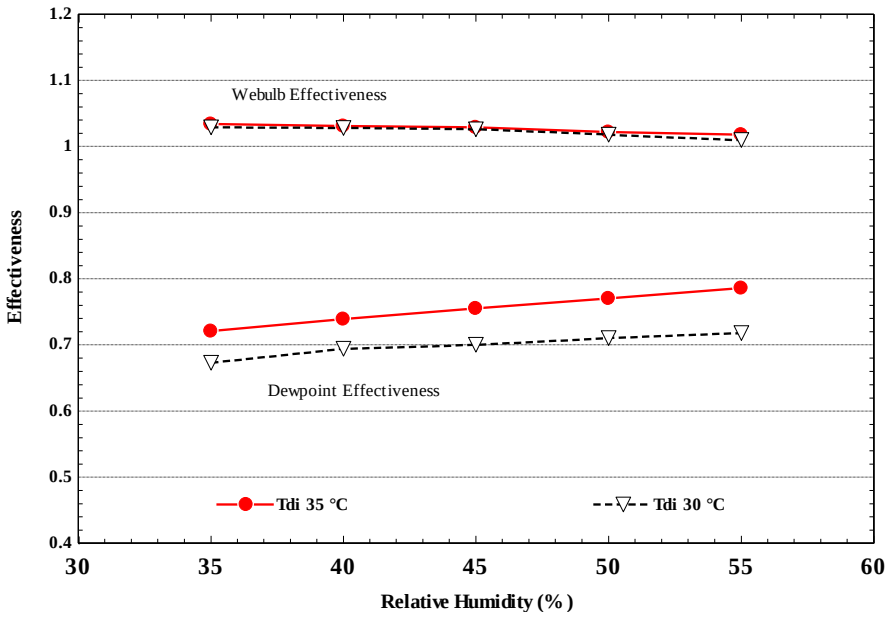

Figure 6.11 Effect of relative humidity on the wet bulb and dew point effectiveness

The wet bulb and dew point effectiveness are evaluated from Equations (3.4) and (4.1) respectively. The wet bulb effectiveness for inlet air temperature of 30 ^{o}C changed from 1.04 to 1.01 and at 35 ^{o}C it varied between 1.05 and 1.025. However, the dew point effectiveness increased with increasing inlet relative humidity; the dew point effectiveness at 35 ^{o}C varied between 0.75 and 0.81 and at 30 ^{o}C it decreased from 0.68 to 0.74. Therefore, it can be noted that higher inlet air temperature gives a higher wet bulb and dew point effectiveness and by increasing inlet relative humidity, a higher dew point effectiveness can be achieved due to increasing of the product air temperature.

6.6 Comparison between modelling and experimental results

6.6.1 The effect of inlet air velocity on effectiveness and product air temperature

Figure 6.12 compares the effectiveness and product air temperature results of modelling and lab tested when the intake air channel velocity varies between 1.0 (m/s) to 3.0 (m/s) and air inlet temperature is set at 35 with 35% relative humidity. The numerical model results show good agreement with the experimental findings. Higher intake air velocity gives a higher product air temperature and lower effectiveness. For velocity less than 2 m/s, the product air for both findings are below their wet bulb temperature and the wet bulb effectiveness also for both results are above 100% when also the intake air velocity is below 2 m/s.

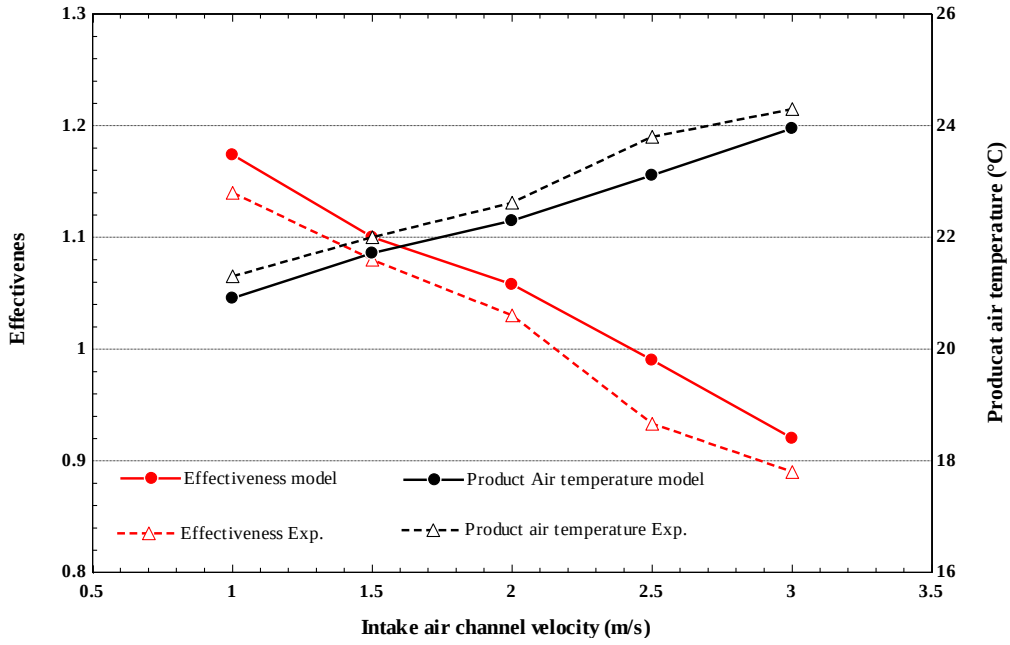

Figure 6.12 Effect of intake air channel velocity on wet bulb effectiveness and product air temperature

6.6.2 The effect of the duct length on product air, working air and water film temperature

The airflow temperature profile along the dry and wet channels is given in Figure 6.13. The computer model predicts that the airflow in the dry channel would be cooled to 22.2^{o} C, achieving sub-web bulb temperature conditions. The airflow along the wet channel, on the other hand, increased from 22.2 ^{o}C to 26.2^{o} C, as it gains latent heat from evaporated water on the surface of the ceramic panels. The experimental measurements, however, show the air temperature at the outlet of the dry channel is about 22.7^{o}C and that of the wet channel is 23.2^{o}C. The discrepancy between the experimental and computer model results, though within the measurement uncertainties of the instruments, is mainly attributed to difficulties in obtaining a uniform airflow distribution in the dry and wet channels.

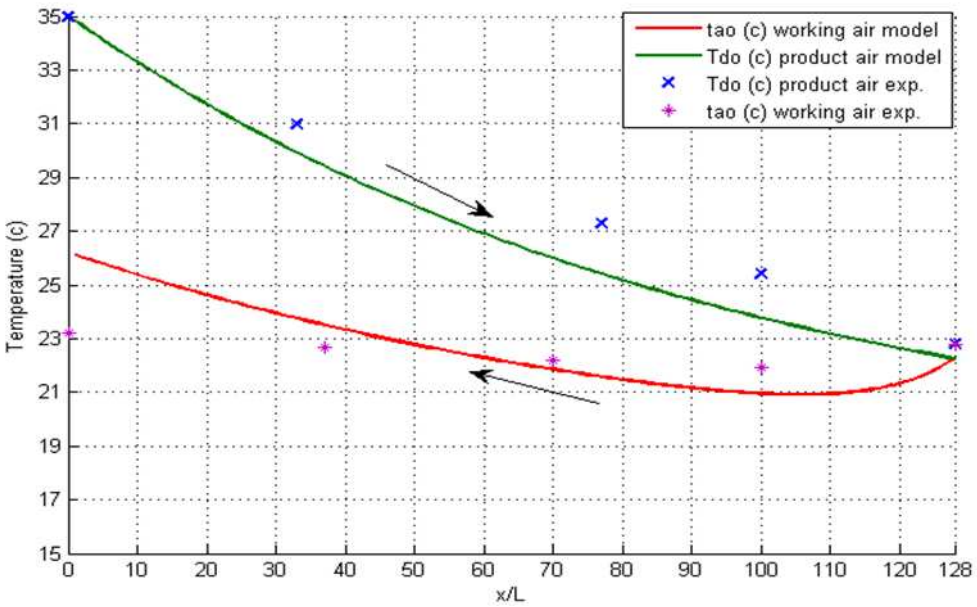

Figure 6.13 Effect of the duct length on product air, working air and water film temperature

6.6.2 The effect of cooler configuration on humidity ratio

Figure 6.14 shows the difference between the modelling result and lab test for humidity ratio of product air and reject air. Form this Figure it can be seen that although the modelling and rig have the same inlet air conditions (i.e., T_{di}=35 and humidity ratio of 12.3 g/kg$_d$), the values of humidity ratio for product air in the dry channel are different. In the modelling the humidity ratio of product air remained constant while it increased from 12.3 g/kg$_d$ to 22 g/kg$_d$ in the wet channel for reject air. However, in the experiment the humidity ratio increased in both channels; it increased from 12.3 g/kg$_d$ to 14.2 g/kg$_d$ in the dry channel for product air and it continued to increase to 16.8 g/kg$_d$ in the wet channel for reject air.

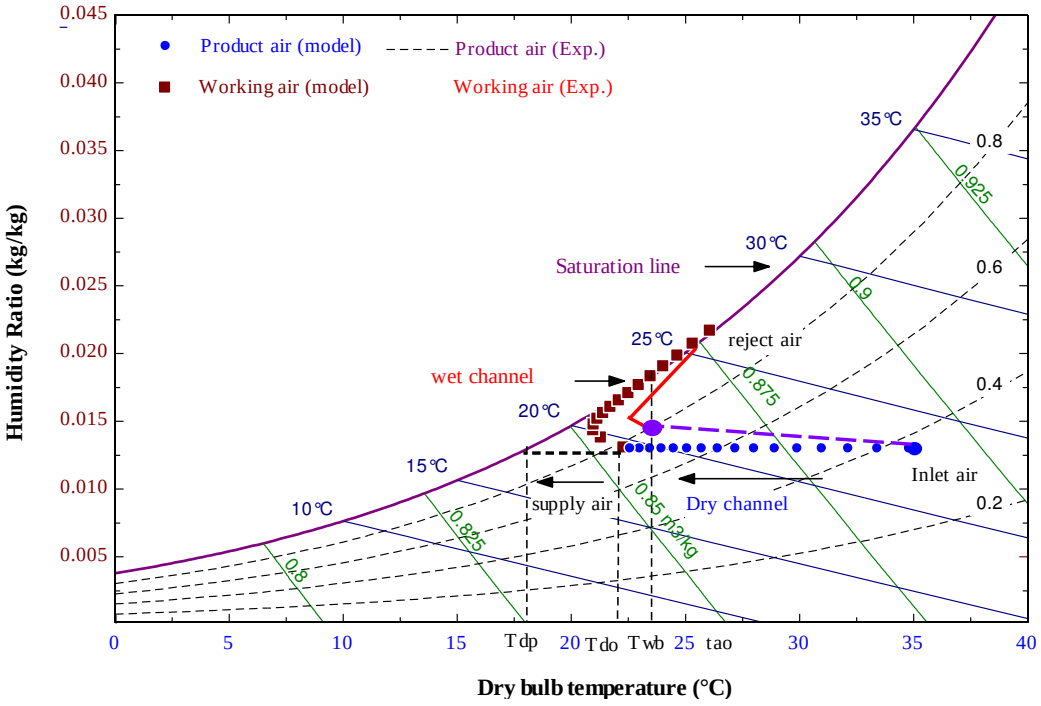

Figure 6.14 Effect of cooler configuration on humidity ratio

6.6.4 The effect of intake air channel and relative humidity on water consumption

The effect of varying intake air velocity and inlet relative humidity on water consumption was compared between the modelling and experimental results. Inlet dry air temperatures set at 35 ^{o}C with two air inlet relative humidity were considered: 35% and 55%, and air velocity ranged from 1 to 2 m/s. The results of this comparison are shown in Figure 6.15

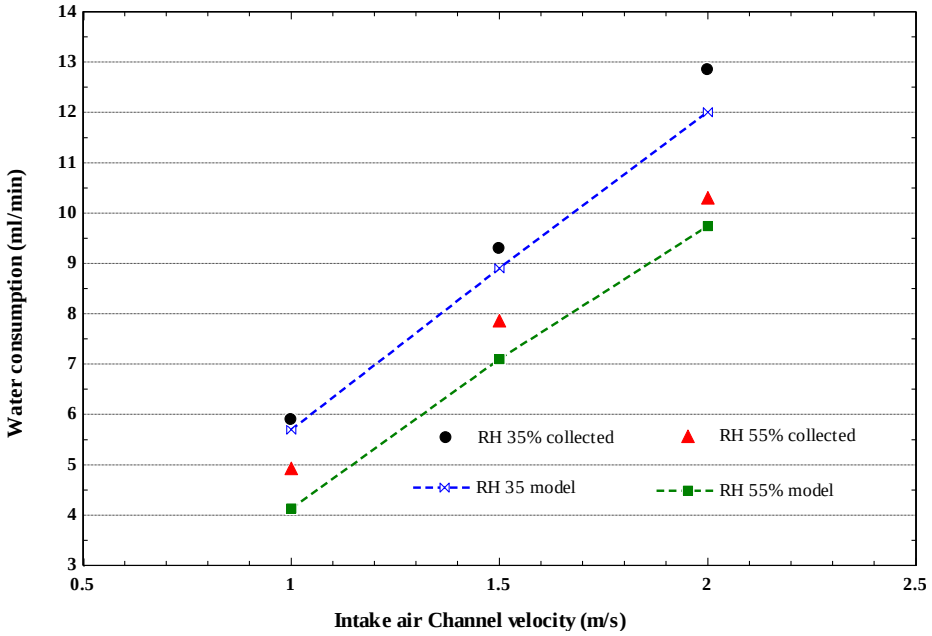

Figure 6.15 Effect of intake air channel and relative humidity on water consumption

6.6.5 The effect of relative humidity on cooling capacity, COP and wet bulb and dew point effectiveness

The modelling results and lab test of the effect of relative humidity on cooling capacity, COP, and wet bulb and dew point effectiveness were comparative with inlet air conditions (i.e., Tdi 35^{o}C, mass flow rate 0.03 kg/s and relative humidity set between 35% and 55%). Figure 6.16 indicated that the lower the inlet relative humidity, the higher the cooling capacity and COP obtained from the collar system.

Figure 6.17 on the other hand, shows that both effectiveness values of modelling and lab tested changed very little with increased relative humidity. It is also shown that similar trends between measured and modelled results were obtained as well as close design values.

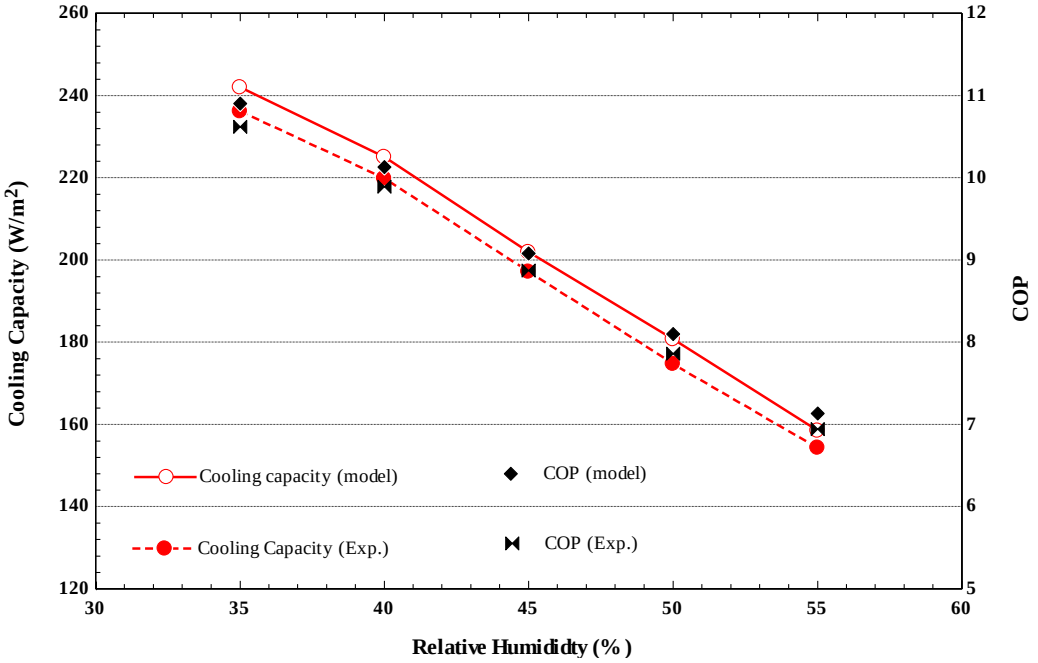

Figure 6.16 Effect of relative humidity on cooling capacity and COP

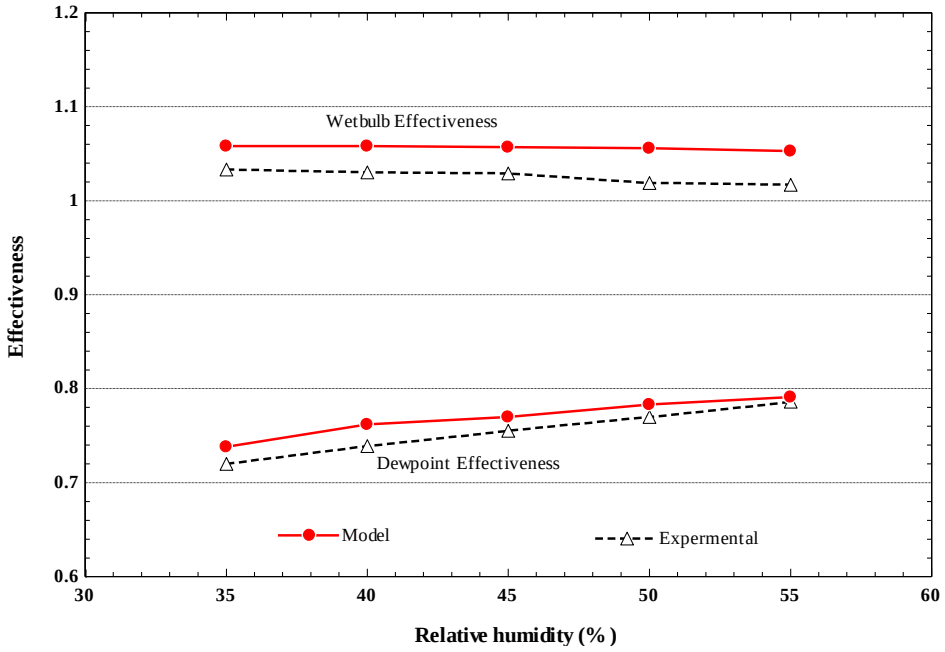

Figure 6.17 Effect of relative humidity on wet bulb and dew point effectiveness

6.7 Comparative performance of current sub-wet bulb temperature evaporative coolers using porous ceramic materials against other published works of direct evaporative cooling systems using porous ceramic

The effect of the temperature drop (difference between inlet air temperature and outlet ΔT) on the cooling capacity of the current work was compared to other works of direct evaporative cooling system using porous ceramic as wet media. Figure 6.18 shows the modelling and experimental results of the cooling capacity for current sub-wet bulb temperature evaporative coolers using porous ceramic materials presented in chapter five and six, and other three works by Ford et al., E. Ibrahim and Musa of direct evaporative cooling systems using porous ceramic. From this figure, it can be seen that the cooling capacity increased with the temperature drop, and the highest values of cooling capacity and temperature drop achieved the current configuration of the sub-wet bulb temperature.

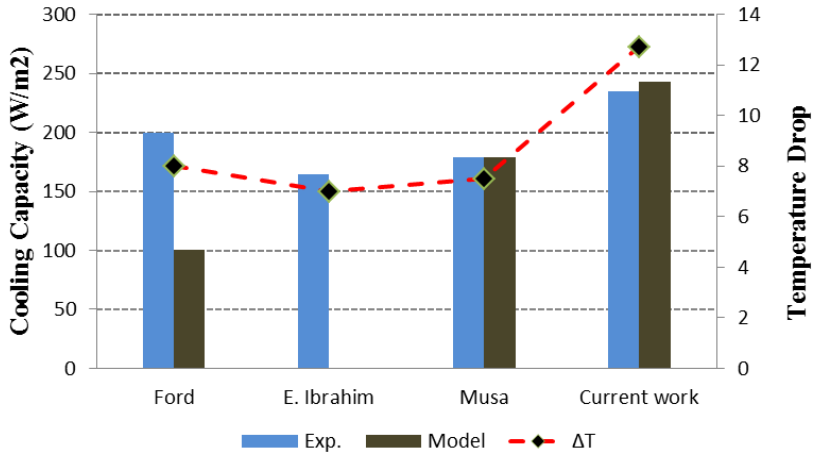

Figure 6.18 Modelling and experimental results of the cooling capacity for current sub-wet bulb temperature evaporative cooler using porous ceramic materials, and other three works by Forod et al, E. Ibrahim and Musa of direct evaporative cooling systems using porous ceramic

The modelling and lab tested results of water consumption and the effectiveness for the current sub-wet bulb temperature evaporative cooler using porous ceramic

materials were compared with the direct evaporative cooling system using the same materials carried out by Musa. For both systems, the air inlet temperature was set at 35 with 35% relative humidity and numerical model results as shown in Figure 6.19 It can see that high water consumption provides a high effectiveness as shown from the current work results. From the results of Figure 6.19 it can be indicated that, although the water consumption of the current sub-wet bulb temperature evaporative coolers using porous ceramic materials is higher than other works on direct evaporative systems using the same materials as wet media, the cooling capacity and effectiveness are higher. This means that the performance of the current system is higher than other direct evaporative cooling systems using porous ceramic as wet media because an optimised design of the evaporative cooling system is a compromise between effectiveness and cooling capacity.

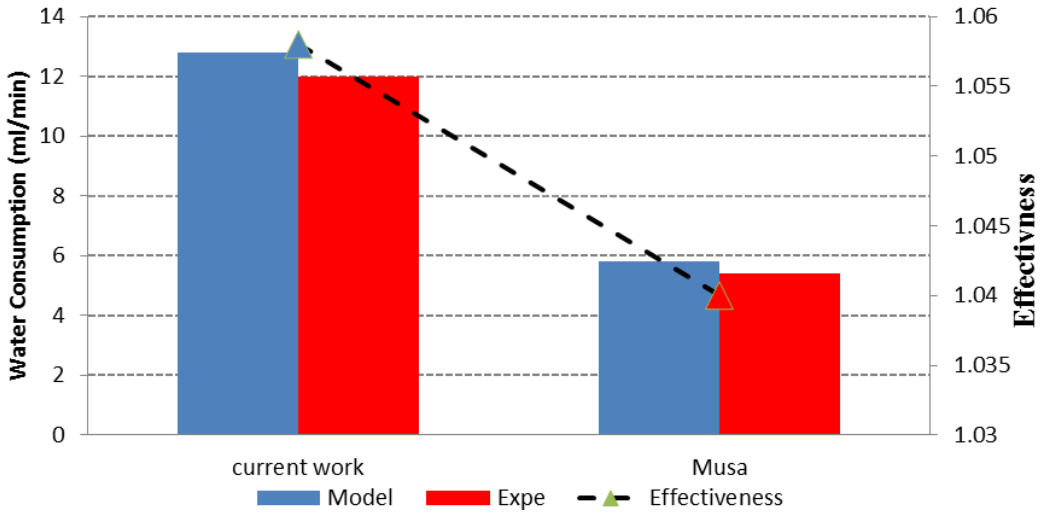

Figure 6.19 Water consumption and effectiveness for current work and Musa work

Chapter 7

Heat pipe-ceramic panels integrated evaporative cooling system

7.1. Introduction

In this arrangement, the heat transfer between the two separate airflows in the dry and wet channels is performed using heat pipes. Heat pipes are passive heat transfer devices with high heat transfer capabilities. The sensible heat exchange between the dry channel and wet channel is accomplished at a minimum temperature drop.

7.2 Description of the system

Similar to the previous rig, porous ceramic panels were used as wet media for water evaporation with the same specific wettability properties. Cylindrical heat pipes with a finned evaporator section were used for heat transfer between the supply airflow in the dry channel and working airflow in the wet channel as shown in Figure 7.1.

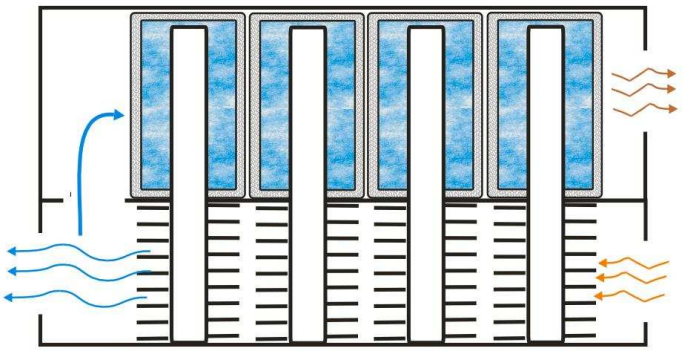

Figure 7.1 A schematic of heat pipe based porous ceramic IEC system

The porous ceramic water containers were placed in a narrow rectangular duct formed using Perspex sheets. The ceramic containers were filled with water which seeped through the micro-pores to form a thin water film on the surface. Air flow around the ceramic containers causes continuous water evaporation from the ceramic surface and subsequently cools the water inside the container. The heat pipes straddle both the dry and wet air channels through which the air supply is cooled indirectly in the dry channel and at constant moisture content.

In operation, when heat is applied to the finned heat pipe section in the dry channel (evaporator), the liquid fluid inside the heat pipe heats up and evaporates. The water vapour then travels along the heat pipe's hollow centre core to the condenser section which is surrounded from the outside by the water body of the ceramic container. The wet channel air flow causes the water from the ceramic container to evaporate and cools in the process the condenser of the heat pipe. The water vapour inside the heat pipe is then condensed to liquid and releases its latent heat and returns to the evaporator section. Figure 7.2 show a cross section of the finned heat pipe.

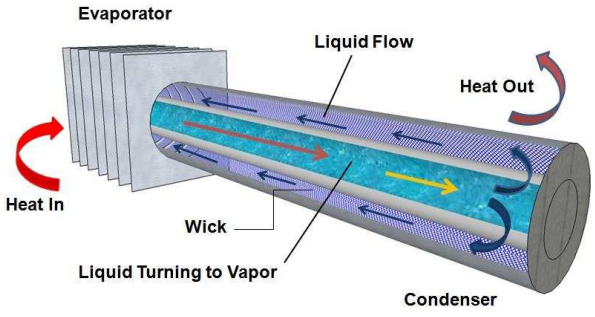

Figure 7.2 Heat pipe structure

7.3 Mathematical model

In the model, the dry and wet channels were divided into small finite and each heat pipe is considered as one control volume where the air properties are homogeneous, as shown in Figure 7.3. The energy and mass conservation equations given in Chapter 5 were equally applied for this design arrangement to evaluate the temperature, moisture content, and heat evolution in both the dry and wet channels. The heat exchange process between the heat pipe working fluid and that of the airflows in the dry and wet channels is very complex and to simplify the analysis, a number of assumptions have been made:

i) The air properties and heat and mass transfer coefficients are constant in each finite control volume.
ii) The masses of product air (m_d) and working air (m_w) are small.
iii) The air velocity of both channels is low to make the air flow laminar.
iv) There is no heat transfer to the surroundings.
v) The air-water interface temperature is assumed to be same as the water film temperature.
vi) To complete the computer model, the initial conditions used in the computer model include known inlet airflow properties for the dry and wet channels and all external surfaces are adiabatic.

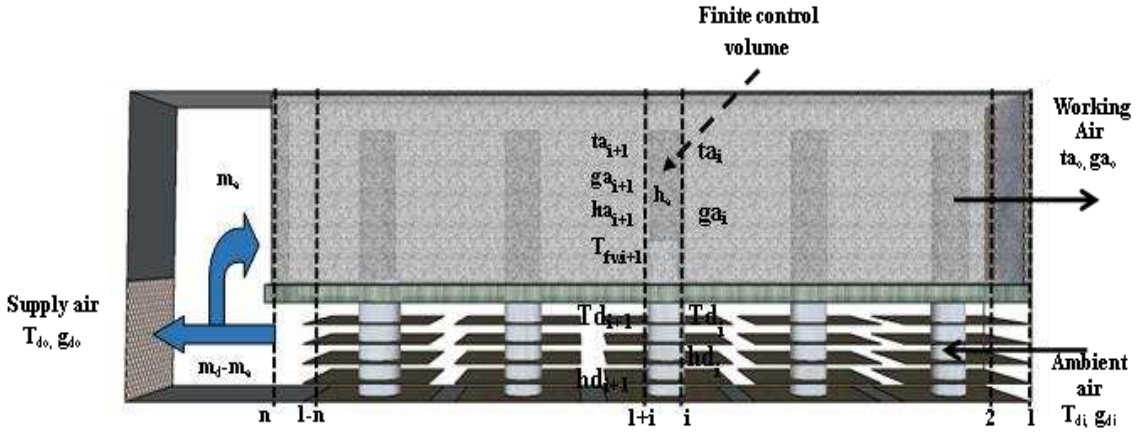

Figure 7.3 Air flow parameters modelling

In this analysis, the heat pipe was modelled using equivalent thermal resistance as heat is transferred in different parts of the heat-pipe ceramic panel module. Figure 7.4 shows a cross section of a module and the thermal resistance of each section.

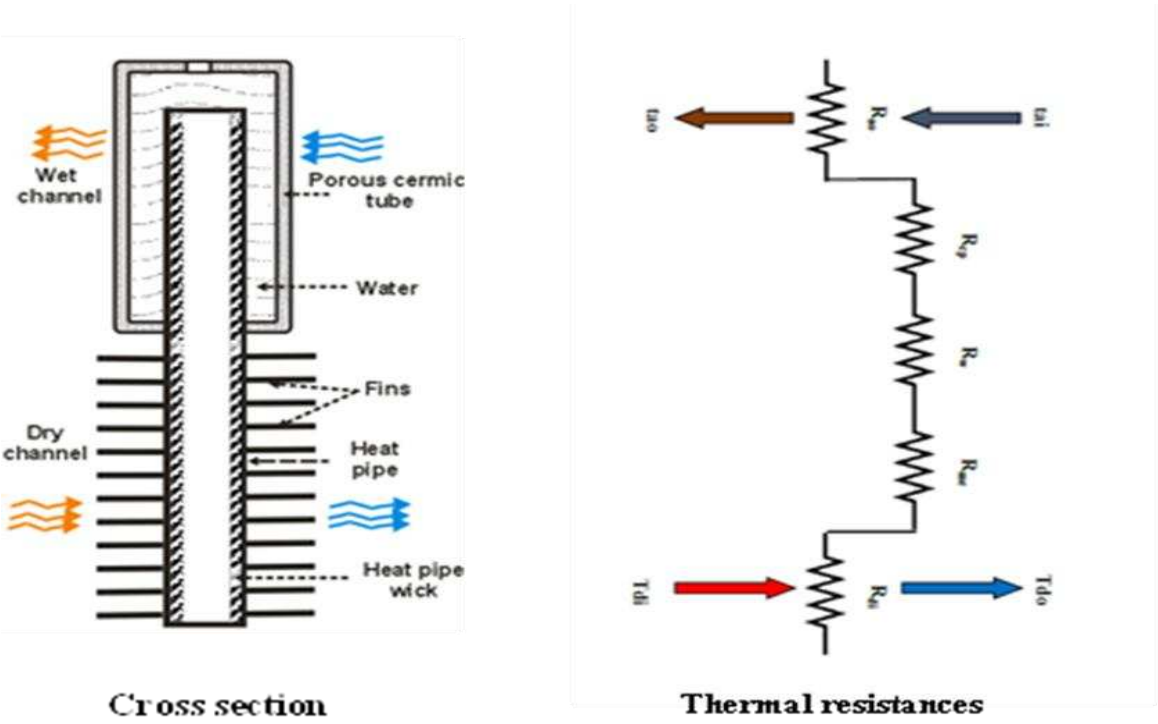

Figure 7.4 A cross section of module and the thermal resistance of each section

The overall heat transfer coefficient of the heat pipe-ceramic panel arrangement, k_s, can be expressed as function of thermal resistance, as following:

$$k_s = \frac{1}{R_{di} + R_{me} + R_w + R_{cp} + R_{ao}} \tag{7.1}$$

The thermal resistance of each section is explained in the following sections.

7.3.1 Thermal resistance of the dry channel

The thermal resistance of the finned section of the heat pipes in the dry channel is given as:

$$R_{di} = \frac{1}{\eta_f \alpha A_f} \tag{7.2}$$

Where, α is the heat transfer coefficient, A_f the finned section heat transfer area, and efficiency of the finned section heat exchanger, η_f can be given by [101]:

$$\eta_f = \frac{\tanh ml}{ml} \tag{7.3}$$

Where parameter m, which depends on the fin properties, is given by:

$$m = \left(\frac{2h}{\lambda_f \delta_f}\right)^{1/2} \tag{7.4}$$

δ_f is the fins thickness and λ_f the fins thermal conductivity.

7.3.2 Thermal resistance of the heat pipe wick of the evaporator and condenser

The analysis of the heat transfer from the dry channel air through the heat pipe assumes that the heat pipe thermal wall's resistance is negligible given that the thermal conductivity of copper is high (380 W/m^2K) compared to the thermal resistance of the saturated wick. The thermal resistance of the tubular wick mesh can be expressed as:

$$R_{me} = \frac{\ln(\frac{r_2}{r_1})}{2\pi l_1 \lambda_{wick}} \tag{7.5}$$

Where r_1, r_2 and l_1 are the inner, outer and length of the wick respectively and λ_{wick} is the effective thermal conductivity of the wick which is expressed as:

$$\lambda_{wick} = \frac{\lambda_1[\lambda_1 + \lambda s - (1-\phi_{wick})(\lambda_1 - \lambda_s)}{\lambda_1 + \lambda_s + (1-\phi_{wick})(\lambda_1 - \lambda_s)} \tag{7.6}$$

Where λ_1 and λ_s are thermal conductivity of the liquid phase of the working fluid and thermal conductivity of heat pipe wick material respectively and ϕ_{wick} wick porosity.

7.3.3 Thermal resistance of the water in the ceramic container

In this analysis, it is assumed that the water layer between the heat pipe outer wall and the ceramic container inner wall is static and the water flow rate due to evaporation is very small and does not affect the overall temperature of the bulk water volume. This is expressed as:

$$R_w = \frac{d_w A_{dh}}{\lambda_w} \tag{7.7}$$

Where d_w water thickness and A_{dh} hydraulic diameter of rectangular ducts which is expressed as:

$$A_{dh} = \frac{2(ab)}{(a+b)}$$

Where a and b are width and height of the duct respectively

λ_w water thermal conductivity.

7.3.4 Thermal resistance of the saturated ceramic panel wall

The ceramic panel is a porous structure and saturated with water. The thermal resistance is given by:

$$R_{cp} = \frac{d_c A}{\lambda_{csw}} \tag{7.8}$$

Where the effective thermal conductivity is expressed in a similar way as that of the heat pipe mesh.

$$\lambda_{csw} = \frac{\lambda_w[\lambda_w + \lambda_c - (1-\phi_c)(\lambda_w - \lambda_c)]}{\lambda_w + \lambda_c + (1-\phi_c)(\lambda_w - \lambda_c)} \tag{7.9}$$

λ_c is the thermal conductivity of the dry ceramic container and ϕ_c is the ceramic container's porosity.

7.3.5 Thermal resistance of the wet channel

The thermal resistance of the wet channel is mainly dominated by the heat transfer coefficient between the ceramic panel wall and the air flow and is given by:

$$R_{ao} = \frac{1}{\alpha A} \tag{7.10}$$

Where the heat transfer coefficient, h, is dependent on the airflow properties and can be given by:

$$\alpha = \frac{Nu\lambda_c}{A} \tag{7.11}$$

Where Nu is Nusselt number and given by[100]:

$$Nu = 1.37(Ra\frac{D}{L})^{0.16} \tag{7.12}$$

Where Ra is Rayleigh number

Furthermore for computer modelling, non-dimensional equations from (5.8) to (5.11) in chapter five were applied to each finite volume element along the dry channel, water film, and wet channel length. The operating parameters, including airflow temperature profiles along the air ducts length, moisture content, and water film temperature, were performed iteratively until converging conditions were satisfied, giving a temperature difference between two consecutive iterations of less than 0.01^{o}C.

7.3.6 Mass transfer coefficient in the wet channel

It assumed that the air flow in the wet channel is in laminar regime and heat and mass transfer can be correlated by the Lewis number formula as follows [99]:

$$\mathbf{Le} = \frac{\alpha_a}{\sigma c_p} \tag{7.13}$$

Where the Lewis number is often in the range of 0.9 to 1.15 and to simplify the model it was taken to be 1.

7.4 Mathematical model analyses and results

The thermal performance of the porous ceramic evaporator cooler shown in Figure 7.1 was evaluated at temperature of 30 and 35^{o}C and corresponding relative humidity of 35% to 55%, prevailing weather conditions in most parts of the Middle East. The effect of intake channel air velocity on wet bulb effectiveness and product air temperature and also the effect of secondary to primary air ratio on cooler effectiveness were modelled to determine the appropriate inlet air velocity and the ratio of working to intake air of this cooler. After that, temperature profiles of air along the dry and wet channels, air moisture content along the wet channel, and temperature profile of the water film on the ceramic panel surface were further modelled. Furthermore, the effect of relative humidity on the cooling capacity and the wet bulb and dew point effectiveness of the cooler were calculated and analysed. The model was defined by the parameters given in Table 7-1.

Table 7-1 Main prototype characteristics

Design parameters	
Porous ceramic panel length	0.72 m
Porous ceramic panel width	0.04 m
Wet channel air gap	0.005 m
Numbers of heat pipes	12
Dry channel width	0.05m
Mass flow rate in the dry channel	0.0031 (kg/s)
Mass flow rate in the wet channel	0.00155 (kg/s)
Water supply temperature	23 (^{0}C)
Porous Ceramic properties	
Materials composition	Al_2O_3, SiO_2, Si_3N_4
Porosity	12%
Density	2300 kg/m^3
Thermal conductivity	1.5 W/mK

7.4.1 The effect of inlet air velocity

The effect of varying intake air velocity on the wet bulb effectiveness and product air temperature were modelled and the results are shown in Figure 7.5. Two inlet air temperatures were considered: 30^o C, 35^o C, with relative humidity set at 35% (i.e., wet bulb temperature, $T_{wbi,}$ of 18.9 ^{o}C and 23^{o}C respectively and air velocity ranged from 1 to 3 m/s. It can also be seen that the wet bulb effectiveness of both inlet air temperatures steadily decreased when the intake air velocity increased from 1 to 2 m/s then the wet bulb effectiveness of T_{di} 35 ^{0}C decreased gradually and the wet bulb effectiveness of T_{di} 30^{0}C fell slightly when the intake air velocity increased from 2 to

3 m/s. Moreover, it can be observed that the wet bulb effectiveness can be more than 1 when the intake air velocity is less than 2 m/s for both inlet air temperatures.

On the other hand, the product air temperature for both 30°C and 35°C inlet temperatures increased linearly with increasing intake air velocity, whereas the dew point temperature can be achieved in this cooler when the intake velocity also less than 2 m/s. This is due to the decreased evaporation rate with increasing intake air channel velocity, because when the working air velocity increases, the time of contact between the working air and wet surfaces will be reduced, which results in decreased capacity of moisture absorbed by working air in the wet channel. Therefore, to decrease the product air temperature for both inlet air temperatures below their wet bulb temperature and achieve a wet bulb effectiveness of more than 100%, the velocity should be set between 1 to 2 m/s for this cooler.

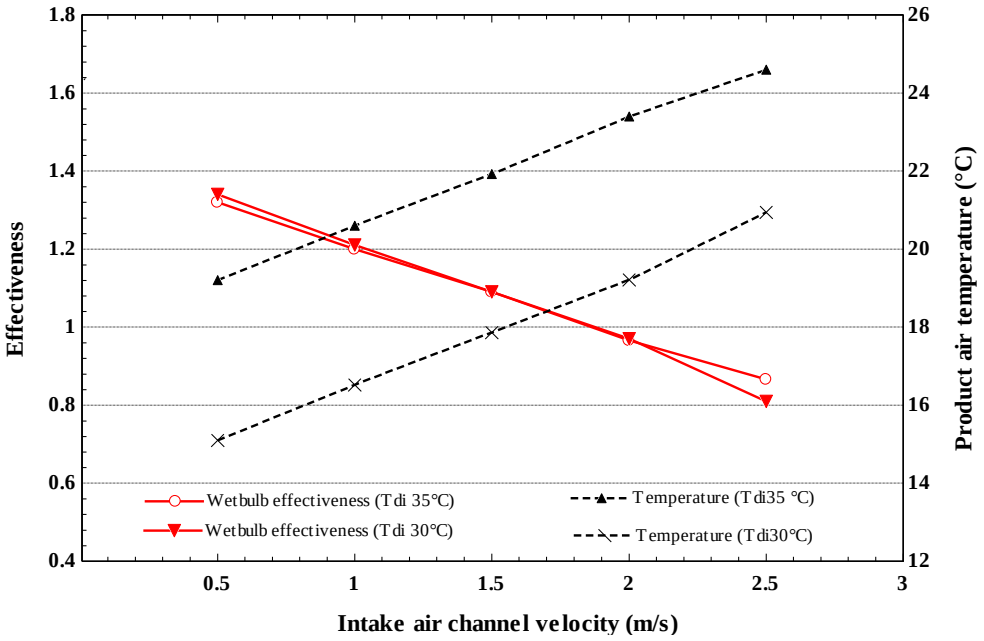

Figure 7.5 Effect of inlet air velocity on effectiveness and product air temperature

7.4.2 The effect of working to intake air ratio

The effect of working to intake air ratio on the cooler effectiveness is further modelled for 30 ^{o}C and 35 ^{o}C inlet air temperatures and intake air mass flow rate of 0.0031kg/s as shown in Figure 7.6. It shown that the wet bulb effectiveness of both inlet air temperatures rose steadily when the working to intake air ratio increased from 0.1 to 0.3, then they gradually increased with the increasing working to intake air ratio. Furthermore, it can be observes that the wet bulb effectiveness can be achieved at more than 100% when the working to intake air ratio ranges between 0.5 and 0.9. However, the dew point effectiveness of the inlet air temperature (Tdi 30 ^{0}C and Tdi 35 ^{0}C) gradually increased from 0.198 to 0.8 and from 0.21 to 0.84 respectively when the working to intake air ratio increased from 0.1 to 0.9. From this finding it can be noted that the cooled supply air should be reduced to increase the effectiveness of this cooler and the working to intake air ratio for this cooler should be set from 0.5 to 0.9 kg/kg.

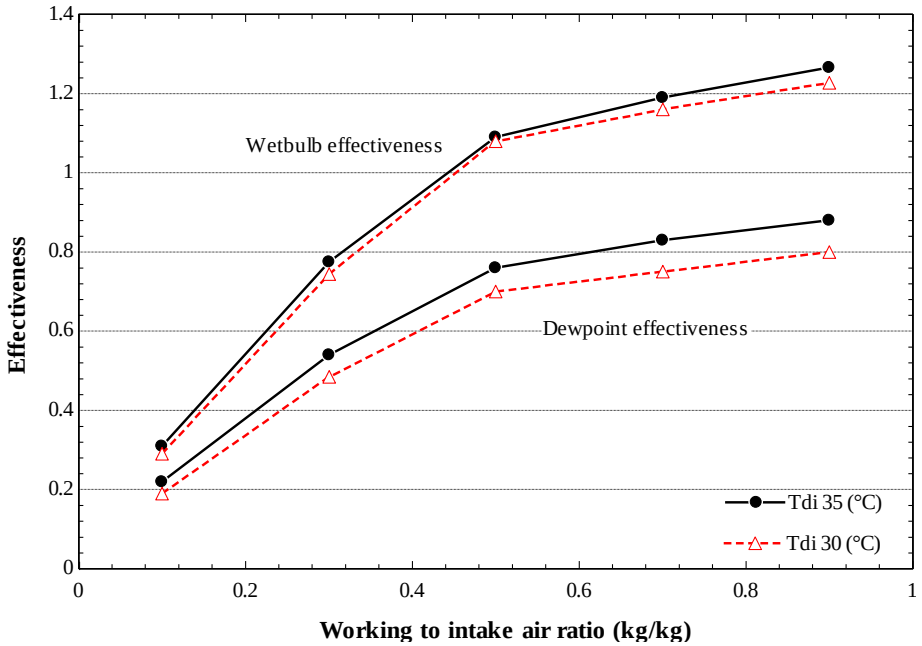

Figure 7.6 Effect of working to intake air ratio on wet bulb and dew point effectiveness

7.4.2 The effect of the duct length on product air, working air and water film temperature

For an initial inlet air (atmospheric air) temperature, T_{dbi}, of 35^{o}C and relative humidity of 35% (i.e., wet bulb temperature, $T_{wbi,}$ of 23^{o}C and dew point of 17.7^{o}C), supply water temperature 23c and mass flow rate of 0.0031kg/s, Figure 7.7 shows the computer model results of product air temperature distribution (T_{do}), working air (t_{ao}) and film of water (T_{fw}) in the sub-wet bulb temperature indirect evaporative cooling system. It can be seen that the temperature of the air in the dry channel decreases from 35 ^{o}C to 21.92 ^{o}C, which is below the wet bulb temperature (T_{wbi}), showing that the evaporative cooler would perform adequately in such climatic conditions. Another important property is that the water film temperature increases from 19.9 ^{o}C to 25.82 ^{o} C along the duct as the balance between heat gain from the air in the dry channel and heat loss by evaporation to the air in the wet channel is positive. The heat loss through evaporation of water to the air in the wet channel is reflected by the increase in both the airflow temperature and water content profiles along the channel. It can also be noticed that the working air temperature, t_{ao}, at the turning point of the airflow is higher than that of the water film and drops from 21.92 ^{o}C to 20.3 ^{o}C, which is below that of the water film, before resuming the normal trend and then being rejected at a temperature of 24.23 ^{o}C. The point at which the water film and wet air temperature profiles intersect depends on the design parameters of the evaporative cooler.

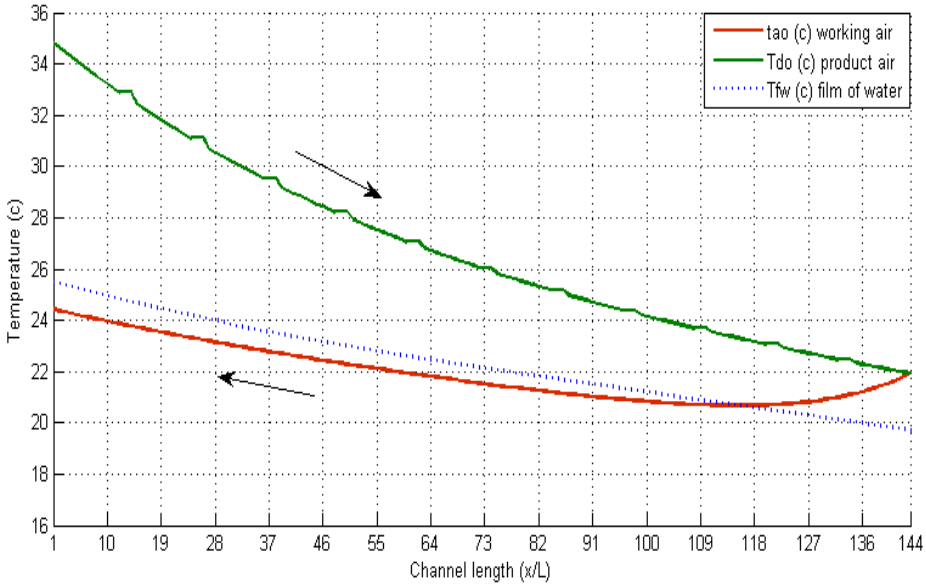

Figure 7.7 Effect of the duct length on product air, working air and water film temperature

7.4.3 The effect of cooler configuration on humidity ratio

The operating properties of the conditioned air in the sub-wet bulb temperature evaporative cooler are further shown on a psychometric chart of Figure 7.8. It can be seen that at design conditions of T_{di} of 35 ^{o}C and relative humidity of 35%, the conditioned air supply has a constant water vapour content of 12.3 (g/kg$_d$) and a temperature lower than the wet bulb temperature, with the ultimate cooling temperature that can be achieved equal to dew point temperature of 17.7 ^{o}C. Equally, Figure 7.8 shows that the working air circulated in the wet channel is rejected at saturation conditions when its characteristic coincides with that of the saturation line on the psychometric chart and exits the evaporative cooler at 24.23 ^{o}C and water vapour content increasing from 13 (g/kg$_d$) to 19 (g/kg$_d$).

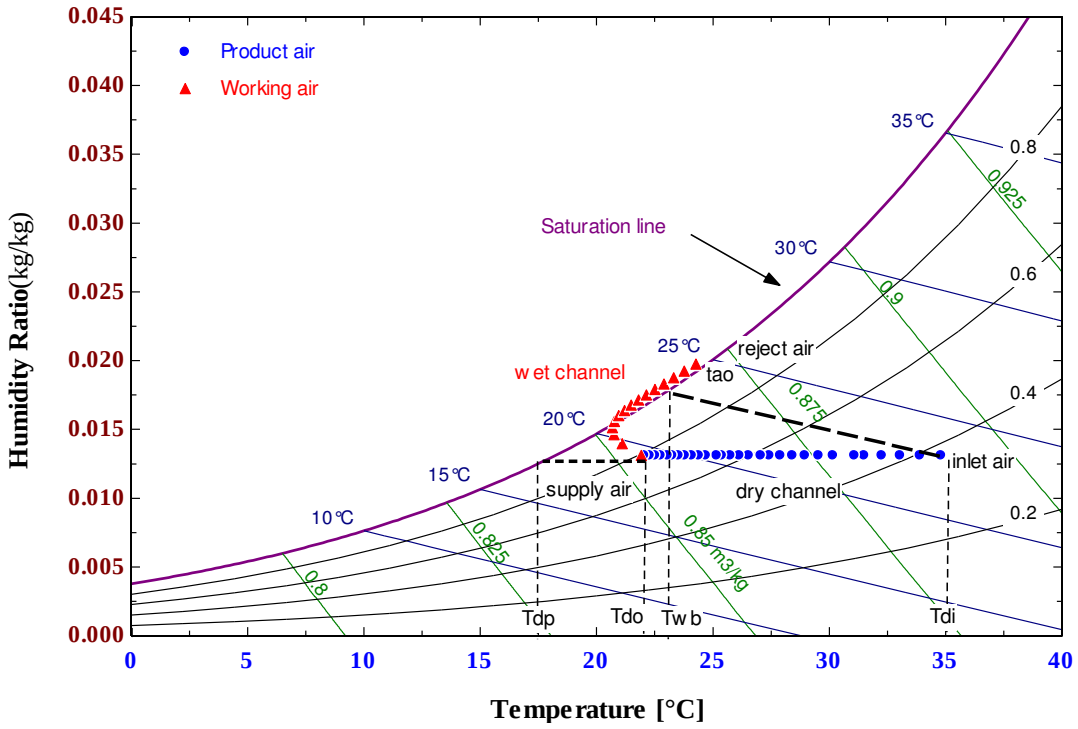

Figure 7.8 Effect of cooler configuration on humidity ratio

7.4.4 The effect of intake air channel velocity and humidity on water consumption

The effect of varying intake air velocity and inlet relative humidity on water consumption was modelled. Three air inlet relative humidities were considered: 35%, 45%, and 55% with inlet dry air temperature set at 35 ^{o}C set and air velocity ranged from 1 to 2 m/s. The results of the model are shown in Figure 7.9. It can be seen that the highest water consummated by cooler achieved when the relative humidity at 35%. Moreover, the water consumption increases with increasing intake air channel velocity.

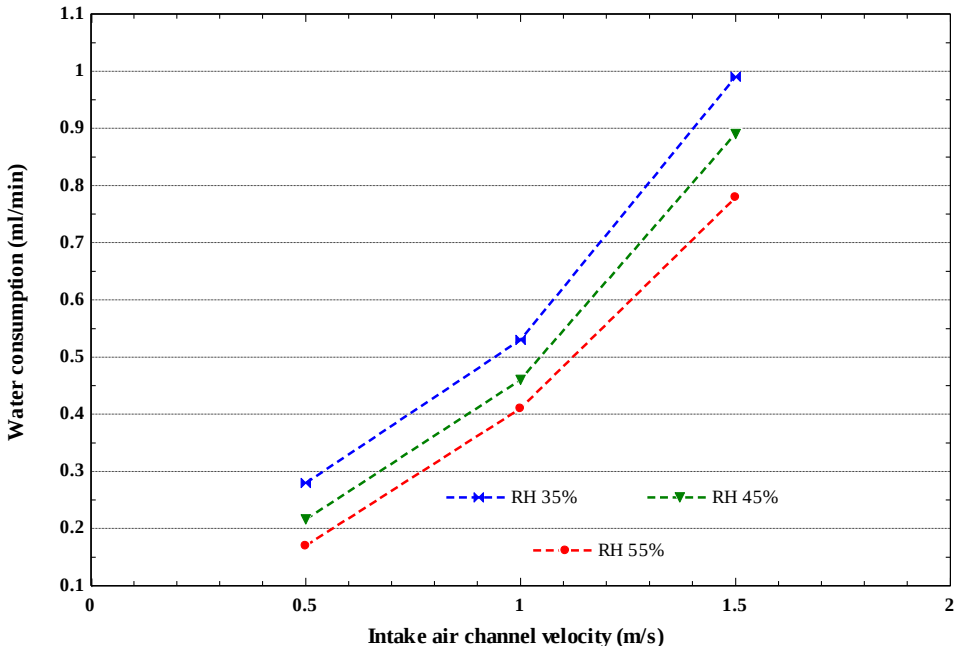

Figure 7.9 Effect of intake air channel velocity and relative humidity in water consumption

7.4.5 The effect of relative humidity on cooling capacity, COP, and wet bulb and dew point effectiveness

The effect of varying inlet air relative humidity on the cooling capacity and COP is further modelled and the results are shown in Figure 7.10. Two inlet air temperatures are considered: 30 ^{o}C, and 35 ^{o}C with relative humidity set at 35%, 40%, 45%, 50%, and 55% with supply air flow rate remaining constant, 0.0031 kg/s. Figure 7.10 shows that the cooling capacity and COP are strongly influenced by relative humidity with the cooling capacity and COP inversely proportional to relative humidity. Similarly the cooling capacity and COP decreased with increasing inlet relative humidity.

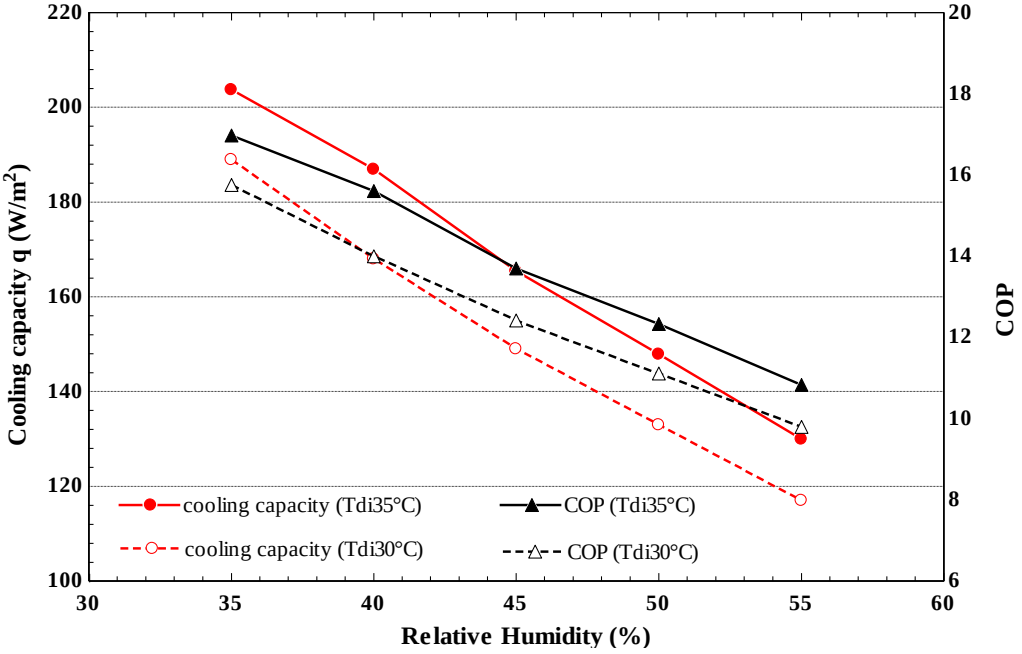

Figure 7.10 Effect of relative humidity on cooling capacity and COP

Moreover, the effect of relative humidity on wet bulb and dew point effectiveness was modelled for the same design inlet air conditions as shown in Figure 7.11. This shows that the wet bulb effectiveness of 30 ^{o}C 35 ^{o}C inlet air temperatures are close together and slightly decreased from about 1.085 when inlet relative humidity is at 35% to 1.05 when relative humidity is at 55%. However, the dew point effectiveness steadily increased with increasing inlet relative humidity for both inlet air temperatures 30 ^{o}C and 35 ^{o}C. The sub wet bulb temperature evaporator cooler would achieve a high thermal performance with wet bulb effectiveness higher than unit (which is the maximum effectiveness a direct evaporative cooler could achieve), reducing overall energy consumption of air conditioning in buildings.

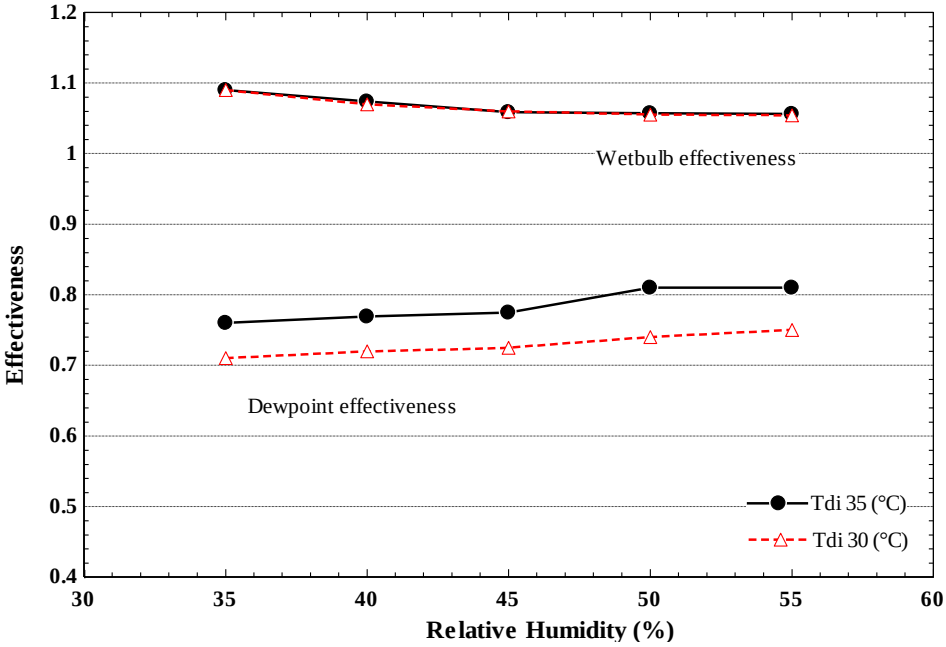

Figure 7.11 Effect of relative humidity on wet bulb and dew point effectiveness

7.5 Description of the experimental set-up

A laboratory test rig experiment was built to test the heat pipe-porous ceramic sub-wet bulb temperature evaporative cooling system. The cooler is made of a 720 x 220 x 42 mm porous ceramic water container with specific wettability properties and a bundle of finned heat pipes for heat transfer. The supply and working airflow streams were staged in separate channels and in counter flow directions as shown in Figure 7.12. The porous ceramic water container was placed in the wet air channel and filled with water through a water feed hose from an overhead tank. Front and back narrow ducts were formed between the ceramic and Perspex material to allow water to seep through the micro-pores to form a thin water film on its surface. The direct evaporation of the water film cools the ceramic panel and its water content which in turn creates a temperature gradient. The heat pipes straddle both the dry and wet air channels through which the air supply is cooled indirectly in the dry channel and at constant moisture content. The airflow in the dry and wet channels was circulated by a fan with

controlled mass flow rate, temperature, and relative humidity. The inlet air temperature and water content were controlled using an environmental chamber. The intake air velocity was adjusted by using an electrical transformer type LAB/SM 270 to supply power rating to a fan between 12 - 20 Volts as shown in Figure 6.2. The rig was fully instrumented to measure the air temperature, moisture content, and flow rates along the dry and wet channels as shown in Table 7-2. The tests were carried out at 30 ^{o}C and 35 ^{o}C inlet air temperatures and relative humidity at 35%, 40%, 45%, 50%, and 55%.

Table 7-2 Measurements instruments used in the experiment

Experimental measurement	
Air flow temperature	K-type thermocouple (±0.5^{o}C)
Relative humidity	HygroClib S3 (0-100 %, ±1.5%rh)
Air flow velocity	Airflow TSI Inco. (0-25 m/s, ±1%)
DC power supply	LAB-SM135 (0-12 V, ±0.05%)

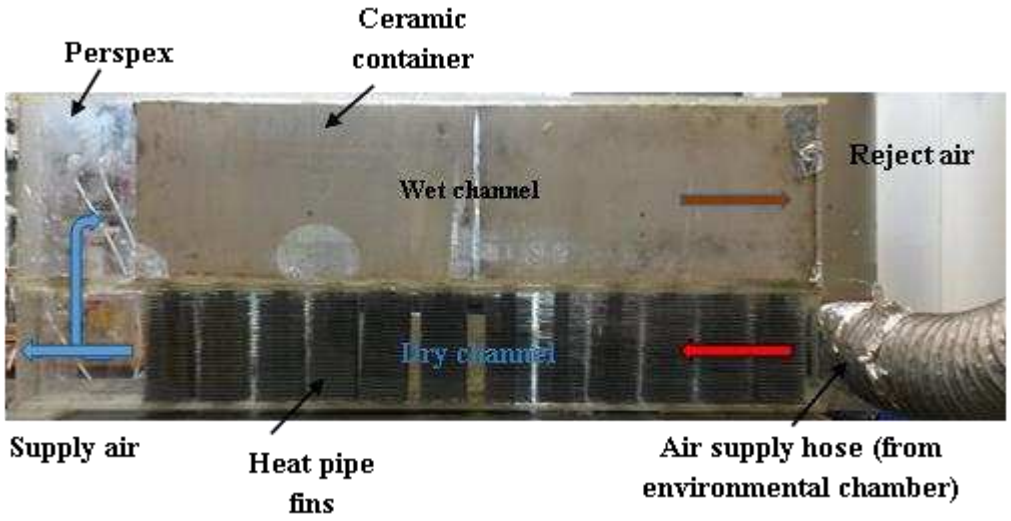

Figure 7.12 Heat pipes and flat ceramic of a laboratory test rig experiment

7.6 Experimental results

The experiment of the indirect evaporative cooler using porous ceramics and heat pipes to achieve wet bulb temperature were carried out to investigate effect of intake air channel velocity and relative humidity and evaluate the thermal performance of this cooler. The intake air velocity considered was between 0.5 (m/s) to 2.5 (m/s) with two inlet air temperatures at 30^{o} C and 35^{o} C, and relative humidity set at 35, 40, 45, 50, and 55%.

7.6.1 The effect of intake air velocity on effectiveness and product air temperature

The test rig results of the effect of varying intake air velocity on the wet bulb effectiveness and product air temperature are shown in Figure 7.13. The intake air velocity considered ranged between 0.5 (m/s) to 2.5 (m/s) with two inlet air temperatures at 30 ^{o}C and 35 ^{o}C (i.e., wet bulb temperature $T_{wbi,}$ of 18.9 ^{o}C and 23^{o}C respectively) and relative humidity set at 35%. From Figure 7.13 it can be seen that the wet bulb effectiveness decreased with increasing velocity of the intake air channel whereas the product air temperature increased almost linearly with increasing air velocity. This is due to the decreased evaporation rate with increasing intake air channel velocity, because when the working air velocity increases, the time of contact between the working air and wet surfaces will be reduced, which results in decreased capacity of moisture absorbed by working air in the wet channel .

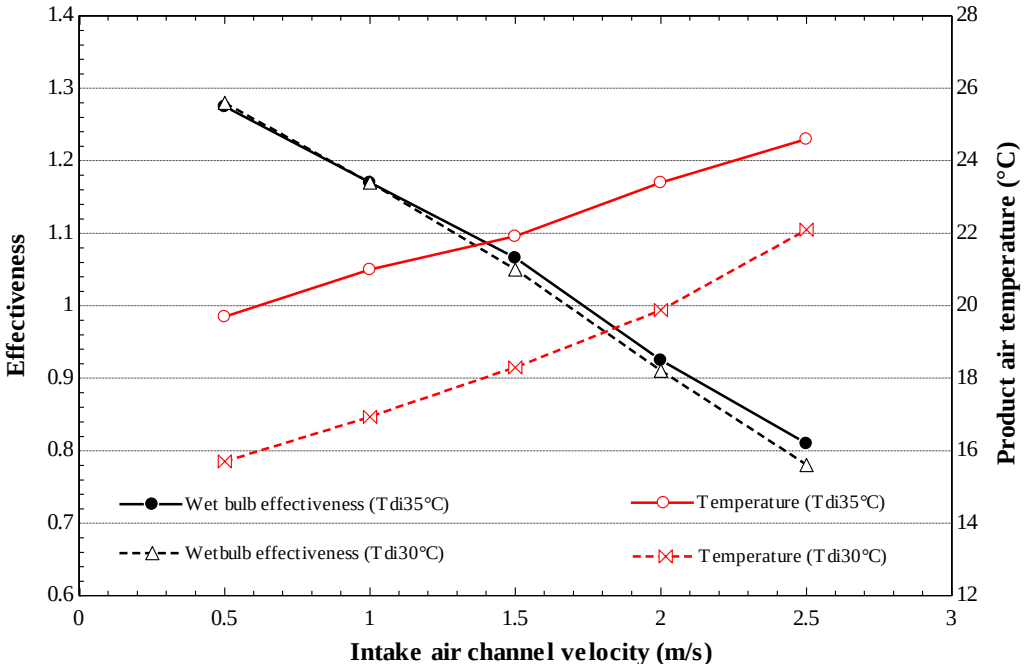

Figure 7.13 Effect of intake air velocity on cooling capacity and product air temperature

The thermal performance of the laboratory porous ceramic evaporator was evaluated at temperatures of 30 ^{o}C and 35 ^{o}C and corresponding relative humidity (%) of 35, 40, 45, 50, and 55, prevailing weather conditions in most parts of the Middle East. For an inlet air temperature of 35 ^{o}C and relative humidity of 35% (i.e., wet bulb temperature, $T_{wb,}$ of 23 ^{o}C and dew point of 17.9 ^{o}C), the steady state measured supply air temperature (airflow temperature at the exit of the dry channel) was 22.4 ^{o}C (a drop of 12.5 ^{o}C) at a mass flow rate of 0.0031kg/s, as shown in Figure 7.14.

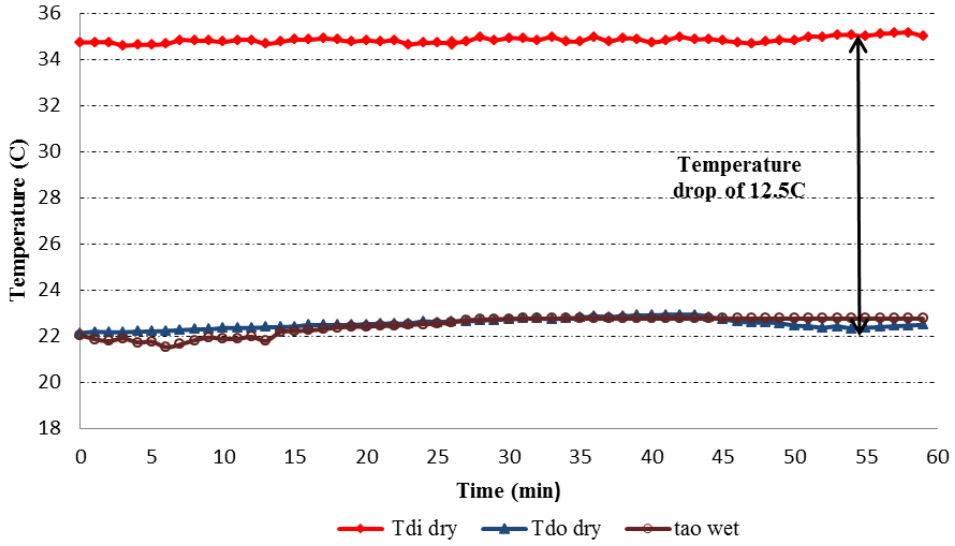

Figure 7.14 Recorded temperature profile in the wet and dry channel

7.6.3 The effect of intake air velocity and relative humidity in water consumption

Figure 7.15 compares the amount of water consumption which was collected from the water drain of cooler, and the water consumption of cooler by using equation (3.5). The air inlet relative humidities were 35% and 55% with inlet dry air temperature set at 35 ^{o}C and air velocity ranged from 1 to 2 (m/s). The results of this comparison indicated that the differential between them is small and the highest values can be achieved when inlet relative humidity is low. In addition, water consumption for both of them increased with increasing intake air channel velocity.

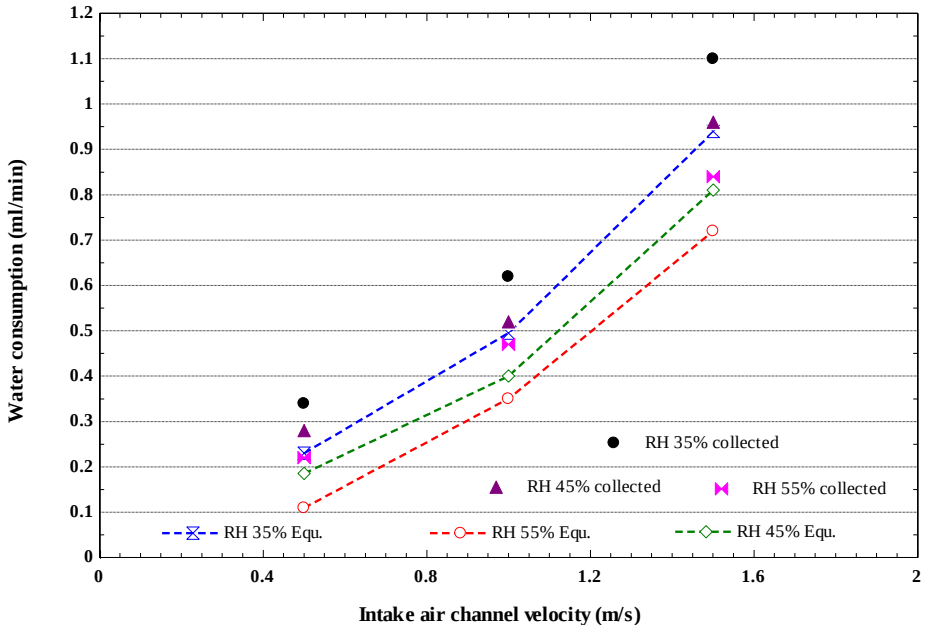

Figure 7.15 Effect of intake air channel and relative humidity on water consumption

7.6.3 The effect of relative humidity on cooling capacity, COP, and wet bulb and dew point effectiveness

The rig tested the effect of varying inlet air relative humidity on cooling capacity, COP, and wet bulb and dew point effectiveness; the results are shown in Figures 7.16 and 7.17. Two inlet air temperatures were considered, 30 ^{o}C and 35 ^{o}C, with relative humidity set at 35%, 40%, 45%, 50%, and 55% and with supply air flow rate remaining constant, 0.0031 kg/s. Figure 7.16 shows that the cooling capacity and COP are strongly influenced by relative humidity when both of them are inversely proportional to relative humidity. The lower the relative humidity level of the inlet air, the higher the cooling capacity and COP that can be obtained from the cooler system. This lead to diverted lower level of inlet air humidity into wet channel more moisture will absorb, since the larger driving force of mass transfer results from the greater vapour pressure difference between the air and the water interface when the inlet air humidity is lower.

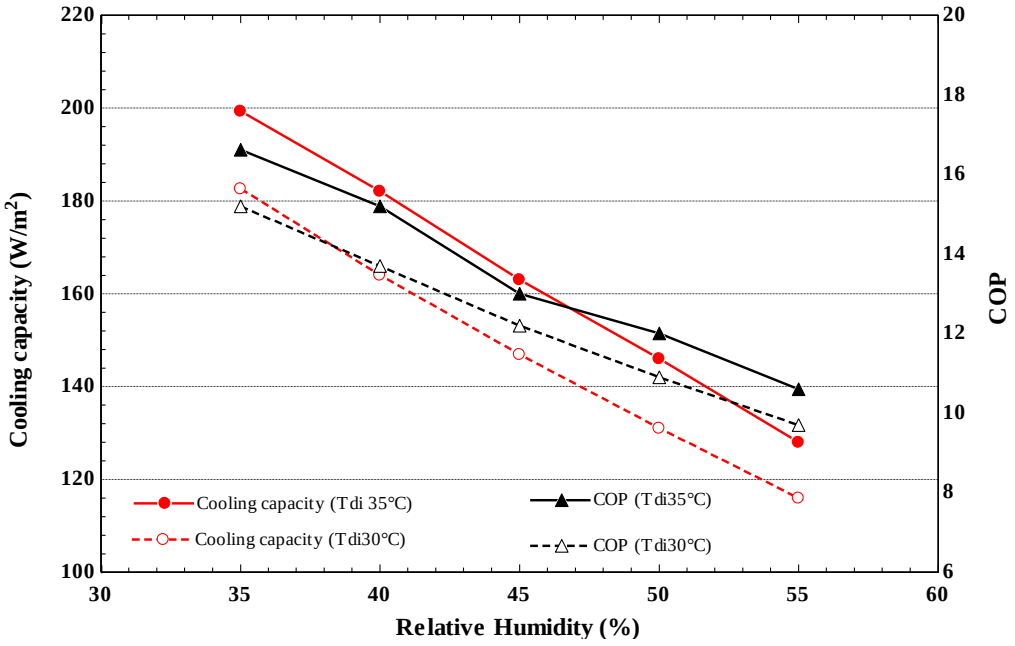

Figure 7.16 Effect of relative humidity on cooling capacity and COP

Figure 7.17 shows the lab test result of the effect of relative humidity on the wet bulb and dew point effectiveness for the cooler when the inlet air temperature was set at 30 and 35 with a relative range between 35% to 55%. Wet bulb and dew point effectiveness can be calculated from the equations (3.4) and (4.1) respectively. The wet bulb effectiveness for the two inlet air temperatures 30 ^{o}C and 35 ^{o}C decreased with increasing inlet air relative humidity, the wet bulb effectiveness of the wet bulb effectiveness of Tdi 30 decreased from 1.056 to 1.04 and Tdi 35 varied between 1.07 to 1.04 and. However, the dew point effectiveness increased with increasing inlet relative humidity, the dew point effectiveness of Tdi 35 varied between 0.75 to 0.81, and the dew point effectiveness of Tdi 30 increased from 0.68 to 0.74. From the above analysis of the experimental results it can be noted that, higher inlet air temperatures give higher wet bulb and dew point effectiveness. Moreover, by increasing the inlet relative humidity, higher dew point effectiveness can be achieved due to increasing the product air temperature as shown in Figure 7.17

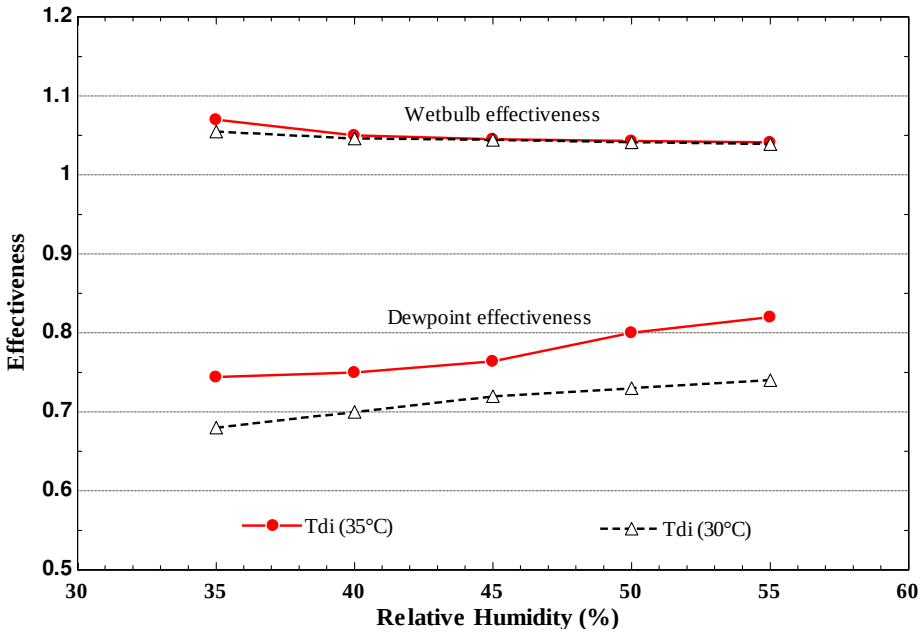

Figure 7.17 Effect of relative humidity on wet bulb and dew point effectiveness

7.7 Comparison between modelling and experimental results

7.7.1 The effect of inlet air velocity on effectiveness and product air temperature

Figure 7.18 compares the effectiveness and product air temperature results of modelling and the lab test when the intake air channel velocity varies between 0.5 (m/s) to 2.5 (m/s) and air inlet temperature is set at 35 with 35% relative humidity. The numerical model results show good agreement with the experimental findings. Higher intake air velocity gives higher product air temperature and lower effectiveness. For velocity less than 1.5 m/s, the product air for both findings are below their wet bulb temperature and the wet bulb effectiveness also for both results are above 100% when also the intake air velocity is below 1.5 (m/s).

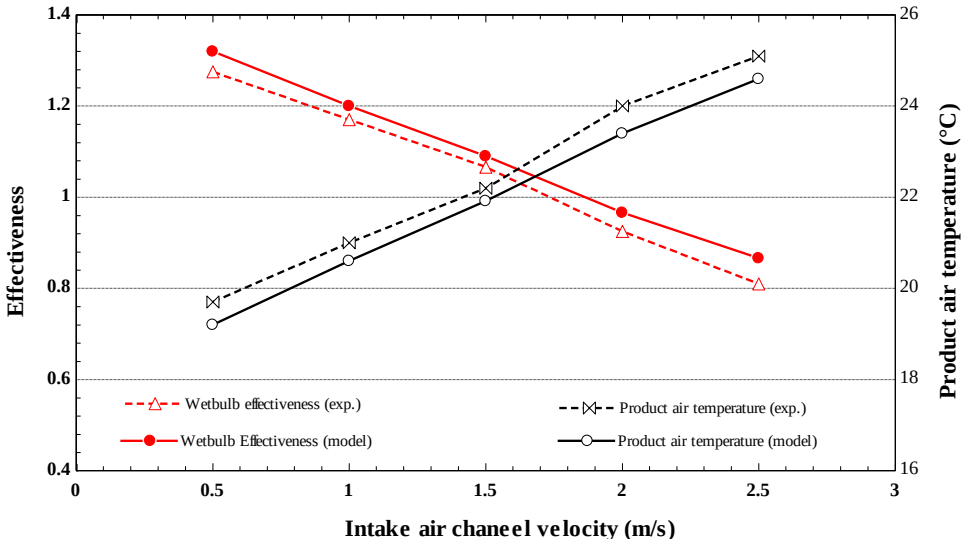

Figure 7.18 Effect of intake air channel velocity on wet bulb effectiveness and product air temperature

7.7.2 The effect of the duct length on product air, working air, and water film temperature

The airflow temperature profile along the dry and wet channels is given in Figure 7.19. The computer model predicted that the airflow in the dry channel would be cooled to

21.9 ^{o}C, achieving sub-web bulb temperature conditions. The airflow along the wet channel, on the other hand, increased from 21.92 ^{o}C to 24.2 ^{o}C, as it gained latent heat from evaporated water on the surface of the ceramic panels. The experimental measurements, however, show the air temperature at the outlet of the dry channel is about 22.3^{o}C and that of the wet channel is 22.8 ^{o}C. The discrepancy between the experimental and computer model results, though within the measurement uncertainties of the instruments, is mainly attributed to difficulties in obtaining a uniform airflow distribution in the dry and wet channels.

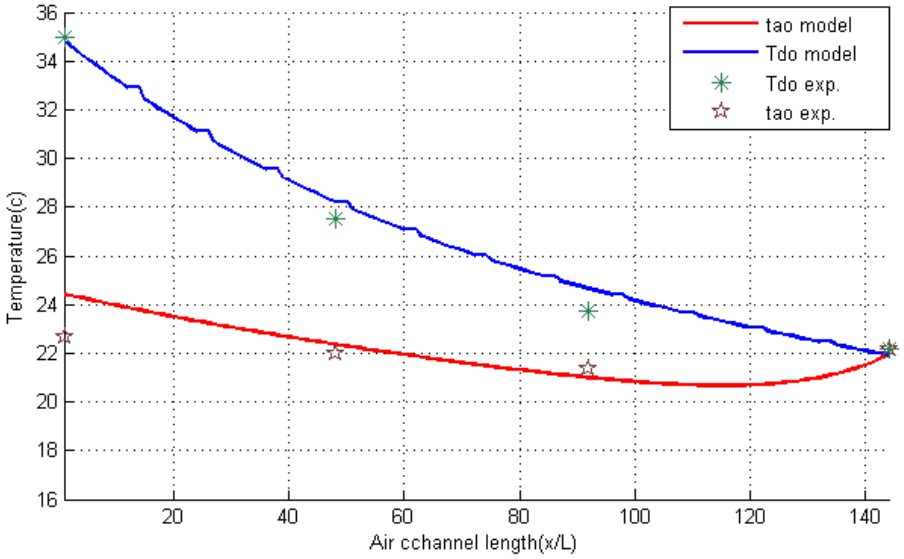

Figure 7.19 Effect of the duct length on product air, working air and water film temperature

7.7.3 The effect of cooler configuration on humidity ratio

Figure 7.20 shows the difference between modelling result and lab test for the humidity ratio of product air and reject air. Form this Figure it can be seen that, although the modelling and rig have the same inlet air conditions (i.e., Tdi 35 ^{0}C and humidity ratio 12.3 (g/kg$_{d}$)), the values of humidity ratios for product air are different. In the modelling, the humidity ratio of product air remained constant when it is

increased from 12.3 (g/kg_d) to 17.2 (g/kg_d) of reject air. However, in the experiment the humidity ratio increased in both channels; it increased from 12.3 (g/kg_d) to 13.2 (g/kg_d) in the dry channel for product air and it is continues to increase to 16.8 (g/kg_d) in the wet channel for reject air.

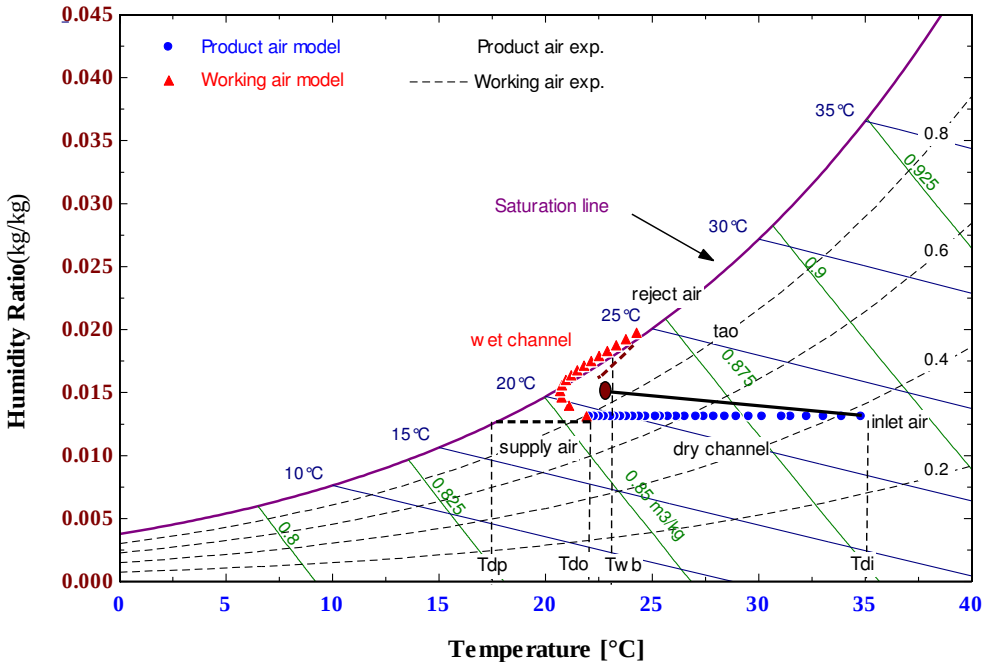

Figure 7.20 Effect of cooler configuration on humidity ratio

7.7.4 The effect of intake air channel and relative humidity on water consumption

The effect of varying intake air velocity and inlet relative humidity on water consumption was compared between the modelling and experimental results. Inlet dry air temperatures set at 35 ^{o}C with two air inlet relative humidity were considered: 35% and 55% and air velocity ranged from 1 to 2 m/s. The results of this comparison are shown in Figure 7.21.

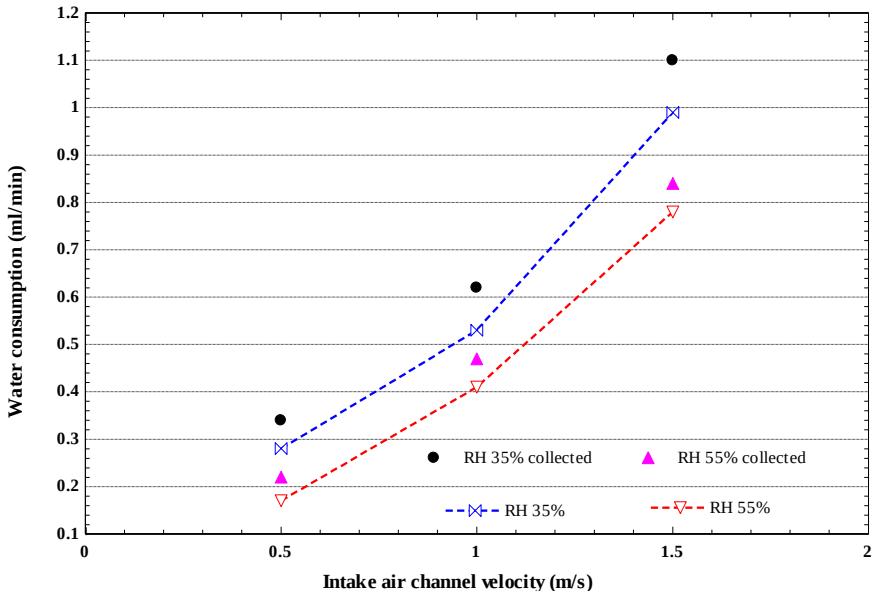

Figure 7.21 Effect of intake air channel and relative humidity on water consumption

7.7.5 The effect of relative humidity on cooling capacity and wet bulb and dew point effectiveness

The modelling results and lab test of the effect of relative humidity on cooling capacity, COP, and wet bulb and dew point effectiveness were compared for inlet air conditions (i.e., T_{di} 35 ^{o}C, mass flow rate 0.0031 kg/s and relative humidity set between 35% and 55%). Figure 7.22 indicates that the lower the inlet relative humidity, the higher the cooling capacity and COP obtained from the collar system. While Figure 7.23 shows that both effectiveness values of modelling and lab test show a significant relationship with relative humidity, wet bulb effectiveness decreased with increasing relative humidity and the best values of wet bulb effectiveness for both lab test and modelling were achieved when inlet relative humidity was set at 35%. On the other hand, dew point effectiveness increased when inlet air relative humidity increased. The higher dew point effectiveness was achieved when relative humidity was set at 55%.

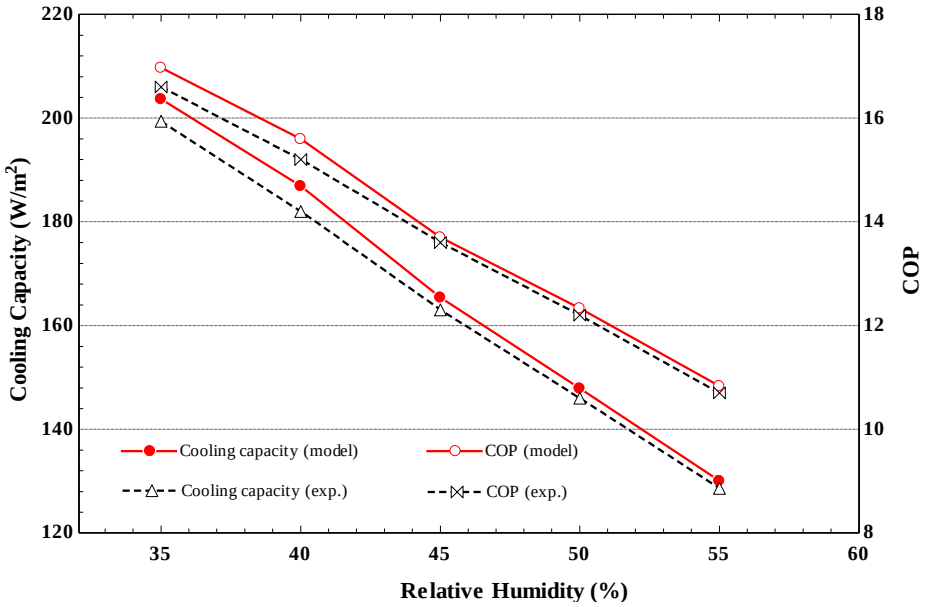

Figure 7.22 Effect of relative humidity on cooling capacity and COP

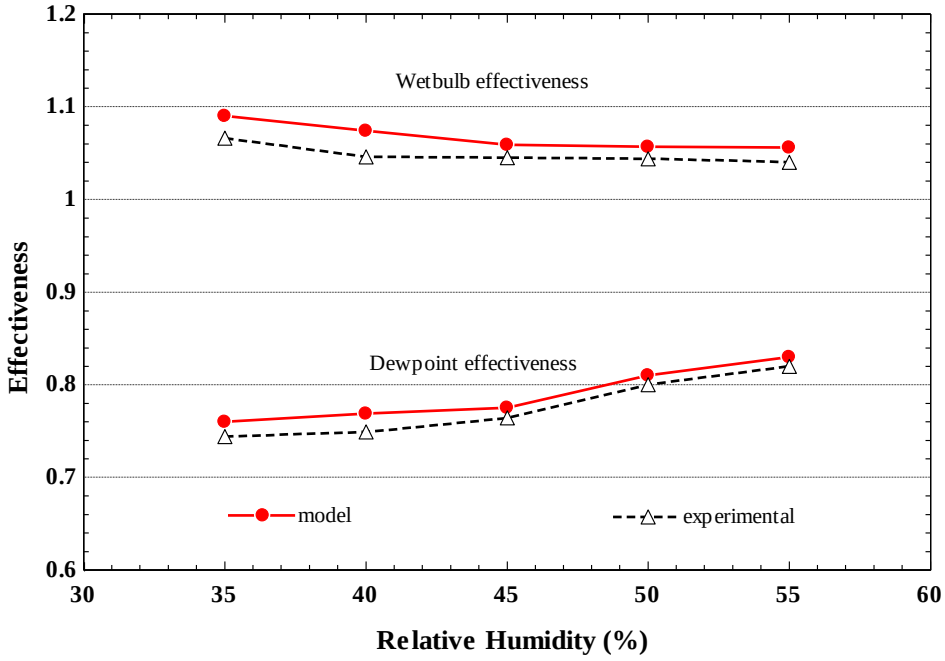

Figure 7.23 Effect of relative humidity on wet bulb and dew point effectiveness

7.7.6 Comparative performance of current sub-wet bulb temperature evaporative coolers using heat pipe-ceramic panels were against Al-Koheji published works of direct evaporative cooling systems using porous ceramic

The modelling and experimental results of the cooling capacity for current sub-wet bulb temperature evaporative coolers using heat pipe-ceramic panels were integrated with the evaporative cooling system presented in chapter 6, and are compared with the indirect evaporative cooler using porous ceramic and heat pipes carried out by Al-Koheji in Figure 7.24. It can be seen that the cooling capacity for both coolers increased with the increasing inlet relative humidity. Although the inlet air velocity for both systems was set at 2 m/s, the cooling capacity achieved by the current cooler is much higher than the cooling capacity result of indirect evaporative cooler. This is due to a high temperature drop, which can be achieved by heat pipe-ceramic panels integrated with the evaporative cooling system.

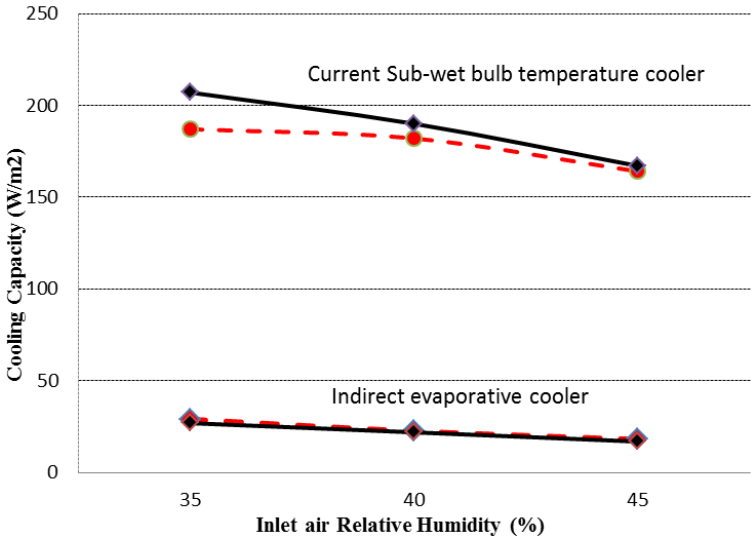

Figure 7.24 The modelling and experimental results of the cooling capacity for current sub-wet bulb temperature evaporative cooler using heat pie-ceramic panels compared with the indirect evaporative cooler using porous ceramic and heat pipes

7.8 Conclusion

An indirect evaporative cooling system consisting of porous ceramic containers and finned heat pipes to achieved sub wet bulb temperatures has been investigated. The modelling was developed and a test rig was constructed and set up in the laboratory to monitor the influence of different parameters (e.g., temperature, air velocity, relative humidity, etc.). Ceramic containers were used as wet media through direct evaporation of the water from the container's external surface that is in direct contact with working air in the wet channel to cool on the end of the heat pipes (condenser). Heat pipes were used to transfer heat from the intake air channel (dry channel) to the ceramic containers.

Results of modelling and lab tests have shown that although the findings values obtained from the modelling are slightly greater than results predicted by the lab tests, the numerical model results show good agreement with the experimental findings. Graphs for both modelling results and lab tests presented that higher intake air channel velocity and relative humidity give lower wet bulb effectiveness, cooling capacity, and COP. Increased of inlet dry air temperature (T_{di}) led to increase in either both effectiveness or product air temperature (T_{do}). Finally, the dew point effectiveness was increased with increasing inlet air relative humidity (%).

Dew point effectiveness can be obtained by using the relationship given by equation (4.1). When inlet temperature ranged from 30 to 45 ^{o}C the dew point effectiveness varied between 63 and 85%. Higher inlet air temperature gives higher dew point effectiveness. Another interesting observation from the experimental results is that higher dew point effectiveness could be obtained by increasing the inlet humidity ratio at constant inlet temperature.

Chapter 8

Thermal Performance and Environmental Assessment of Evaporative Cooling Systems: Case of Mina Valley, Saudi Arabia

8.1 Introduction

Saudi Arabia receives millions of pilgrims in the holy city of Makkah every year and energy consumption for air conditioning in buildings and pilgrims open spaces is huge. To alleviate energy consumption for air conditioning, the Saudi government opted for large scale installations of evaporative cooling systems in places like Mina Valley in Makkah where over 3 million pilgrims converge on to the city every year. Figure 8.1 shows an example of rooftop mounted evaporative cooling units for space cooling in purpose built pilgrims' accommodations. There are over 48,000 units installed in Mina Valley alone [102][5]. This chapter presents a detailed description of evaporative cooling systems used for space cooling in Mina Valley, Saudi Arabia. The thermal performance and environmental impact of the evaporative coolers were also evaluated.

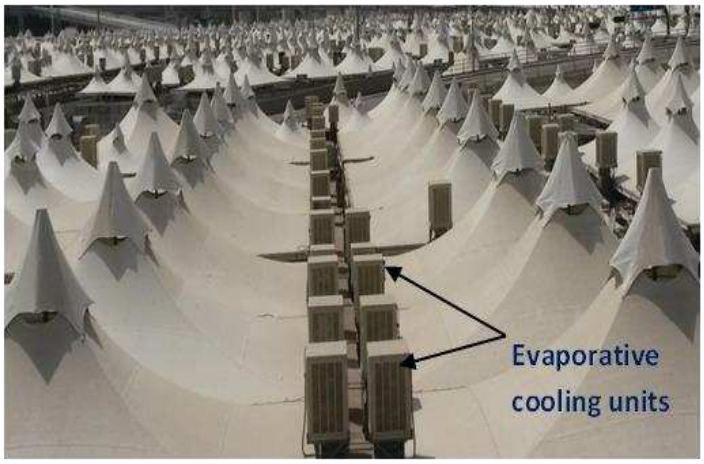

Figure 8.1 Roof top mounted evaporative cooler for cooling in pilgrims' accommodations

8.2 Evaporative Cooling Technology in Mina Valley

Mina Valley is a residence to over 2 million pilgrims for a short period of only 6 days per year during the annual pilgrimage to the holy places in Saudi Arabia. It is located about 7 km from Makkah city and is known as 'The Tent City'. The location is known for its hot and dry climate where typical temperatures vary between 19 and 43°C and relative humidity ranges from 20 to 57% in July and January respectively. Figure 8.2 shows a psychrometric plot for a range of prevailing daily average temperatures and relative humidity of Mina Valley in Makkah

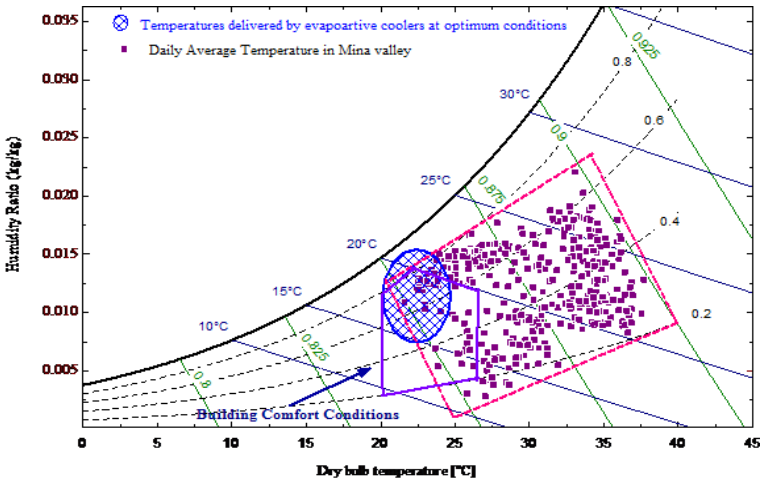

Figure 8.2 Daily average temperature at Mina valley (Saudi Arabia) and Temperatures delivered by evaporative coolers at optimum conditions

The use of evaporative cooling technology, particularly direct evaporative cooling systems, is widely practiced in Saudi Arabia. However, there are few publications on the subject with the focus on measuring the operating parameters and cooling temperatures. Alamari et al. (2002) [103]evaluated the performance of evaporative coolers in sixteen permanent tents that accommodate pilgrims' in Mina Valley during the Hajj period. The author measured the indoor space conditions including dry-bulb temperature, wet-bulb temperature, and relative humidity of inlet and outlet supply air. The data collected was related to the number of occupants per tent with cases of crowded tents with occupants and semi-empty tents. However, apart from the measured air temperature and moisture content it is hard to draw any firm conclusion about the performance of the system. Similarly the there is little data on durability and maintenance of wet media materials used in direct evaporative coolers. Figure 8.3 (a) shows an example of new Aspen Wood wet media while Figure 8.3 (b) shows a spent materials, however there is no indication on the life span of the materials.

a) b)

Figure 8.3 Aspen Wood wet media material a) New material b) Spent materials

Other research work on the wet media materials was published by Habeebullah[104] in which the author investigated the possibility of using Celdek paper and Luffa sponge material as substitutes for Aspen wood to improve the efficiency of evaporative coolers. The results indicate that, the pressed Luffa sponge of 175 mg/cm^3 density could be a viable alternative with recorded . cooling effectiveness approaches 96% for an air volume flow rate of 1.01 m^3/s. Figure 8.4 shows an example of Celdek material and Luffa respectively.

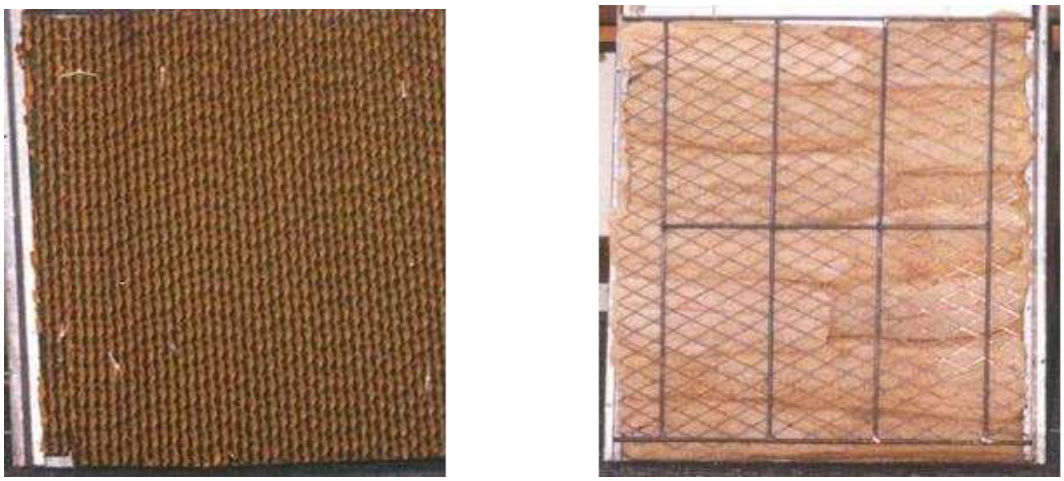

a) b)

Figure 8.4 Alternative wet media a) Celdek b) Luffa

Similarly, Masha et al. [5] presented an experimental study of an evaporative cooler using a 3 cm thick Aspen wood as wet media deployed in a direct evaporative cooler in the Mina Valley. An indication of the thermal performance of the cooler is summarised in Table 8-1.

Table 8-1 An experimental study of evaporative cooler using a 3cm thick aspen wood as wet media

Parameters	
Inlet Dry Bulb Air Temperature (^{O}C)	40.33
Outlet Dry Bulb Air Temperature (^{O}C)	27.01
Inlet Wet Bulb Air Temperature (^{O}C)	24.55
Outlet Wet Bulb Air Temperature (^{O}C)	24.2
Inlet Air Relative Humidity (%)	26.39
Outlet Air Relative Humidity (%)	73.88
Air Velocity (m/s)	3.6
Air Flow Rate (m^3/s)	0.84
Water Evaporation (kg/h)	15.85
Cooling Effectiveness (%)	84.41
Cooling Capacity (kW)	14.32
Air Velocity (m/s)	3.6

8.2.1 Evaporative cooling in tents accommodation

There are approximately 48,000 permanently erected tents with a total area of about 2.5 km^2, as shown in Figure 8.5 (a). Each tent is equipped with one or more evaporative air cooler units, air distribution ducts and a complete water supply network. Air distribution ducts made from galvanized steel deliver cool air to the occupied space at a rate of 1500 cfm for tent floor areas of 16m^2.

Two types of evaporative coolers have been installed depending on required air flow rate. There are about 37,411 evaporative coolers with a flow rate capacity of 6,000 cfm and a motor drive, of 1.5 hp and 6,312 units with 3,000 cfm capacity and ¾ hp motor. The average ambient inlet air condition in summer 2013 was 37^{o}C and 22% RH and the supply air delivered by evaporative coolers was 25^{o}C and 63% RH. Figure 8.5 (b) shows the evaporative cooling unit assembly.

Figure 8.5 (a) Mina valley pilgrims' tents (b) roof-top evaporative cooler unit

8.2.2 Evaporative Coolers in Aljamaraat Bridge

This is a 4-story walk through bridge used in the spiritual rituals shown in Figure 8.6 (a). The large number of pilgrims converging on these walkthrough spaces requires the deployment of 114 evaporative cooling units rated at 60,000 cfm on each floor to provide comfortable climatic conditions as shown in Figure 8.6 (b). All the evaporative coolers are centrally controlled. The averages for inlet and supply air temperature and relative humidity delivered by evaporative coolers in July 2013 were 39^{o}C and 24%; and 27^{o}C and 62%, respectively.

Figure 8.6 (a) Aljamarrat Bridge

(b) Evaporative cooler unit

8.2.3 Evaporative Coolers at Mashair Railway Station

The railway station has the capacity for the transit of half a million pilgrims in only six hours. The waiting areas for pilgrims are equipped with evaporative coolers to provide comfortable conditions. There are 279 evaporative cooling units installed in nine train stations half of which are cooled by evaporative coolers rated at 26,000 cfm with 12 hp motors and the other half by those rated at 13,000 cfm with 6hp motors. Figure 8.7 shows an example of the cooling units. Centrally controlled, the average inlet and supply air temperature and relative humidity delivered by those evaporative coolers during July 2013 was equivalent to that of the units installed on the Aljamaraat Bridge in the previous section.

Figure 8.7 Evaporative cooling units in the train station

8.3 Thermal and Economic Evaluation of the Evaporative Cooling Systems

The performance and environmental impact of the evaporative cooling systems installed in different parts of Mina Valley were evaluated estimating the cooling capacity, energy consumption, cost of energy consumption and the total carbon dioxide emission.

i) Cooling load

The direct evaporative unit cooling capacity is calculated from:

$$Q_c = C_p \rho \dot{V} (T_i - T_o) \tag{8.1}$$

Where Q_c is given here in BTU/h, $\dot{V}$ is the flow rate in cfm, Cp is the specific heat capacity (0.24 BTU's), ρ is the density (0.075 lbs/cu.ft) and T_i and T_o are the ambient and supply air temperatures in (^oF)

ii) Coefficient of performance

The thermal performance is evaluated directly from measured cooling loads and power consumption of the driving fan motor:

$$COP = \frac{Q_c}{P} \tag{8.3}$$

Where P is power consumption by driving fan motor.

iii) Electrical power consumption

The power consumption over a specify period of time is then calculated:

$$E_c = Pt \tag{8.5}$$

Where E_c is given in (kWh) and t is the number of running hour

iv) Cost of electricity consumption

$$C_c = E_c E_{tariff} \tag{8.7}$$

Where $E_{tarriff}$ is the cost of a unit of electricity (SAR/kWh)

v) Carbon dioxide (CO_2) emission

$$Co_2 \text{emission} = E_c \, f_{Co_2} \tag{8.8}$$

Where f_{CO2} (kg/kWh) is the emission factor of the electricity generation mix in Saudi Arabia.

A summary of the thermal performance of the evaporative cooling systems installed in different parts of Mina Valley in terms of the cooling capacity rates and volume flow rates is given in Table 8-2.

Table 8-2 Installed evaporative cooler

Cooled Site	Number Of EC Units	Flow Rate (M^3/S)	Cooling Capacity (Kw)	Motor Rating (Kw)
Accommodation – EC1	37411	1.42	12	0.56
Accommodation – EC2	6312	2.83	24	1.12
Railway Station – EC3	139	6.14	53	4.47
Railway Station – EC4	139	12.27	107	8.95
AljamaraatBridge – EC5	456	28.32	246.8	37.28

The five evaporative cooler units (EC1 to EC5) recorded a cooling temperature difference of 12^oC and an increase in relative humidity of about 39%.

In the following analysis, it is assumed that the tents are fully occupied for 6 days per annum and the railway stations are at maximum capacity for 5 days and the Aljamaraat Bridge is used for 3 days. For comparison, it is also assumed that a conventional vapour compression air conditioning system would have a COP of 3.5 [11].

Compared to traditional vapour compression, the power consumption of evaporative coolers is limited to the power used by the fan and associated electric controls and water pump. In this analysis, it was assumed that a given cooling load, the vapour compression air conditioning system would operate at a COP of 3. Hence, the overall energy consumption of both types of coolers is shown in Figure 8.8. It is also estimated that the deployment of evaporative cooling systems would reduce peak electricity demand from the grid by about 163 MW.

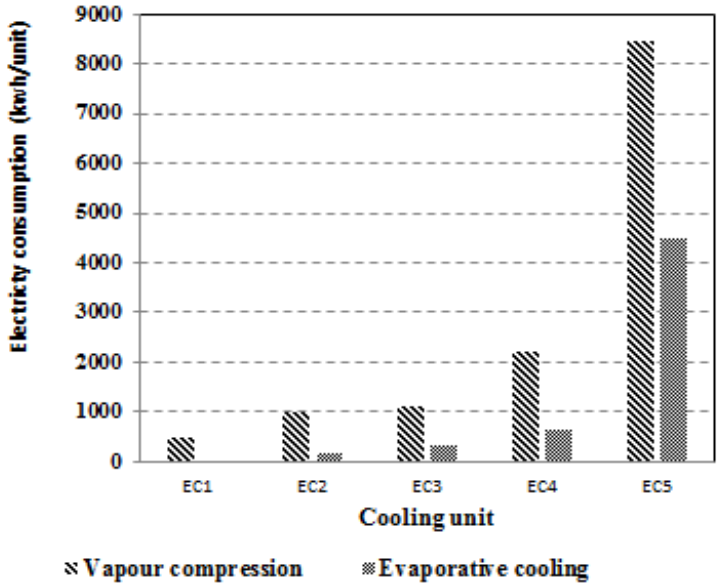

Figure 8.8 Electricity consumption between evaporative cooler and vapour compression

The total running cost of the evaporative cooling units over the period of the pilgrimage is estimated to be SAR 1.06 million, based on the current grid power tariffs of 0.175 SAR/kWh. If, however, a vapour compression system was deployed for air conditioning over the same period of time, the energy consumption cost will be as high as SAR 5 million. Hence, the installed evaporative cooling systems save on average over 70% in the running energy cost. Figure 8.9 shows the savings realized by each scheme and the corresponding COP.

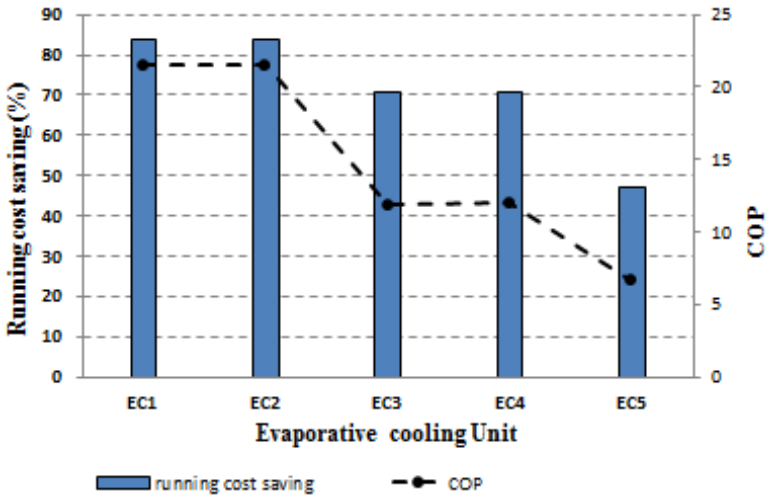

Figure 8.9 Running cost savings

The evaporative cooling has a positive impact on both providing constantly fresh air and reducing electricity demand and therefore carbon emissions. Based on the emission factor of the Saudi electricity generation mix of 0.75kgCO_2/kWh, the total amount of CO_2 reduction when comparing evaporative cooling and vapour compression systems to provide an equivalent cooling load is estimated to be 24600 tonne (i.e., a saving of 78%). Figure 8.10 shows the emission savings from each evaporative cooler.

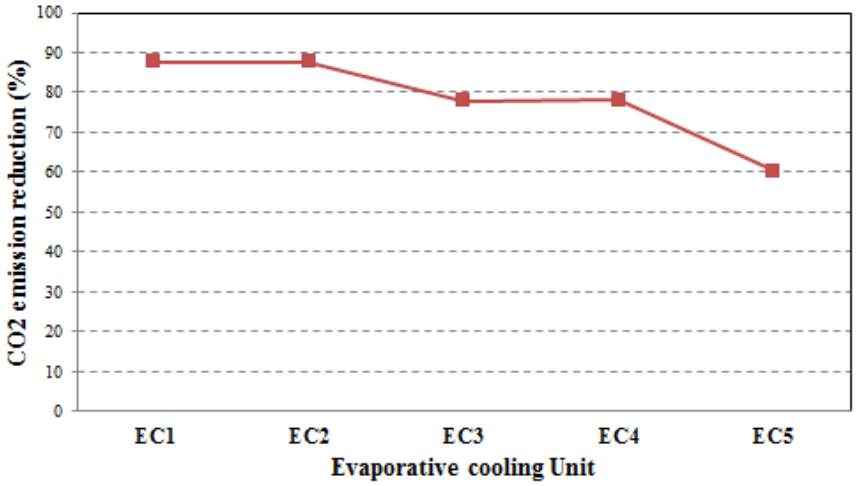

Figure 8.10 The emission savings from each evaporative cooler

8.4 Water consumption

Water consumption of the evaporative cooler depends on the air flow velocity, air temperature and relative humidity, solar radiation and the properties of the evaporative materials. The overall water consumption of the evaporative cooler is determined by equation 3.5. Figure 8.11 shows the water consumption rate in (M^3/min) of all types of direct evaporative coolers installed in Mina valley. According to the running hours of evaporative coolers, the water consumption of the evaporative coolers EC1 and EC2 in tents accommodation for 6 days was 657290118.2L, the water consumption of the evaporative coolers EC3 and EC4 at the Mashair railway station was 2436585.17 L over a period of 5days and the water consumption of the evaporative cooler EC5 in the Aljamaraat Bridge was 12203271L over a period of 3days. therefore, the total water consumption of all evaporative coolers installed in Mina valley was 671929974.4 L (6.7 million m3) during the Hijj period.

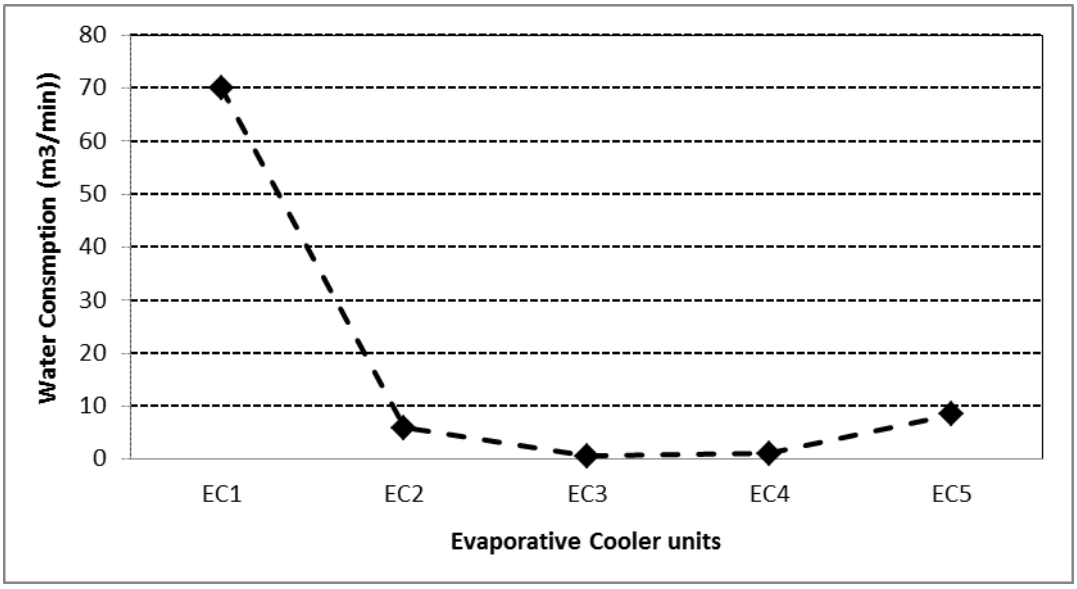

Figure 8.11 Water consumption rate (M^3/min) for all direct evaporative coolers installed in Mina valley

8.4 Conclusion

It is shown in this simplified analysis that the evaporative cooling system is very suitable in a site like Mina Valley where the weather is hot and dry. The evaporative cooling system saves over 70% in energy consumption costs and reduces carbon dioxide emissions by 78% compared to using mechanical vapour compression systems. The evaporative cooling provides the required comfort level using 100% fresh air.

Chapter 9

How and where the system can be integrated into a typical building

9.1 Introduction

The integration method for buildings is an important part of the holistic design of the cooling system. This can minimise the use of the envelope materials, improve efficiency by properly positioning the systems and enhance the comfort level in the building. According to Ibrahim, when the evaporative cooler is integrated correctly in the building, comfort will be improved, occupants will receive the best cooling performance of the space and energy bills will be decreased. The study of the integration of direct evaporative cooling systems using prototypes of porous ceramic carried out by Ford et al. showed that these systems can be integrated within walls or roofs as shown in Figure 9.1 to deliver cooling to perimeter areas of both existing and new buildings.

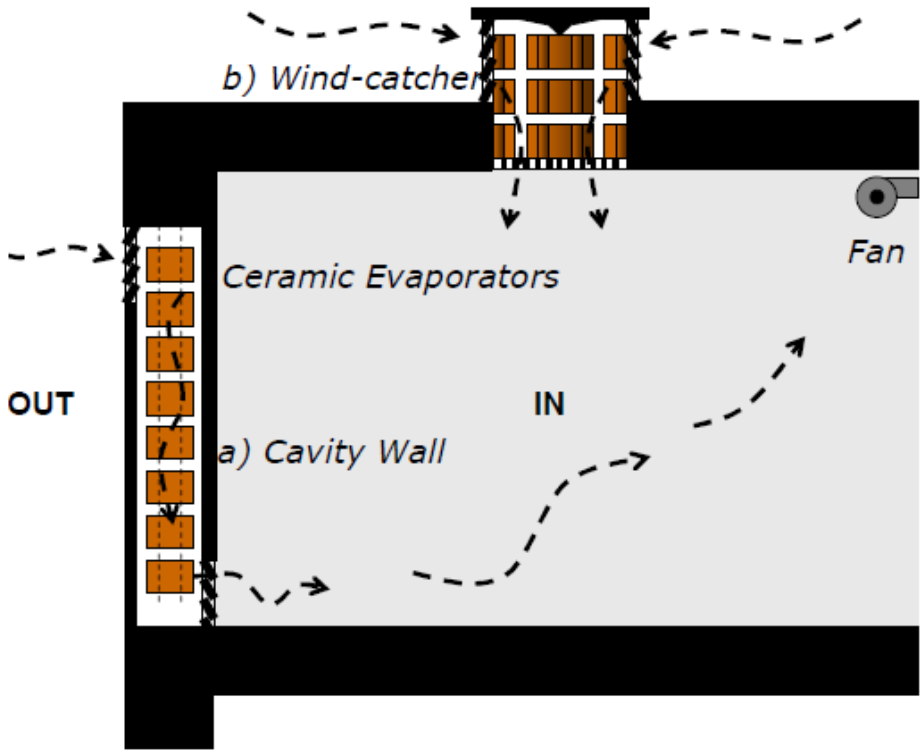

Figure 9.1 Principle of operation of direct system [90]

9.11 Roof mounting

Evaporative cooling systems on domestic, public and private buildings are mostly mounted on the roof, as shown in Figure 9.2 and Figure 9.3

Figure 9.2 Evaporative cooler installed in Jamarat train station in Mina Valley

Figure 9.3 Evaporative cooler installed in Mina Valley

The current sub-wet bulb temperature evaporative coolers using porous ceramic materials can be installed as roof mounted cooling systems as shown in Figure 9.4. In the system, the hot and dry air is supplied at the top of the unit where the air is circulated in the dry channel before it splits at the supply end, and where part of the air flows through the wet channel to perform the necessary evaporation and generate the cooling effect. The top roof installation method is a compromise between the cost and maintenance requirements as well as the constant exposure to weather conditions. In addition, maintenance will require gaining access to the roof of the house, and which will need a trained and qualified installer. Similarly, the roof-top mounted systems are secure from vandalism and offer the shortest air distribution ductworks, and hence, are less costly. The ductworks would be installed in the loft and supply the below occupants' space with air.

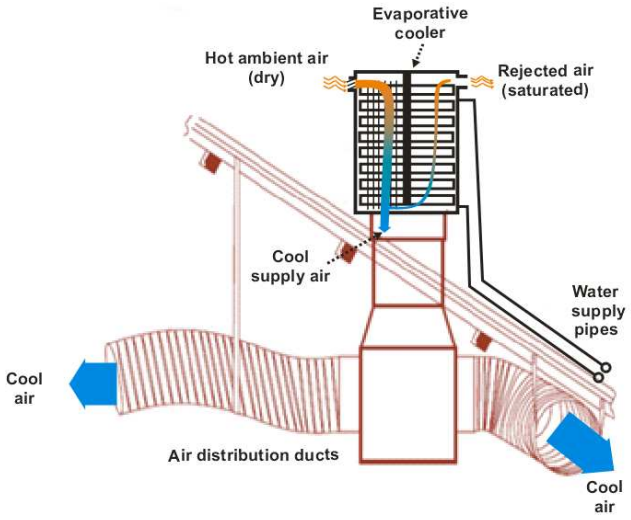

Figure 9.4 Roof mounted cooling system

9.1.2 Wall mounted

However, wall mounted evaporative cooling could be another alternative to ceiling mounted units to form a cool wall. According to Rosa [91], the most effective option is the wall integrated system, where a column of modular porous ceramic evaporators is integrated into a perimeter cavity wall as shown in Figure 9.5, and the use of a room-integrated fan might be necessary in still conditions to assure a constant air flow.

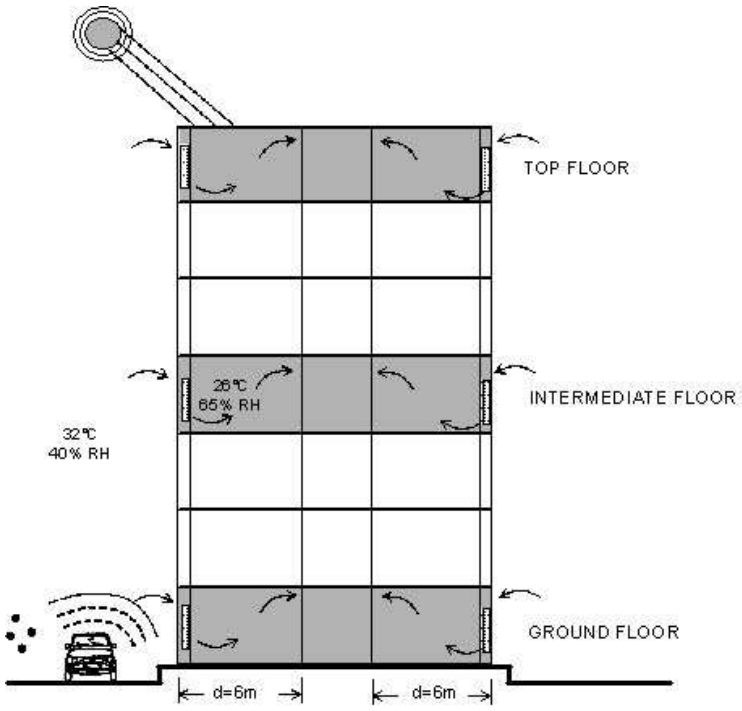

Figure 9.5 Strategy of integration for existing apartment blocks [91]

The current sub-wet bulb temperature evaporative cooler using porous ceramic materials can be integrated into a perimeter cavity wall. In this system, the ambient air is to be supplied and circulated through the dry side of the ceramic material, and part of the cool air is supplied to the building at the ceiling level as well as the through radiation directly into the occupied space. Figure 9.6 shows a schematic of this configuration.

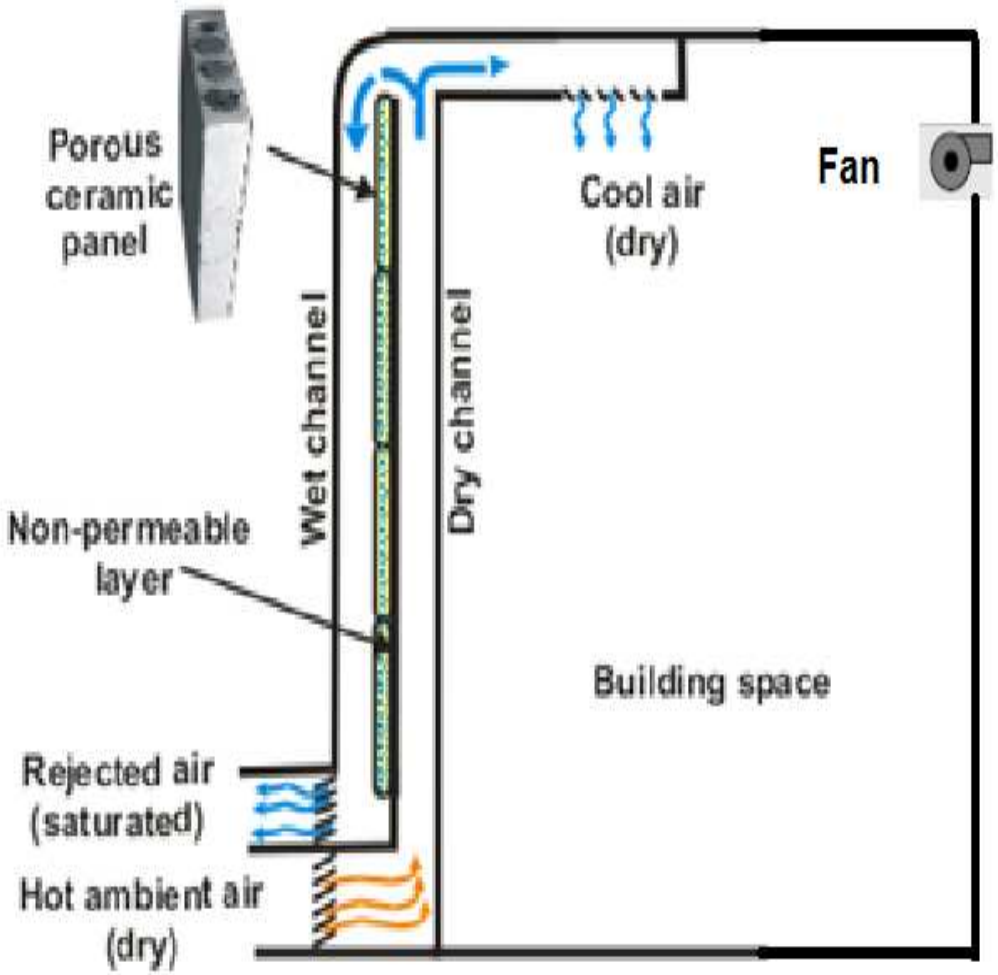

Figure 9.6 A schematic of current sub-wet bulb temperature evaporative cooler using porous ceramic materials can be integrated into a perimeter cavity

In private buildings and apartments with large wall areas (i.e., large exposed room walls), the cooling system could be fitted to two opposite walls to increase the cooling effect. In this instance, care should be taken to make sure that there is water moisture

penetration into the wall fabric, and special impermeable layers should be used to eliminate vapour propagation.

Chapter 10

Conclusions and further work

10.1 Introduction

The concept of a sub-wet bulb temperature evaporative cooling system and the overall aims of the research project were investigated and discussed in this thesis. It also demonstrated the technical feasibility of the technology as compared to the more energy intensive vapour compression systems and the potential of further work to maximise the economic and environmental benefit of the technology.

10.2 Conclusions

The thesis covered the analytical and experimental investigation of sub-wet bulb temperature evaporative cooling using porous ceramic materials as wet media materials for integration into building elements. The thesis also explored briefly the economic viability and environmental impact of evaporative cooling compared to traditional vapour compression through an existing large scale installation case study.

A mathematical model using common energy and mass conservation laws was developed and the computer codes were written using Matlab Software. The computer model results of the evaporative cooling system were extensively analysed to determine the cooling capacity and effectiveness for various design parameters such as ambient air dry bulb temperature, humidity, air flow velocity, etc.

The validation of the computer model was also carried out by constructing and testing two small scale laboratory prototypes using flat panel porous ceramic materials. In the first rig, hollow flat panel ceramic material had one side water proof sealed through which heat is transferred from the dry channel to wet channel. In the second rig, the flat panel ceramic was combined with heat pipes devices for heat exchange between the airflow in the dry and wet channels.

10.2.1 Computer modelling and experimental results validation

The thermal performance results of the design prototypes, including the cooling capacity and effectiveness at different air ambient temperature, showed good overall agreement and trends with the experimental results. An environmental chamber was used to provide different air temperature, dry bulb temperature, and humidity to replicate the mathematical model design parameters.

The work demonstrated that using porous ceramic materials is a feasible option for integrating evaporative cooling systems into building elements (wall, ceiling, etc.). Ceramic materials have the added benefit of stability, reliability, and ease of manufacturing. It was found that both modelling and experimental results show a strong influence of air relative humidity on the thermal performance of the evaporative cooler. For low relative humidity, the tested prototypes achieve air supply temperatures below the wet bulb temperature (sub-wet bulb) and cooling capacity as high as 240W/m^2 of wet ceramic materials surface area as shown in Figure 10.1. Similarly, Figure 10.2 shows that the tested prototypes achieved “wet bulb effectiveness” higher than unity.

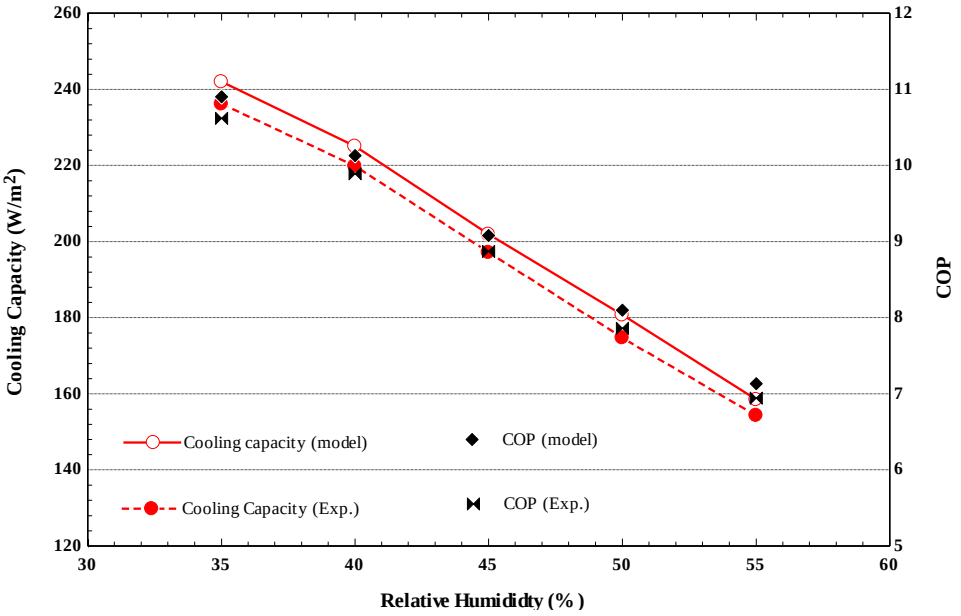

Figure 10.1 Effect of relative humidity on cooling capacity and COP

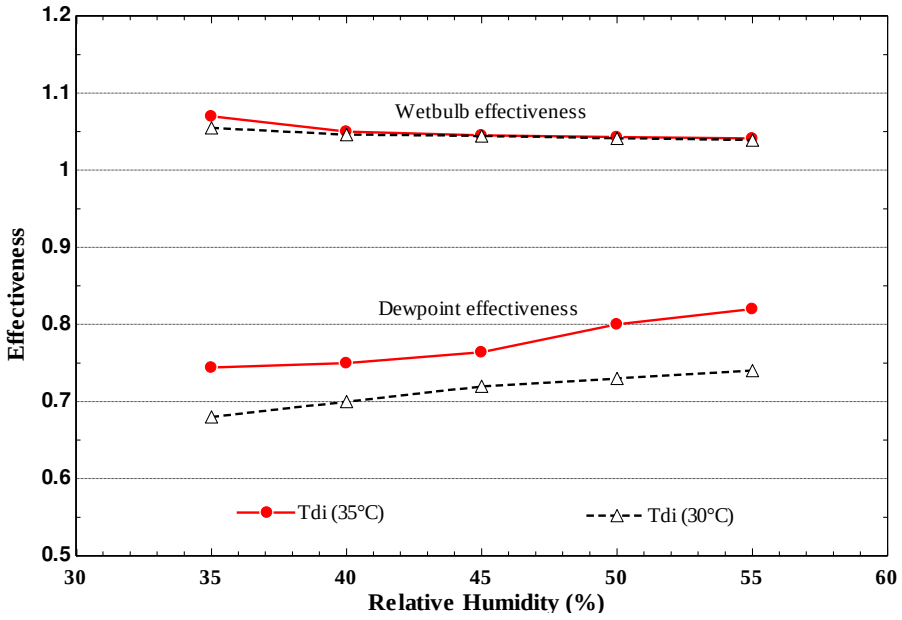

Figure 10.2 Effect of relative humidity on effectiveness

10.2.2 Feasibility and environmental case study

The economic and environmental feasibility study was carried out using data gathering from a large scale installation of evaporative coolers in Mina Valley, Saudi Arabia. Given the geographical location, which is characterised by dry and hot weather

conditions, evaporative cooling proved to be a suitable cooling technology alternative to more energy intensive vapour compression systems. The study showed that evaporative cooling systems save on average over 70% in energy consumption costs and reduce carbon dioxide emissions by 78% compared to using mechanical vapour compression systems as shown in Figure 10.3(a,b).

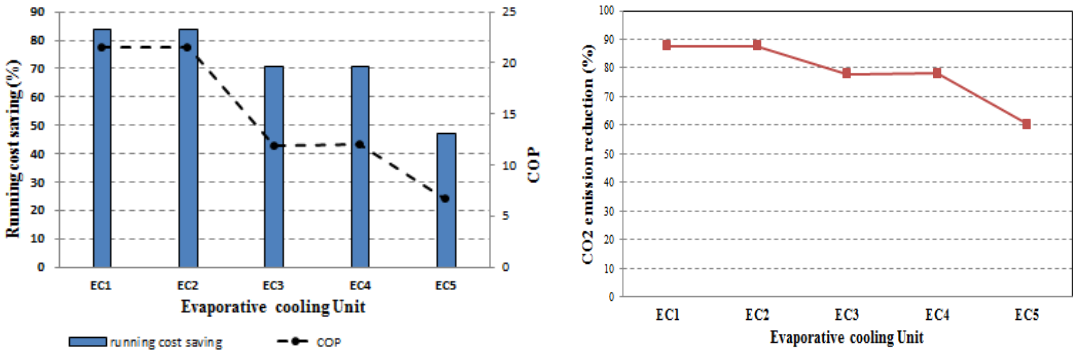

(a) (b)

Figure 10.3 Running cost savings and environmental analysis

10.3 Further work

The work carried out in this thesis demonstrated the principles of sub-wet bulb temperature using porous ceramic materials as wet media in the form of flat panel configurations with and without the application of the heat pipes. It is envisaged that the work could be extended to tests different ceramic media geometries, including flat surfaces with groves and nibbles to augment heat and mass transfer surface area. In addition, cylindrical shaped ceramics could be another option for integrating tubular heat pipes with the ceramics. Figure 10.4 shows a schematic of the proposed further work design of an integrated tubular ceramic and heat pipes.

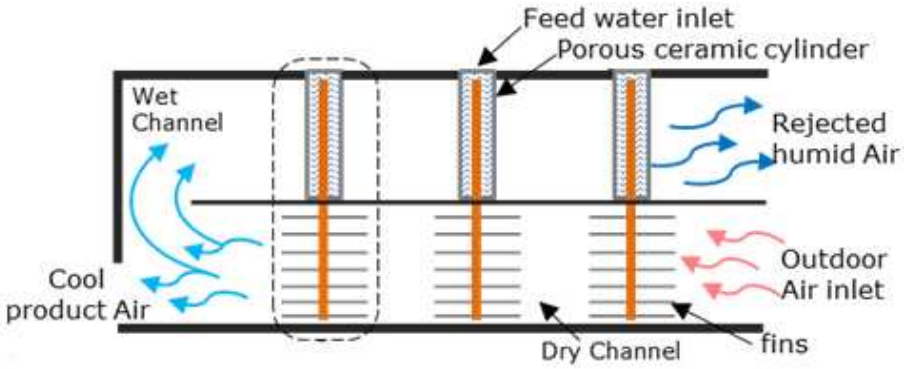

Figure 10.4 Proposed further work configuration

In effect, this work has been initiated by another researcher in the department to investigate its feasibility.

References

1. Resources, E. *Fossil Fuel*. 2011 2011 [cited 2011 5 March]; Available from: http://home.clara.net/darvill/altenerg/fossil.htm#intro.
2. Fules, E.R.F. *energy from fossilised organic materials*. 2013 [cited 2014 15/01]; Available from: http://home.clara.net/darvill/altenerg/fossil.htm#intro.
3. Dodoo, A., L. Gustavsson, and R. Sathre, *Building energy-efficiency standards in a life cycle primary energy perspective.* Energy and Buildings, 2011. **43**(7): p. 1589-1597.
4. Pérez-Lombard, L., et al., *A review of HVAC systems requirements in building energy regulations.* Energy and Buildings, 2011. **43**(2-3): p. 255-268.
5. Book, B.E.D. *Buildin Sector*. 2012 [cited 2013 02/12]; Available from: http://buildingsdatabook.eren.doe.gov/ChapterIntro1.aspx?1#4.
6. Maisotsenko V, G.L., Heaton TL. Gillan Ad., *Method and plate appartus for dew point evaporative cooler,* . 2003: Uinted State.
7. Ibrahim, E., L. Shao, and S.B. Riffat, *Performance of porous ceramic evaporators for building cooling application.* Energy and Buildings, 2003. **35**(9): p. 941-949.
8. Schiano-Phan, R. *The use of porous ceramic for passsive evapoartaive cooling in buildings*. 2009; Available from: http://www.phdc.eu/uploads/media/PHDC_Cooling_with_porous_ceramic_01-06-09.pdf.
9. Riffat, S.B. and J. Zhu, *Mathematical model of indirect evaporative cooler using porous ceramic and heat pipe.* Applied Thermal Engineering, 2004. **24**(4): p. 457-470.
10. Slingo, R.H.a.J., *Climate: Observations, projections and impacts, Saudi Arabia*. 2011: UK.
11. GCC, S.B.H., *Cleantech Business in the GCC*. 2009: Dubai.
12. Al-Homoud, M., *Thermal Design Optimazation of Mosques in Saudi arabia.* Architectural Engineering Department, King Fahd University of Petroleum and Minerals.
13. Chan Doi yan, C.K., Lam Long and Lam Sui San *Saudi Arabia - hot and arid.* Building Technology, 2013.
14. Taleb, H.M. and S. Sharples, *Developing sustainable residential buildings in Saudi Arabia: A case study.* Applied Energy, 2011. **88**(1): p. 383-391.
15. Spark, W. *Average Weather for Makkah, Sausi Arabi*. 2014 [cited 2014 08/05/2014]; Available from: http://weatherspark.com/averages/32773/Mecca-Makkah-Saudi-Arabia.
16. ASHRAE, *Thermal Environmental Condidtions for Human Occupancy*, in *Conditions That Provide Thermal Comfort*. 2004, Amaerican Society of heating, Refrigeration and Air-Conditioning Engineers, Inc.
17. Santamouris, m.A., D, *Passive Cooling of Buildings*. 1996, Londone: James & Lames Ltd.
18. Bank, W., *Evaporative Air- Conditioning, Application for Envirnmentallly Friendly Cooling*. 1999.
19. Elzaidabi, A., *Low Energy, Wind Catcher assisted Indirect- Evaporative Cooling System for Building Applications*. 2009, Nottingham University: UK.
20. Tassou, S., ed. *Air Conditioning* Building Servuces Engineering, MSc Programme. 2001, Brunel University: London. 1.
21. Jones, W., *Air Conitioning Engineering*. 4 ed. 1994, London: Hodder Headline Group.
22. Al-Helal, I., *A pilot-scale study for evaluationg the performance of a fan -pad cooling system under different climatic conditions of Saudi Arabia.* Biological Engineering, 2009.

23. Rahim, S.A., *Climate and Socioeconomic Influence on House Design* College of Architecture and Planning, King Saud University, Riyada, Saudi arbia, 2008: p. 37-55.
24. Limited, M.I.C. *A Trainer Resource Manual for Sustainable Energy Efficiency*. 2012 [cited 2014 13/05].
25. Donnelly, J., *Energy Efficincy in Traditional Buildings*, H.a.L.G. Environmental, Editor. 2010, Stationery Office: Dublin.
26. Fardeheb, F., *Examination and review of passive solar cooling strategies in middle eastern and north african vernacular architecture*, in *Proceeding of ISES World Congress*. 2007, Springer. p. 2512-2513.
27. Feeney, J. *The Magic of the Mashrabiyas*. 1974 [cited 2014 18/02]; Available from: https://www.saudiaramcoworld.com/issue/197404/the.magic.of.the.mashrabiyas.htm.
28. Foudazi, F., M'Rithaa and Mugendi. *Sustainable Solutions for Cooling Systems in Residential Buildings Case Study in the Western Cape Province, South Africa* [cited 2014 03/04]; Available from: http://www.thesustainabilitysociety.org.nz/conference/2010/papers/Foudazi-M'Rithaa.pdf.
29. Solaripedia. *Wind Towers Catch the Breezes (Mid East)*. 2014 [cited 2014 14/05]; Available from: http://www.solaripedia.com/13/205/2077/wind_tower_dubai_bastakiyya_overview.html.
30. Anawar, M. *Eavaporaetive cooling* [cited 2014 02/02]; Available from: http://greenpassivesolar.com/wp-content/uploads/2012/02/Evaporative-Cooling.pdf.
31. *Evaporative Cooling Energy Engineering*. 2014 [cited 2014 15/06]; Available from: http://what-when-how.com/energy-engineering/evaporative-cooling-energy-engineering/.
32. Smith, S.T., V.I. Hanby, and C. Harpham, *A probabilistic analysis of the future potential of evaporative cooling systems in a temperate climate.* Energy and Buildings, 2011. **43**(2–3): p. 507-516.
33. Baca, I.M., et al., *Evaporative cooling efficiency according to climate conditions.* Procedia Engineering, 2011. **21**(0): p. 283-290.
34. Renato M, L., *Introduction of a simple diagram-based method for analyzing evaporative cooling.* Applied Thermal Engineering, 2007. **27**(11–12): p. 2011-2025.
35. Gert Jan Bom, R.F., Ebel Dijkstra, Marja Tummers, *Evaporative Air-Conditioning Applications for Environmentally*. 1999, The Word Bank Washington, D.C.
36. J. D. Palmer, P.E., C. E.M. , *Evaporative Cooling Design Guidelines Manual for New Mexico Schools and Commercial Building*. 2002.
37. coolers, W.a. *Evaporative air coolers*. 2010 [cited 2011; Available from: http://www.alibaba.com/product-gs/490046732/workshop_air_coolers.html.
38. Chen, Q., et al., *A new approach to analysis and optimization of evaporative cooling system I: Theory.* Energy, 2010. **35**(6): p. 2448-2454.
39. Frank, B., *On-site experimental testing of a novel dew point evaporative cooler.* Energy and Buildings, 2011. **43**(12): p. 3475-3483.
40. Koheji, M.A.-. *Application of Porous Cramics and Wind-catchers for Direct and Indirect Evaporative Cooling in Buildings*, in *Built Environment Institute of Building Technology*. 2003, The University of Nottingham: Nottingham. p. 16.
41. Bhatai, A. *Altrenatives to Active HVAC Sysyem*.
42. Afonso, C.F.A., *Recent advances in building air conditioning systems.* Applied Thermal Engineering, 2006. **26**(16): p. 1961-1971.

43. Kalkan, N., E.A. Young, and A. Celiktas, *Solar thermal air conditioning technology reducing the footprint of solar thermal air conditioning.* Renewable and Sustainable Energy Reviews, 2012. **16**(8): p. 6352-6383.
44. *Refrigeration Cycles*. [cited 2013 10/11]; Available from: http://www.eng.su.ac.th/me/elearning/ThermodynamicsII/3RefrigerationCycle.pdf.
45. Proctor Engineering Group, L., *High EEr at 46C Kingdom of Saudi Arabia Air Conditioner Project*. 2013: Saudi Arabia.
46. SPA, *20 million units of air conditioning in Saudi Arabia*, in *OKAZ*

2014: Saudi Arabia.
47. CIBSE, *Heating, Vantilation, Air conditioning and Refrigeration*, in *Guide B*

2005.
48. Jradi, M. and S. Riffat, *Tri-generation systems: Energy policies, prime movers, cooling technologies, configurations and operation strategies.* Renewable and Sustainable Energy Reviews, 2014. **32**(0): p. 396-415.
49. Duan, Z., et al., *Indirect evaporative cooling: Past, present and future potentials.* Renewable and Sustainable Energy Reviews, 2012. **16**(9): p. 6823-6850.
50. ASHRAE, *HVAC applications*, in *Evaporative cooling applications*. 2003, American Socity of Heating , Refirageration and Air-Conditioning Engineers: Atlanta, USA. p. 52 of 57.
51. Heidarinejad, G., et al., *Experimental investigation of two-stage indirect/direct evaporative cooling system in various climatic conditions.* Building and Environment, 2009. **44**(10): p. 2073-2079.
52. El-Dessouky, H., H. Ettouney, and A. Al-Zeefari, *Performance analysis of two-stage evaporative coolers.* Chemical Engineering Journal, 2004. **102**(3): p. 255-266.
53. Steeman, M., A. Janssens, and M. De Paepe, *Performance evaluation of indirect evaporative cooling using whole-building hygrothermal simulations.* Applied Thermal Engineering, 2009. **29**(14–15): p. 2870-2875.
54. Maheshwari, G.P., F. Al-Ragom, and R.K. Suri, *Energy-saving potential of an indirect evaporative cooler.* Applied Energy, 2001. **69**(1): p. 69-76.
55. Delfani, S., et al., *Energy saving potential of an indirect evaporative cooler as a pre-cooling unit for mechanical cooling systems in Iran.* Energy and Buildings, 2010. **42**(11): p. 2169-2176.
56. Hsu, S.T., Z. Lavan, and W.M. Worek, *Optimization of wet-surface heat exchangers.* Energy, 1989. **14**(11): p. 757-770.
57. Hasan, A., *Indirect evaporative cooling of air to a sub-wet bulb temperature.* Applied Thermal Engineering, 2010. **30**(16): p. 2460-2468.
58. Ala, H., *Going below the wet-bulb temperature by indirect evaporative cooling: Analysis using a modified ε-NTU method.* Applied Energy, 2012. **89**(1): p. 237-245.
59. Riangvilaikul, B. and S. Kumar, *Numerical study of a novel dew point evaporative cooling system.* Energy and Buildings, 2010. **42**(11): p. 2241-2250.
60. Riangvilaikul, B. and S. Kumar, *An experimental study of a novel dew point evaporative cooling system.* Energy and Buildings, 2010. **42**(5): p. 637-644.
61. Anisimov, S. and D. Pandelidis, *Numerical study of the Maisotsenko cycle heat and mass exchanger.* International Journal of Heat and Mass Transfer, 2014. **75**(0): p. 75-96.
62. Cui, X., et al., *Studying the performance of an improved dew-point evaporative design for cooling application.* Applied Thermal Engineering, 2014. **63**(2): p. 624-633.
63. Rogdakis, E.D., I.P. Koronaki, and D.N. Tertipis, *Experimental and computational evaluation of a Maisotsenko evaporative cooler at Greek climate.* Energy and Buildings, 2014. **70**(0): p. 497-506.

64. Zhao, X., et al., *Feasibility study of a novel dew point air conditioning system for China building application.* Building and Environment, 2009. **44**(9): p. 1990-1999.
65. Zhao, X., J.M. Li, and S.B. Riffat, *Numerical study of a novel counter-flow heat and mass exchanger for dew point evaporative cooling.* Applied Thermal Engineering, 2008. **28**(14-15): p. 1942-1951.
66. Zhan, C., et al., *Comparative study of the performance of the M-cycle counter-flow and cross-flow heat exchangers for indirect evaporative cooling – Paving the path toward sustainable cooling of buildings.* Energy, 2011. **36**(12): p. 6790-6805.
67. Duan, Z., *Investigation of a Novel Dew Point Indirect Evaporative Air Conditioning System for Buildings*, in *Architecture and Built Environment*. 2011, The University of Nottingham: Nottingham.
68. Elberling, L., *Laboratory Evaluation of the Coolerado Cooler Indirect Evaporative Cooling Unit*. 2006: USA.
69. Jesse Dean, L.H., Eric Kozubal and Jesse Geriger, *Dew Point Evaporative Comfort Cooling* 2012.
70. Wanphen, S. and K. Nagano, *Experimental study of the performance of porous materials to moderate the roof surface temperature by its evaporative cooling effect.* Building and Environment, 2009. **44**(2): p. 338-351.
71. Fouda, A. and Z. Melikyan, *A simplified model for analysis of heat and mass transfer in a direct evaporative cooler.* Applied Thermal Engineering, 2011. **31**(5): p. 932-936.
72. Wu, J.M., X. Huang, and H. Zhang, *Numerical investigation on the heat and mass transfer in a direct evaporative cooler.* Applied Thermal Engineering, 2009. **29**(1): p. 195-201.
73. Wu, J.M., X. Huang, and H. Zhang, *Theoretical analysis on heat and mass transfer in a direct evaporative cooler.* Applied Thermal Engineering, 2009. **29**(5-6): p. 980-984.
74. Velasco Gómez, E., F.J. Rey Martínez, and A. Tejero González, *Experimental characterisation of the operation and comparative study of two semi-indirect evaporative systems.* Applied Thermal Engineering, 2010. **30**(11-12): p. 1447-1454.
75. Naticchia, B., et al., *Energy performance evaluation of a novel evaporative cooling technique.* Energy and Buildings, 2010. **42**(10): p. 1926-1938.
76. Dai, Y.J. and K. Sumathy, *Theoretical study on a cross-flow direct evaporative cooler using honeycomb paper as packing material.* Applied Thermal Engineering, 2002. **22**(13): p. 1417-1430.
77. Zhao, X., S. Liu, and S.B. Riffat, *Comparative study of heat and mass exchanging materials for indirect evaporative cooling systems.* Building and Environment, 2008. **43**(11): p. 1902-1911.
78. Musa, M., *Novel Evaporative Cooling Systems for Building application*, in *Architectur and Built Environment*. May 2008, The University of Nottingham: Nottingham. p. 61-70, 234.
79. ABDUL-WAHAB S. MASHAT* , A.A.M.a.T.M.H., *Using Alternative Materials to Wood Flacks to improve the Efficiency of Evaporative Cooler.* Meteorology, Environment and Arid Land Agriculture Sciences Journal, 2005. **16**(2).
80. Al-Sulaiman, F., *Evaluation of the performance of local fibers in evaporative cooling.* Energy Conversion and Management, 2002(43): p. 2267-2273.
81. CSC. *What are Ceramics*. 2013 [cited 2013 15/03]; Available from: http://www.ceramic-substrates.co.uk/ceramics.html.
82. Ceramices, M.T. *properties and Advantages of Porous Ceramics*. 2013 [cited 2013 13/03]; Available from: http://www.mantectechnicalceramics.com/products/porous-products.

83. Zhu, S.R.a.J., *Experimental Investigation of an Indirect Evaporative Cooler Consisting of a Heat pipe Embedded in porous ceramic.* The journal of engineering Research, 2004: p. 47-52.
84. Lomas, K.J., et al., *Building bioclimatic charts for non-domestic buildings and passive downdraught evaporative cooling.* Building and Environment, 2004. **39**(6): p. 661-676.
85. He, J. and A. Hoyano, *Experimental study of cooling effects of a passive evaporative cooling wall constructed of porous ceramics with high water soaking-up ability.* Building and Environment, 2010. **45**(2): p. 461-472.
86. He, J. and A. Hoyano, *Experimental study of practical applications of a passive evaporative cooling wall with high water soaking-up ability.* Building and Environment, 2011. **46**(1): p. 98-108.
87. Velasco Gómez, E., et al., *Description and experimental results of a semi-indirect ceramic evaporative cooler.* International Journal of Refrigeration, 2005. **28**(5): p. 654-662.
88. Rey Martínez, F.J., et al., *Comparative study of two different evaporative systems: an indirect evaporative cooler and a semi-indirect ceramic evaporative cooler.* Energy and Buildings, 2004. **36**(7): p. 696-708.
89. Jiang, H., *A design supporting simulation system for predicting and evaluating the cool microclimate creating effect of passive evaporative cooling walls.* Building and Environment, 2011. **46**(3): p. 584-596.
90. *Passive Downdraught Cooling Systems Using Porous Ceramic Evaporators*. 2003: UNIVERSITY OF NOTTINGHAM, UK.
91. Schiano-Phan, R., *The Development of Passive Downdraught Evaporative Cooling Systems Using Porous Ceramic Evaporators and their application in residential buildings*, in *Plea2004 - The 21th Conference on Passive and Low Energy Architecture. Eindhoven, The Netherlands*. 2004. p. 1-6.
92. THERMALLOY, A. *How A Heat Pipe Works*. 2014 [cited 2014 26/01]; Available from: http://www.aavid.com/product-group/heatpipe/operate.
93. David Reay, P.K.a.R.M.G., *Heat Pipes theory, Design and Applications*. Sixth Edition ed. 2014, Oxford, UK: ELSEVIER.
94. Wan, J.W., J.L. Zhang, and W.M. Zhang, *The effect of heat-pipe air-handling coil on energy consumption in central air-conditioning system.* Energy and Buildings, 2007. **39**(9): p. 1035-1040.
95. Martínez, F.J.R., et al., *Design and experimental study of a mixed energy recovery system, heat pipes and indirect evaporative equipment for air conditioning.* Energy and Buildings, 2003. **35**(10): p. 1021-1030.
96. Beckwith, W.B., *Novel application of heat pipes for economical dehumidification in air conditioning systmes*, in *Ameraican heat pipes*. 2004. p. 1-8.
97. Xuan, Y.M., et al., *Research and application of evaporative cooling in China: A review (I) – Research.* Renewable and Sustainable Energy Reviews, 2012. **16**(5): p. 3535-3546.
98. Chandrakant Wani , S.G., Chaitanya Shrivastava M.Tech. Student , Associate Professor *A Review on Potential of Maisotsenko Cycle in Energy Saving Applications Using Evaporative Cooling.* International Journal of Advance Research in Science, Engineering and Technology, 2012. **01**(01): p. 15-20.
99. Halasz, B., *A general mathematical model of evaporative cooling devices.* Elsevier, Paris, 1998: p. 245-255.
100. Burmeister, L.C., *Convective Heat Transfer*. Second Edition ed. 1993, New York: John Wiley & Sons, Inc.

101. Sekulic, R.K.S.a.D., *fundamentals of heat exchanger design*. 2003, Canada: Jon Wiley& Sons.
102. ABDUL-WAHAB S. MASHAT* , A.A.M.a.T.M.H., *Evaluation of the Efficiency of Evaporative Cooler Using Cooling Efficiency Equation and Heat Transfer Equation.* Journal of King Abdulaziz University , Meteorology,Environment and Arid Land Agriculture Siences, 2005. **16**.
103. R. Alameri, A.A., T. Habeebullah, *Evaluated and developing of evaporative coolers in Mina valley.* Umm Al-Qura University, The Institute of The Tow Holy Mosques for Hajj and Omrah Research. , 2002.
104. Habeebullah, T., *Using Alternative Materials to Wood Flacks improve the Efficiency of Evaporative Cooler*, in *Meteorology, Environment and Arid Land Agriculture King Abdulaziz university*. 2004, King Abdulaziz: Jeedah.

Appendix 1

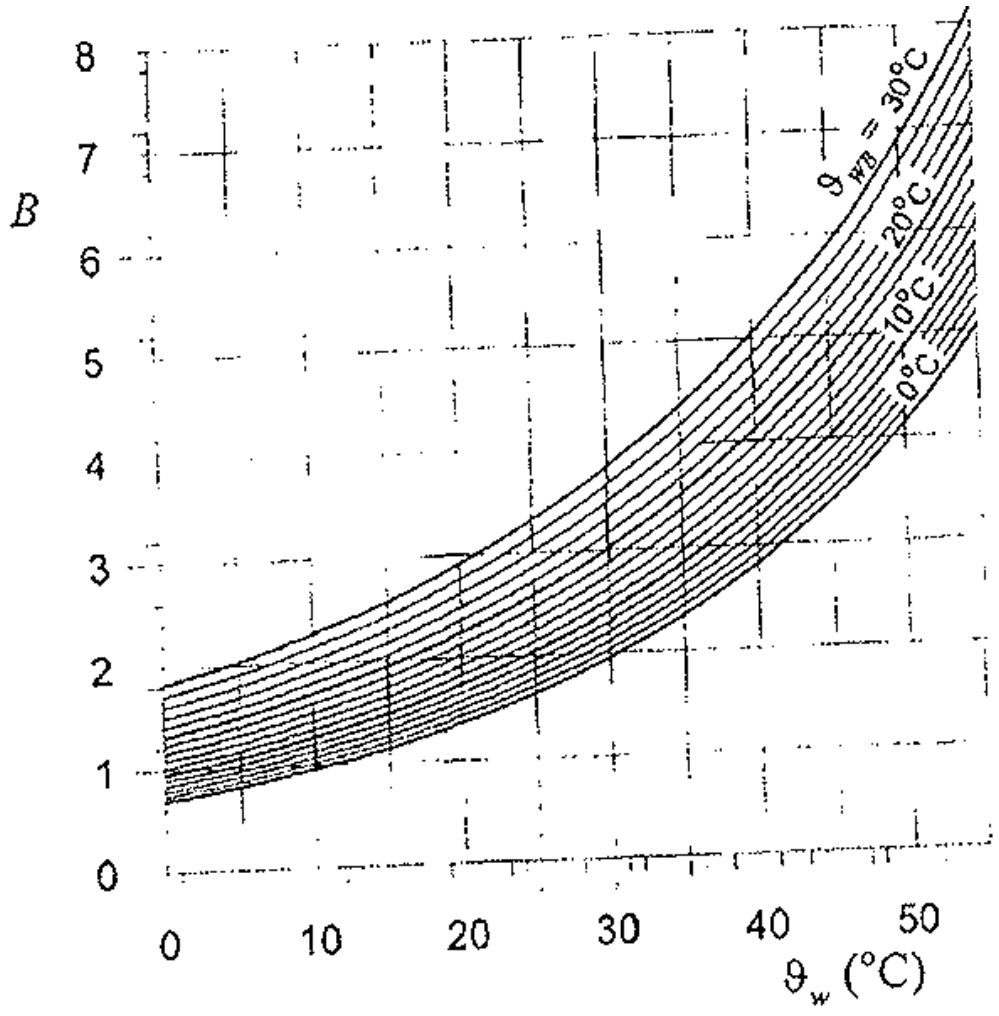

The value B as a function of θ_w and θ_{wB}

Appendix 2

Tdi30 ^{o}C and RH from 35% to 75%

```
clear all;

U1=0.0069;

U=0.0069;

Xoo=8.5;

Xo=7.5;

Ko=0.62;

K=0.52;

C=0.55;

Tdi(1,1)= 1;

Tfwi(1,1)=-0.101;

%twi(1,1)= 0.9570;

gi(1,1)=-1;

Le=1;

B=2.55;

%W=0.023;

%Xo/W=Z
```

```
Z=326;

%K+1+Le*B=D

D=4.55;

km=1;

%First Stage

%Dry Channel first stage

for i=1:144

Tdo(km,i)=((2*Tdi(km,i))-
(U1*Ko*C*Xoo*Tdi(km,i))+(2*U1*Ko*C*Xoo*Tfwi(km,1)))/(2+(U1*Ko*C*Xoo));

Tdi(km,i+1)=Tdo(km,i);

end

for j=1:12:144

   Tdo(j+12)=Tdo(j+11)

   Tdo(j+13)=Tdo(j+11)

end

%wet channel

%twi1=Tdo100=0.9570

twi(1,1)=Tdo(km,144);

for i=1:168
```

```
    two(km,i)=(2*twi(km,i)-(U*Xo*twi(km,i))+(2*U*Xo*Tfwi(km,1)))/(2+(U*Xo));

    twi(km,i+1)=two(km,i);

end

%Humidaity ratios

for i=1:144

go(km,i)=((2*gi(km,i))(U*Le*Xo*gi(km,i))+(2*U*Le*B*Xo*Tfwi(km,1)))/(2+(U*L
e*Xo));

    gi(km,i+1)=go(km,i);

end

%T film of water

for i=1:144

Tfwo(km,i)=((2*Tfwi(km,1))+(2*U*Z*K*Tdo(km,145i))+(2*U*Z*two(km,i))+(2*U
*Z*go(km,i))-(U*Z*D*Tfwi(km,1)))/(2+(U*Z*D));

Tfwi(km,i+1)=Tfwo(km,i);

end

%Second stage

%Dry Channel second stage

for km=2:100
```

```
Tdi(km,1)=1;

for i=1:144

Tdo(km,i)=((2*Tdi(km,i))-
(U1*Ko*C*Xoo*Tdi(km,i))+(2*U1*Ko*C*Xoo*Tfwo(km-1,145-
i)))/(2+(U1*Ko*C*Xoo));

Tdi(km,i+1)=Tdo(km,i);

end

%Wet Channel

twi(km,1)=Tdo(km,144);

for i=1:144

   two(km,i)=((2*twi(km,i)-U*Xo*twi(km,i))+(2*U*Xo*Tfwo(km-1,i)))/(2+(U*Xo));

   twi(km,i+1)=two(km,i);

end

%Humidaity ratios

gi(km,1)=-1;

for i=1:144

   go(km,i)=((2*gi(km,i))-(U*Le*Xo*gi(km,i))+(2*U*Le*B*Xo*Tfwo(km-
1,i)))/(2+(U*Le*Xo));

   gi(km,i+1)=go(km,i);
```

```
    end
%T film of water
%Tfwi(km,1)=0.27;
Tfwi(km,1)=Tfwo(km-1,145-i);
for i=1:144
Tfwo(km,i)=((2*Tfwi(km,i))+(2*U*Z*K*Tdo(km-1,145-i))+(2*U*Z*two(km-
1,i))+(2*U*Z*go(km-1,i))-(U*Z*D*Tfwi(km,i)))/(2+(U*Z*D));
Tfwi(km,i+1)=Tfwo(km,i);
end
end
for j=1:12:144
    Tdo(km,j+12)=Tdo(km,j+11)
    Tdo(km,j+13)=Tdo(km,j+11)
end
%RH35
for i=1:144
    Td(i)=Tdo(km-1,145-i)*11.1+18.9;
    tw(i)=twi(km,i)*11.1+18.9;
    g(i)=go(km,i)*0.0045+0.0137;
```

```
    Tf(i)=Tfwo(km,i)*11.1+18.9;
    Td30(i)=Tdo(km,i)*11.1+18.9;
end
%RH45
for i=1:144
    %Td(i)=Tdo(km-1,145-i)*9.05+20.95;
    %tw(i)=twi(km,i)*9.05+20.95;
    %g(i)=go(km,i)*0.0037+0.0146;
    %Tf(i)=Tfwo(km,i)*9.05+20.95;
    %Td30(i)=Tdo(km,i)*9.05+20.95;
end
%RH55
for i=1:144
    %Td(i)=Tdo(km-1,145-i)*7.16+22.84;
    %tw(i)=twi(km,i)*7.16+22.84;
    %g(i)=go(km,i)*0.0031+0.01756;
    %Tf(i)=Tfwo(km,i)*7.16+22.84;
    %Td30(i)=Tdo(km,i)*7.16+22.84;
end
```

```
%RH65
for i=1:144
    %Td(i)=Tdo(km-1,145-i)*5.4+24.6;
    %tw(i)=twi(km,i)*5.4+24.6;
    %g(i)=go(km,i)*0.00219+0.01959;
    %Tf(i)=Tfwo(km,i)*5.4+24.6;
    %Td30(i)=Tdo(km,i)*5.4+24.6;
end
%RH75
for i=1:144
   %Td(i)=Tdo(km-1,145-i)*3.74+26.26;
    %tw(i)=twi(km,i)*4.1+30.9;
    %g(i)=go(km,i)*0.00169+0.02169;
    %Tf(i)=Tfwo(km,i)*3.74+26.26;
    %Td30(i)=Tdo(km,i)*3.74+26.26;
end
```

```
for o=1:144

xx(o)=tw(end,145-o);

ss(o)=Tf(end,145-o);

end

hold on;

plot(xx)

plot(Td30(end,:))

plot(ss,':b'), grid on
```

Appendix 3

Tdi35 °C and RH from 35% to 75%

```
clear all;

U=0.0078;

Xo=11;

K=0.5;

C=0.55;

Tdi(1,1)= 1;

Tfwi(1,1)=-0.101;

%twi(1,1)= 0.9570;

gi(1,1)=-1;

Le=1;

B=3;

%W=0.045;

%Xo/W=Z

Z=154;

%K+1+Le*B=D

D=4.5;
```

```
km=1;

%First Stage

%Dry Channel first stage

for i=1:128

Tdo(km,i)=((2*Tdi(km,i))-
(U*K*C*Xo*Tdi(km,i))+(2*U*K*C*Xo*Tfwi(km,1)))/(2+(U*K*C*Xo));

Tdi(km,i+1)=Tdo(km,i);

end

%wet channel

%twi1=Tdo100=0.9570

twi(1,1)=Tdo(km,128);

for i=1:128

   two(km,i)=(2*twi(km,i)-(U*Xo*twi(km,i))+(2*U*Xo*Tfwi(km,1)))/(2+(U*Xo));

   twi(km,i+1)=two(km,i);

end

%Humidaity ratios

for i=1:128

   go(km,i)=((2*gi(km,i))-
(U*Le*Xo*gi(km,i))+(2*U*Le*B*Xo*Tfwi(km,1)))/(2+(U*Le*Xo));
```

```
    gi(km,i+1)=go(km,i);
end
%T film of water
for i=1:128
Tfwo(km,i)=((2*Tfwi(km,1))+(2*U*Z*K*Tdo(km,129-
i))+(2*U*Z*two(km,i))+(2*U*Z*go(km,i))-(U*Z*D*Tfwi(km,1)))/(2+(U*Z*D));
Tfwi(km,i+1)=Tfwo(km,i);
end
%Second stage
%Dry Channel second stage
for km=2:128
Tdi(km,1)=1;
for i=1:128
Tdo(km,i)=((2*Tdi(km,i))-(U*K*C*Xo*Tdi(km,i))+(2*U*K*C*Xo*Tfwo(km-1,129-
i)))/(2+(U*K*C*Xo));
Tdi(km,i+1)=Tdo(km,i);
end
%Wet Channel
```

```
twi(km,1)=Tdo(km,128);

for i=1:128

   two(km,i)=((2*twi(km,i)-U*Xo*twi(km,i))+(2*U*Xo*Tfwo(km-1,i)))/(2+(U*Xo));

   twi(km,i+1)=two(km,i);

end

%Humidaity ratios

gi(km,1)=-1;

for i=1:128

   go(km,i)=((2*gi(km,i))-(U*Le*Xo*gi(km,i))+(2*U*Le*B*Xo*Tfwo(km-
1,i)))/(2+(U*Le*Xo));

   gi(km,i+1)=go(km,i);

   end

%T film of water

%Tfwi(km,1)=0.27;

Tfwi(km,1)=Tfwo(km-1,129-i);

for i=1:128

Tfwo(km,i)=((2*Tfwi(km,i))+(2*U*Z*K*Tdo(km-1,129-i))+(2*U*Z*two(km-
1,i))+(2*U*Z*go(km-1,i))-(U*Z*D*Tfwi(km,i)))/(2+(U*Z*D));

Tfwi(km,i+1)=Tfwo(km,i)
```

```
end

end

%RH35

for i=1:128

    Td(i)=Tdo(km-1,129-i)*12.38+22.62;

    tw(i)=twi(km,i)*12.38+22.62;

    g(i)=go(km,i)*0.005+0.018;

    Tf(i)=Tfwo(km,i)*12.38+22.62;

    Td30(i)=Tdo(km,i)*12.38+22.62;

end

%RH45

for i=1:128

    %Td(i)=Tdo(km-1,129-i)*10.05+24.95;

    %tw(i)=twi(km,i)*10.05+24.95;

    %g(i)=go(km,i)*0.005+0.02;

    %Tf(i)=Tfwo(km,i)*10.05+24.95;

    %Td30(i)=Tdo(km,i)*10.05+24.95;

end

%RH55
```

```
for i=1:128
    %Td(i)=Tdo(km-1,129-i)*7.9+27.1;
    %tw(i)=twi(km,i)*7.9+27.1;
    %g(i)=go(km,i)*0.0033+0.0228;
    %Tf(i)=Tfwo(km,i)*7.9+27.1;
    %Td30(i)=Tdo(km,i)*7.9+27.1;
end
%RH65
for i=1:128
    %Td(i)=Tdo(km-1,129-i)*5.9+29.1;
    %tw(i)=twi(km,i)*5.9+29.1;
    %g(i)=go(km,i)*0.0028+0.0258;
    %Tf(i)=Tfwo(km,i)*5.9+29.1;
    %Td30(i)=Tdo(km,i)*5.9+29.1;
end
%RH75
for i=1:128
    %Td(i)=Tdo(km-1,129-i)*4.1+30.9;
    %tw(i)=twi(km,i)*4.1+30.9;
```

```
    %g(i)=go(km,i)*0.0017+0.0287;

    %Tf(i)=Tfwo(km,i)*4.1+30.9;

    %Td30(i)=Tdo(km,i)*4.1+30.9;

end

for o=1:128

xx(o)=tw(end,129-o);

ss(o)=Tf(end,129-o);

end

hold on;

plot(xx)

plot(Td30(end,:))

plot(ss,':b'), grid on

sub = [35,31,27.3, 25.4,22.8];

XX1 = [0,33,77,100, 128];

hold on

%plot(XX1,sub)
%hold on
wo = [23.2,22.7,22.2,21.9,22.8];
ss= [0,37,70,100,128]
%plot(ss,wo)
```

Appendix 4

Heat pipe

Tdi30 ^{o}C and RH from 35% to 75%

```
clear all;

U1=0.0069;

U=0.0069;

Xoo=8.5;

Xo=7.5;

Ko=0.62;

K=0.52;

C=0.55;

Tdi(1,1)= 1;

Tfwi(1,1)=-0.101;

%twi(1,1)= 0.9570;

gi(1,1)=-1;

Le=1;

B=2.55;

%W=0.023;

%Xo/W=Z
```

```
Z=326;

%K+1+Le*B=D

D=4.55;

km=1;

%First Stage

%Dry Channel first stage

for i=1:144

Tdo(km,i)=((2*Tdi(km,i))-
(U1*Ko*C*Xoo*Tdi(km,i))+(2*U1*Ko*C*Xoo*Tfwi(km,1)))/(2+(U1*Ko*C*Xoo));

Tdi(km,i+1)=Tdo(km,i);

end

for j=1:12:144

    Tdo(j+12)=Tdo(j+11)

    Tdo(j+13)=Tdo(j+11)

end

%wet channel

%twi1=Tdo100=0.9570

twi(1,1)=Tdo(km,144);

for i=1:168
```

```
    two(km,i)=(2*twi(km,i)-(U*Xo*twi(km,i))+(2*U*Xo*Tfwi(km,1)))/(2+(U*Xo));

    twi(km,i+1)=two(km,i);

end

%Humidaity ratios

for i=1:144

    go(km,i)=((2*gi(km,i))-
(U*Le*Xo*gi(km,i))+(2*U*Le*B*Xo*Tfwi(km,1)))/(2+(U*Le*Xo));

    gi(km,i+1)=go(km,i);

end

%T film of water

for i=1:144

Tfwo(km,i)=((2*Tfwi(km,1))+(2*U*Z*K*Tdo(km,145-
i))+(2*U*Z*two(km,i))+(2*U*Z*go(km,i))-(U*Z*D*Tfwi(km,1)))/(2+(U*Z*D));

Tfwi(km,i+1)=Tfwo(km,i);

end

%Second stage

%Dry Channel second stage

for km=2:100
```

```
Tdi(km,1)=1;

for i=1:144

Tdo(km,i)=((2*Tdi(km,i))-
(U1*Ko*C*Xoo*Tdi(km,i))+(2*U1*Ko*C*Xoo*Tfwo(km-1,145-
i)))/(2+(U1*Ko*C*Xoo));

Tdi(km,i+1)=Tdo(km,i);

end

%Wet Channel

twi(km,1)=Tdo(km,144);

for i=1:144

   two(km,i)=((2*twi(km,i)-U*Xo*twi(km,i))+(2*U*Xo*Tfwo(km-1,i)))/(2+(U*Xo));

   twi(km,i+1)=two(km,i);

end

%Humidaity ratios

gi(km,1)=-1;

for i=1:144

   go(km,i)=((2*gi(km,i))-(U*Le*Xo*gi(km,i))+(2*U*Le*B*Xo*Tfwo(km-
1,i)))/(2+(U*Le*Xo));

   gi(km,i+1)=go(km,i);
```

```
    end
%T film of water
%Tfwi(km,1)=0.27;
Tfwi(km,1)=Tfwo(km-1,145-i);
for i=1:144
Tfwo(km,i)=((2*Tfwi(km,i))+(2*U*Z*K*Tdo(km-1,145-i))+(2*U*Z*two(km-
1,i))+(2*U*Z*go(km-1,i))-(U*Z*D*Tfwi(km,i)))/(2+(U*Z*D));
Tfwi(km,i+1)=Tfwo(km,i);
end
end
for j=1:12:144
    Tdo(km,j+12)=Tdo(km,j+11)
    Tdo(km,j+13)=Tdo(km,j+11)
end
%RH35
for i=1:144
    %Td(i)=Tdo(km-1,145-i)*11.1+18.9;
    %tw(i)=twi(km,i)*11.1+18.9;
    %g(i)=go(km,i)*0.0045+0.0137;
```

```
    %Tf(i)=Tfwo(km,i)*11.1+18.9;
    %Td30(i)=Tdo(km,i)*11.1+18.9;
end
%RH45
for i=1:144
    %Td(i)=Tdo(km-1,145-i)*9.05+20.95;
    %tw(i)=twi(km,i)*9.05+20.95;
    %g(i)=go(km,i)*0.0037+0.0146;
    %Tf(i)=Tfwo(km,i)*9.05+20.95;
    %Td30(i)=Tdo(km,i)*9.05+20.95;
end
%RH55
for i=1:144
    Td(i)=Tdo(km-1,145-i)*7.16+22.84;
    tw(i)=twi(km,i)*7.16+22.84;
    g(i)=go(km,i)*0.0031+0.01756;
    Tf(i)=Tfwo(km,i)*7.16+22.84;
    Td30(i)=Tdo(km,i)*7.16+22.84;
end
```

```
%RH65
for i=1:144
    %Td(i)=Tdo(km-1,145-i)*5.4+24.6;
    %tw(i)=twi(km,i)*5.4+24.6;
    %g(i)=go(km,i)*0.00219+0.01959;
    %Tf(i)=Tfwo(km,i)*5.4+24.6;
    %Td30(i)=Tdo(km,i)*5.4+24.6;
end
%RH75
for i=1:144
   %Td(i)=Tdo(km-1,145-i)*3.74+26.26;
    %tw(i)=twi(km,i)*4.1+30.9;
    %g(i)=go(km,i)*0.00169+0.02169;
    %Tf(i)=Tfwo(km,i)*3.74+26.26;
    %Td30(i)=Tdo(km,i)*3.74+26.26;
end
for o=1:144
xx(o)=tw(end,145-o);
ss(o)=Tf(end,145-o);
```

```
end

hold on;

plot(xx)

plot(Td30(end,:))

plot(ss,':b'), grid on
```

Appendix 5

Heat pipe

Tdi35 ^{o}C and RH from 35% to 75%

```
clear all;

U1=0.0069;

U=0.0069;

Xoo=8.5;

Xo=7.5;

Ko=0.62;

K=0.52;

C=0.55;

Tdi(1,1)= 1;

Tfwi(1,1)=-0.101;

%twi(1,1)= 0.9570;

gi(1,1)=-1;

Le=1;

B=2.55;

%W=0.023;
```

```
%Xo/W=Z

Z=326;

%K+1+Le*B=D

D=4.55;

km=1;

%First Stage

%Dry Channel first stage

for i=1:144

Tdo(km,i)=((2*Tdi(km,i))-
(U1*Ko*C*Xoo*Tdi(km,i))+(2*U1*Ko*C*Xoo*Tfwi(km,1)))/(2+(U1*Ko*C*Xoo));

Tdi(km,i+1)=Tdo(km,i);

end

for j=1:12:144

    Tdo(j+12)=Tdo(j+11)

    Tdo(j+13)=Tdo(j+11)

end

%wet channel

%twi1=Tdo100=0.9570
```

```
twi(1,1)=Tdo(km,144);

for i=1:168

   two(km,i)=(2*twi(km,i)-(U*Xo*twi(km,i))+(2*U*Xo*Tfwi(km,1)))/(2+(U*Xo));

   twi(km,i+1)=two(km,i);

end

%Humidaity ratios

for i=1:144

   go(km,i)=((2*gi(km,i))-
(U*Le*Xo*gi(km,i))+(2*U*Le*B*Xo*Tfwi(km,1)))/(2+(U*Le*Xo));

   gi(km,i+1)=go(km,i);

end

%T film of water

for i=1:144

Tfwo(km,i)=((2*Tfwi(km,1))+(2*U*Z*K*Tdo(km,145-
i))+(2*U*Z*two(km,i))+(2*U*Z*go(km,i))-(U*Z*D*Tfwi(km,1)))/(2+(U*Z*D));

Tfwi(km,i+1)=Tfwo(km,i);

end



%Second stage
```

```
%Dry Channel second stage

for km=2:100

Tdi(km,1)=1;

for i=1:144

Tdo(km,i)=((2*Tdi(km,i))-
(U1*Ko*C*Xoo*Tdi(km,i))+(2*U1*Ko*C*Xoo*Tfwo(km-1,145-
i)))/(2+(U1*Ko*C*Xoo));

Tdi(km,i+1)=Tdo(km,i);

end

%Wet Channel

twi(km,1)=Tdo(km,144);

for i=1:144

   two(km,i)=((2*twi(km,i)-U*Xo*twi(km,i))+(2*U*Xo*Tfwo(km-1,i)))/(2+(U*Xo));

   twi(km,i+1)=two(km,i);

end



%Humidaity ratios

gi(km,1)=-1;

for i=1:144
```

```
    go(km,i)=((2*gi(km,i))-(U*Le*Xo*gi(km,i))+(2*U*Le*B*Xo*Tfwo(km-
1,i)))/(2+(U*Le*Xo));
    gi(km,i+1)=go(km,i);
    end
%T film of water
%Tfwi(km,1)=0.27;
Tfwi(km,1)=Tfwo(km-1,145-i);
for i=1:144
Tfwo(km,i)=((2*Tfwi(km,i))+(2*U*Z*K*Tdo(km-1,145-i))+(2*U*Z*two(km-
1,i))+(2*U*Z*go(km-1,i))-(U*Z*D*Tfwi(km,i)))/(2+(U*Z*D));
Tfwi(km,i+1)=Tfwo(km,i);
end


end
for j=1:12:144
    Tdo(km,j+12)=Tdo(km,j+11)
    Tdo(km,j+13)=Tdo(km,j+11)
end
%RH35
```

```
for i=1:144
    Td(i)=Tdo(km-1,145-i)*12.38+22.62;
    tw(i)=twi(km,i)*12.38+22.62;
    g(i)=go(km,i)*0.005+0.018;
    Tf(i)=Tfwo(km,i)*12.38+22.62;
    Td30(i)=Tdo(km,i)*12.38+22.62;
end
%RH45
for i=1:144
    %Td(i)=Tdo(km-1,145-i)*10.05+24.95;
    %tw(i)=twi(km,i)*10.05+24.95;
    %g(i)=go(km,i)*0.005+0.02;
    %Tf(i)=Tfwo(km,i)*10.05+24.95;
    %Td30(i)=Tdo(km,i)*10.05+24.95;
end
%RH55
for i=1:144
    %Td(i)=Tdo(km-1,145-i)*7.9+27.1;
    %tw(i)=twi(km,i)*7.9+27.1;
```

```
    %g(i)=go(km,i)*0.0033+0.0228;
    %Tf(i)=Tfwo(km,i)*7.9+27.1;
    %Td30(i)=Tdo(km,i)*7.9+27.1;
end
%RH65
for i=1:144
    %Td(i)=Tdo(km-1,145-i)*5.9+29.1;
    %tw(i)=twi(km,i)*5.9+29.1;
    %g(i)=go(km,i)*0.0028+0.0258;
    %Tf(i)=Tfwo(km,i)*5.9+29.1;
    %Td30(i)=Tdo(km,i)*5.9+29.1;
end
%RH75
for i=1:144
    %Td(i)=Tdo(km-1,145-i)*4.1+30.9;
    %tw(i)=twi(km,i)*4.1+30.9;
    %g(i)=go(km,i)*0.0017+0.0287;
    %Tf(i)=Tfwo(km,i)*4.1+30.9;
    %Td30(i)=Tdo(km,i)*4.1+30.9;
```

```
end

for o=1:144

xx(o)=tw(end,145-o);

ss(o)=Tf(end,145-o);

end

hold on;

plot(xx)

%plot(Td35)

plot(Td30(end,:))

plot(ss,':b'), grid on
```